Mathematical and numerical analysis of capillarity problems and processes

Liliana Braescu, Simona Epure, Thierry Duffar

Mathematical and Numerical Analysis of Capillarity Problems and Processes

Liliana Braescu
West University of Timisoara

Simona Epure
SIMaP-EPM and West University of Timisoara

Thierry Duffar
SIMaP-EPM

One major problem confronting crystal growth researchers has been the development of techniques capable of monitoring and controlling the external shape of melt-grown crystals, and simultaneously improving the crystal structures. In the EFG, Cz, dewetted Bridgman and FZ processes, the shape and the dimensions of the crystal are determined by the liquid meniscus and by the heat transfer at the melt–crystal interface. In addition, the meniscus is also of great practical use for techniques of diameter control: in the weighing method ([Bardsley 1974, Bardsley 1977, Dijk 1974, Johansen 1992, Chapter 3]) the weight of the melt enclosed by the meniscus appears as an essential parameter; when using video observation ([Gartner 1972, Gartner 1973, O'Kane 1972, Sachs 1980]), the crystal diameter and the interface height have to be measured exactly.

Historically, the physical origin and the shape of a liquid meniscus were among the first phenomena to be studied in capillarity [Hauksbee 1709]. The first formal analytical expression was given by Laplace [Laplace 1806], after introduction of the *mean curvature* κ defined as the average (arithmetic mean) of the principal curvatures $\kappa = \frac{1}{2}(1/R_1 + 1/R_2)$

[Young 1805]. Laplace showed that the *mean curvature* of the free surface is proportional to the pressure change across the surface. The proportionality coefficient is the surface tension γ_{lv}. The pressure change across the surface contains p_v the pressure of the external gas on the melt; p_O, the internal pressure applied on the liquid, which can generally be defined at the origin; $\rho_l g z$, the hydrostatic pressure; $\frac{1}{2}\rho_l \Omega_l^2 (x^2 + y^2)$, the pressure determined by the centrifugal force due to a possible liquid rotation $\frac{1}{2}\rho_l \Omega_l^2 (x^2 + y^2)$ where Ω_l is the angular velocity of the liquid (around the Oz axis in crystal growth techniques), and, when magnetic fields are used, the Maxwell pressure which is proportional to the square of the magnetic induction $B^2(x, y) / 2\mu$ (μ-magnetic permeability). The following equality known as the Young–Laplace equation must hold:

$$\frac{1}{R_1} + \frac{1}{R_2} = \pm \frac{p_O - p_v - \rho_l g z + \frac{1}{2}\rho_l \Omega_l^2 (x^2 + y^2) - [B^2(x, y)/2\mu]}{\gamma_{lv}}. \tag{8.1}$$

As quoted in [Landau 1971], the choice of the positive sign is a convention which generally follows the physical meaning. However, from the mathematical point of view, the positive or negative signs depend on the axis frame convention. Generally, the curvature is taken to be positive if the curve turns in the same direction as the surface's chosen normal, and negative otherwise.

The result can be summarized as follows: the positive sign corresponds to the cases where the liquid has the shape of a sessile or pendant drop (Figure 8.1a), e.g. floating zone (FZ), dewetting or Verneuil configurations, and the negative sign corresponds to the cases where the liquid has the shape of an external meniscus (Figure 8.1b), e.g. EFG or Cz configurations [Hartland 1976].

Denoting the meniscus surface by A: $z(x, y)$, it is known from differential geometry, that the mean curvature is expressed as [Finn 1986]:

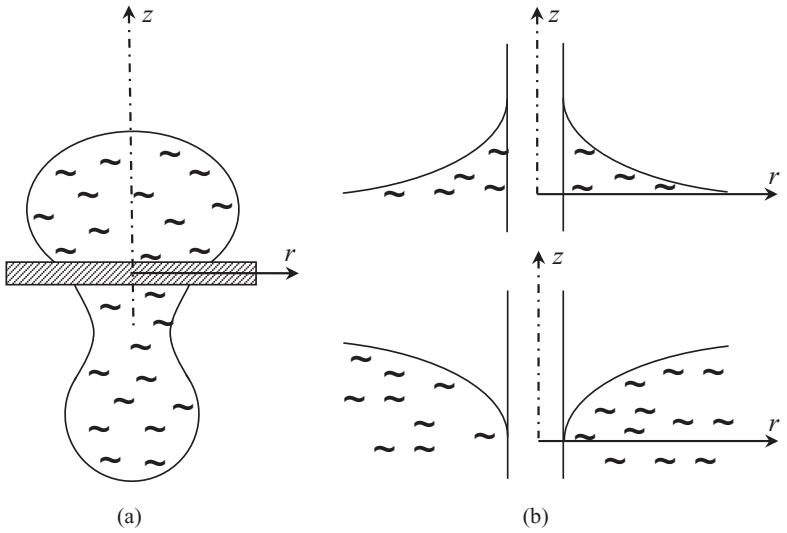

Figure 8.1 *(a) Sessile or pendant drop: + positive sign in Young-Laplace equation. (b) External meniscus: – negative sign in Young-Laplace equation.*

$$\kappa = \frac{E_{\mathrm{I}} G_{\mathrm{II}} - 2F_{\mathrm{I}} F_{\mathrm{II}} + G_{\mathrm{I}} E_{\mathrm{II}}}{2\left(E_{\mathrm{I}} G_{\mathrm{I}} - F_{\mathrm{I}}^2\right)}, \tag{8.2}$$

where E_{I}, F_{I}, G_{I} represent the coefficients of the first fundamental form of the surface A and E_{II}, F_{II}, G_{II} represent the coefficients of the second fundamental form. According to Finn, for a surface given in explicit form $z = z(x, y)$, these coefficients are given by:

$$E_{\mathrm{I}} = 1 + \left(\frac{\partial z}{\partial x}\right)^2, \quad F_{\mathrm{I}} = \frac{\partial z}{\partial x} \cdot \frac{\partial z}{\partial y}, \quad G_{\mathrm{I}} = 1 + \left(\frac{\partial z}{\partial y}\right)^2,$$

$$E_{\mathrm{II}} = \frac{\partial^2 z / \partial x^2}{\sqrt{1 + (\partial z/\partial x)^2 + (\partial z/\partial y)^2}},$$

$$F_{II} = \frac{\partial^2 z / (\partial x \partial y)}{\sqrt{1 + (\partial z/\partial x)^2 + (\partial z/\partial y)^2}},$$

$$G_{\mathrm{II}} = \frac{\partial^2 z / \partial y^2}{\sqrt{1 + (\partial z/\partial x)^2 + (\partial z/\partial y)^2}},$$

and hence the Young–Laplace equation (8.1) becomes:

$$\frac{\left[1 + \left(\frac{\partial z}{\partial y}\right)^2\right] \cdot \frac{\partial^2 z}{\partial x^2} - 2 \cdot \frac{\partial z}{\partial x} \cdot \frac{\partial z}{\partial y} \cdot \frac{\partial^2 z}{\partial x \partial y} + \left[1 + \left(\frac{\partial z}{\partial x}\right)^2\right] \cdot \frac{\partial^2 z}{\partial y^2}}{\left[1 + \left(\frac{\partial z}{\partial x}\right)^2 + \left(\frac{\partial z}{\partial y}\right)^2\right]^{3/2}}$$

$$= \pm \frac{p_{\mathrm{O}} - p_{\mathrm{v}} - \rho_{\mathrm{l}} g z + \frac{1}{2} \rho_{\mathrm{l}} \Omega_{\mathrm{l}}^2 \left(x^2 + y^2\right) - \left[B^2(x, y)/2\mu\right]}{\gamma_{\mathrm{lv}}}. \tag{8.3}$$

This equation is a nonlinear partial differential equation (PDE) of second order, and the unknown function $z(x, y)$ represents the meniscus surface. Because of the nonlinearity of this equation, it is necessary to do qualitative analysis and to develop specific numerical tools for finding the meniscus surface, which, furthermore, should satisfy the boundary conditions depending on the chosen configuration.

Section 8.1 below contains a mathematical formulation of the capillary problem. The boundary value problem for the Young–Laplace equation in the three-dimensional and axisymmetric cases is presented, and the initial and boundary condition of the axisymmetric meniscus problem are given. The growth angle criterion and some approximated solutions of the axisymmetric meniscus problem are also included.

In sections 8.2–8.4 some analytical and numerical solutions for the meniscus equation in the Cz, EFG and dewetted Bridgman growth techniques are presented. The case of the FZ process is extensively described in Chapter 4 and is not treated here.

8.1 Mathematical Formulation of the Capillary Problem

8.1.1 Boundary Value Problems for the Young–Laplace Equation

8.1.1.1 Three-Dimensional Case

In order to find physically sound solutions of the Young–Laplace equation, it is generally necessary to formulate the model as a 'well posed' PDE problem. A PDE problem is said to be well posed if: (i) a solution to the problem exists; (ii) the solution is unique; and (iii) the solution depends continuously on the problem data. In practice, the question of whether a PDE problem is well posed can be difficult to settle.

The Young–Laplace equation (8.3) can be written as follows:

$$a(x,y)\cdot\frac{\partial^2 z}{\partial x^2}+2\cdot b(x,y)\cdot\frac{\partial^2 z}{\partial x\partial y}+c(x,y)\cdot\frac{\partial^2 z}{\partial y^2}+d(x,y)\cdot z=e(x,y), \tag{8.4}$$

where

$$a(x,y)=\frac{1+\left(\dfrac{\partial z}{\partial y}\right)^2}{\left[1+\left(\dfrac{\partial z}{\partial x}\right)^2+\left(\dfrac{\partial z}{\partial y}\right)^2\right]^{3/2}}, \tag{8.5}$$

$$b(x,y)=\frac{-\dfrac{\partial z}{\partial x}\cdot\dfrac{\partial z}{\partial y}}{\left[1+\left(\dfrac{\partial z}{\partial x}\right)^2+\left(\dfrac{\partial z}{\partial y}\right)^2\right]^{3/2}}, \tag{8.6}$$

$$d(x,y)=\frac{\rho_{\mathrm{l}}g}{\gamma_{\mathrm{lv}}}, \tag{8.7}$$

$$c(x,y)=\frac{1+\left(\dfrac{\partial z}{\partial x}\right)^2}{\left[1+\left(\dfrac{\partial z}{\partial x}\right)^2+\left(\dfrac{\partial z}{\partial y}\right)^2\right]^{3/2}}, \tag{8.8}$$

$$e(x,y)=\pm\frac{p_{\mathrm{O}}-p_{\mathrm{v}}+\dfrac{1}{2}\rho_{\mathrm{l}}\Omega_{\mathrm{l}}^2\left(x^2+y^2\right)-B^2(x,y)/2\mu}{\gamma_{\mathrm{lv}}}. \tag{8.9}$$

The inequality

$$a(x,y)\cdot c(x,y)-b^2(x,y)=\frac{1}{\sqrt{1+(\partial z/\partial x)^2+(\partial z/\partial y)^2}}>0$$

looks like an elliptic type of any solution $z(x,y)$ [Finn 1986]. Unfortunately Equation (8.4) cannot be included in the general theory of the elliptic PDE from variational calculus because the functions a, b, c, d, e: $\Omega \subset \mathbb{R}^2 \rightarrow \mathbb{R}$ are unknown and strongly nonlinear. Moreover, a well-posed elliptic PDE problem usually takes the form of a boundary value problem (BVP) with the solution required to satisfy a single boundary condition (Dirichlet, Neumann or Robin boundary condition) at each point on the boundary $\partial\Omega$ of the region.

These circumstances have important consequences for the behaviour of the solutions, reasons for which each problem containing the Young–Laplace equation should be treated separately. The peculiarities of each problem will lead to a corresponding mathematical context capable of providing conditions that ensure the existence and uniqueness of the solution.

Because of the complexity of the BVP associated to the Young–Laplace equation, there is no general analytical solution and the problem must be addressed numerically [Clanet 2002]. In some particular domains Ω, e.g. those obtained from crystal growth configurations (Cz, EFG, dewetted Bridgman, FZ), certain approximations can be made in order to simplify the problem and hence the equation can be integrated. In the following, the approximations most commonly used in the literature are presented, i.e. the domain Ω is two-dimensional or axisymmetric. These two-dimensional models will then be developed for EFG, Cz and dewetted Bridgman growth techniques. In some particular conditions, analytical solutions will be given.

8.1.1.2 Axisymmetric Case

In the axisymmetric case, the Young–Laplace equation (8.3) can be written using cylindrical polar coordinates $x = r \cdot \cos\theta$, $y = r \cdot \sin\theta$, $z = z$ (the meniscus is axisymmetric). Expressing r and θ as functions of x and y, i.e. $r = \sqrt{x^2 + y^2}$, $\theta = \arctan(y/x)$, the partial derivatives of the function $z(x,y)$ are:

$$\frac{\partial z}{\partial x} = \frac{\mathrm{d}z}{\mathrm{d}r}\cdot\frac{x}{r}, \quad \frac{\partial z}{\partial y} = \frac{\mathrm{d}z}{\mathrm{d}r}\cdot\frac{y}{r},$$

$$\frac{\partial^2 z}{\partial x^2} = \frac{\mathrm{d}^2 z}{\mathrm{d}r^2}\cdot\frac{x^2}{r^2} + \frac{\mathrm{d}z}{\mathrm{d}r}\cdot\frac{y^2}{r^3}, \quad \frac{\partial^2 z}{\partial y^2} = \frac{\mathrm{d}^2 z}{\mathrm{d}r^2}\cdot\frac{y^2}{r^2} + \frac{\mathrm{d}z}{\mathrm{d}r}\cdot\frac{x^2}{r^3}, \quad \frac{\partial^2 z}{\partial x \partial y} = \frac{\mathrm{d}^2 z}{\mathrm{d}r^2}\cdot\frac{xy}{r^2} - \frac{\mathrm{d}z}{\mathrm{d}r}\cdot\frac{xy}{r^3}.$$

Replacing these derivatives in Equation (8.3), the Young–Laplace equation written in cylindrical coordinates is:

$$\frac{\dfrac{\mathrm{d}^2 z}{\mathrm{d}r^2} + \dfrac{1}{r}\cdot\dfrac{\mathrm{d}z}{\mathrm{d}r}\cdot\left[1+\left(\dfrac{\mathrm{d}z}{\mathrm{d}r}\right)^2\right]}{\left[1+(\mathrm{d}z/\mathrm{d}r)^2\right]^{3/2}} = \pm\frac{p_\mathrm{O} - p_\mathrm{v} - \rho_\mathrm{l} g z + \dfrac{1}{2}\rho_\mathrm{l}\Omega_\mathrm{l}^2\cdot r^2 - \dfrac{B^2(r)}{2\mu}}{\gamma_\mathrm{lv}}, \tag{8.10}$$

for which the solution $z = z(r)$ is sought depending on the radial coordinate $r = \sqrt{x^2 + y^2}$. An equivalent formulation of Equation (8.10) is given in terms of the principal curvatures:

$$\frac{\dfrac{\mathrm{d}^2 z}{\mathrm{d}r^2}}{\left[1+(\mathrm{d}z/\mathrm{d}r)^2\right]^{3/2}} + \frac{\dfrac{1}{r}\cdot\dfrac{\mathrm{d}z}{\mathrm{d}r}}{\left[1+(\mathrm{d}z/\mathrm{d}r)^2\right]^{1/2}} = \pm\frac{p_\mathrm{O} - p_\mathrm{v} - \rho_\mathrm{l} g z + \dfrac{1}{2}\rho_\mathrm{l}\Omega_\mathrm{l}^2\cdot r^2 - \left[B^2(r)/2\mu\right]}{\gamma_\mathrm{lv}} \tag{8.11}$$

where

$$\frac{\mathrm{d}^2 z/\mathrm{d}r^2}{\left[1+(\mathrm{d}z/\mathrm{d}r)^2\right]^{3/2}}=\frac{1}{R_1}\quad\text{and}\quad\frac{(1/r)\cdot(\mathrm{d}z/\mathrm{d}r)}{\left[1+(\mathrm{d}z/\mathrm{d}r)^2\right]^{1/2}}=\frac{1}{R_2},$$

but the most useful formulation is:

$$\frac{\mathrm{d}^2 z}{\mathrm{d}r^2}=\pm\frac{p_\mathrm{O}-p_\mathrm{v}-\rho_\mathrm{l}gz+\frac{1}{2}\rho_\mathrm{l}\Omega_\mathrm{l}^2\cdot r^2-\frac{B^2(r)}{2\mu}}{\gamma_\mathrm{lv}}\cdot\left[1+\left(\frac{\mathrm{d}z}{\mathrm{d}r}\right)^2\right]^{3/2}-\frac{1}{r}\cdot\frac{\mathrm{d}z}{\mathrm{d}r}\cdot\left[1+\left(\frac{\mathrm{d}z}{\mathrm{d}r}\right)^2\right].\quad(8.12)$$

This is a nonlinear second-order differential equation and to obtain its solution $z = z(r)$ two conditions are needed, which, in association with Equation (8.12), give the BVP or initial value problem (IVP). In general, because of its nonlinearity, the problem does not have a solution expressed in an analytical form.

To solve the BVP (or IVP) it is necessary do a qualitative analysis and to develop specific numerical tools. To this end, Equation (8.12) is transformed into a nonlinear first-order system of differential equations. In the literature, two equivalent systems are known: one having three differential equations, and another having two differential equations. In both formulations, the angle ϕ between the tangent to the meniscus (at an arbitrary point) and the horizontal axis, called meridian angle [Boucher 1980], is involved.

First, Princen and Mason [Princen 1965] introduced the arc length s along the curve which generates the surface of revolution $z(r)$: $\mathrm{d}r/\mathrm{d}s = \cos\phi$, $\mathrm{d}z/\mathrm{d}s = \pm\sin\phi$ (the positive or negative signs depend on the axis frame convention in the same way as in Equation (8.1)). Taking into account that $\mathrm{d}r/\mathrm{d}s = \cos\phi$, $\mathrm{d}z/\mathrm{d}s = \sin\phi$ imply the curvatures $1/R_1 = \mathrm{d}\phi/\mathrm{d}s$ and $1/R_2 = (\sin\phi)/r$ (e.g. configuration Figure 8.1a), and $\mathrm{d}r/\mathrm{d}s = \cos\phi$, $\mathrm{d}z/\mathrm{d}s = -\sin\phi$ imply $1/R_1 = -\mathrm{d}\phi/\mathrm{d}s$, $1/R_2 = -(\sin\phi)/r$ (e.g. configuration Figure 8.1b)), Equation (8.11) is transformed into a system of three parametric differential equations:

$$\begin{cases}\dfrac{\mathrm{d}r}{\mathrm{d}s}=\cos\phi\\[2ex]\dfrac{\mathrm{d}z}{\mathrm{d}s}=\pm\sin\phi\\[2ex]\dfrac{\mathrm{d}\phi}{\mathrm{d}s}=-\dfrac{\sin\phi}{r}\pm\dfrac{p_\mathrm{O}-p_\mathrm{v}-\rho_\mathrm{l}gz+\frac{1}{2}\rho_\mathrm{l}\Omega_\mathrm{l}^2\cdot r^2-\left[B^2(r)/2\mu\right]}{\gamma_\mathrm{lv}}\end{cases}\quad(8.13)$$

Later, Huh and Scriven [Huh 1969] eliminated the parameter s using the notation $\mathrm{d}z/\mathrm{d}r = \pm\tan\phi$ (with the sign convention mentioned above). Thus, Equation (8.11) was transformed into a system of two differential equations:

$$\begin{cases}\dfrac{\mathrm{d}z}{\mathrm{d}r}=\pm\tan\phi\\[2ex]\dfrac{\mathrm{d}\phi}{\mathrm{d}r}=\pm\dfrac{p_\mathrm{O}-p_\mathrm{v}-\rho_\mathrm{l}gz+\frac{1}{2}\rho_\mathrm{l}\Omega_\mathrm{l}^2\cdot r^2-\left[B^2(r)/2\mu\right]}{\gamma_\mathrm{lv}}\cdot\dfrac{1}{\cos\phi}-\dfrac{1}{r}\cdot\tan\phi.\end{cases}\quad(8.14)$$

In order to make the analytical and numerical analysis easier, a dimensionless form of the Young–Laplace equation is also used, by introducing the following dimensionless parameters with L a characteristic dimension of the problem or the capillary constant of the material (see Chapter 2):

$$\tilde{r} = \frac{r}{L}; \quad \tilde{z} = \frac{z}{L}; \quad \phi(r) \to \phi(\tilde{r}), \tag{8.15}$$

which leads to:

$$\frac{\mathrm{d}z}{\mathrm{d}r} = \frac{\mathrm{d}(\tilde{z}\cdot L)}{\mathrm{d}(\tilde{r}\cdot L)} = \frac{\mathrm{d}\tilde{z}}{\mathrm{d}\tilde{r}}, \quad \frac{\mathrm{d}^2 z}{\mathrm{d}r^2} = \frac{\mathrm{d}}{\mathrm{d}r}\left(\frac{\mathrm{d}z}{\mathrm{d}r}\right) = \frac{1}{L}\frac{\mathrm{d}}{\mathrm{d}\tilde{r}}\left(\frac{\mathrm{d}\tilde{z}}{\mathrm{d}\tilde{r}}\right) = \frac{1}{L}\frac{\mathrm{d}^2\tilde{z}}{\mathrm{d}\tilde{r}^2}.$$

Using the above dimensionless parameters, Equation (8.12) can be written as:

$$\frac{\mathrm{d}^2\tilde{z}}{\mathrm{d}\tilde{r}^2} = \pm\left[La - Bo\cdot\tilde{z} + \frac{1}{2}\left(We\cdot\tilde{r}^2 - Bo_{\mathrm{em}}\right)\right]\cdot\left[1+\left(\frac{\mathrm{d}\tilde{z}}{\mathrm{d}\tilde{r}}\right)^2\right]^{3/2} - \frac{1}{\tilde{r}}\frac{\mathrm{d}\tilde{z}}{\mathrm{d}\tilde{r}}\left[1+\left(\frac{\mathrm{d}\tilde{z}}{\mathrm{d}\tilde{r}}\right)^2\right], \tag{8.16}$$

where $Bo = \rho_{\mathrm{l}}\cdot g\cdot L^2/\gamma_{\mathrm{lv}}$ denotes the Bond number, $La = (p_{\mathrm{o}} - p_{\mathrm{v}})\cdot L/\gamma_{\mathrm{lv}}$ the Laplace number, $We = \rho_{\mathrm{l}}\Omega_{\mathrm{l}}L^3/\gamma_{\mathrm{lv}}$ the Weber number and $Bo_{\mathrm{em}} = (B^2(r)\cdot L)/(\mu\cdot\gamma_{\mathrm{lv}})$ is the electromagnetic Bond number. Because after the dimensionless analysis ϕ depends on the non-dimensional parameter $\tilde{r}$, in the following $\tilde{\phi}$ is used instead of $\phi(\tilde{r})$.

Taking into account that:

$$\begin{aligned}
&\frac{\mathrm{d}z}{\mathrm{d}r} = \pm\tan\phi \overset{\phi\to\tilde{\phi}}{\Rightarrow} \frac{\mathrm{d}\tilde{z}}{\mathrm{d}\tilde{r}} = \pm\tan\tilde{\phi}\\
&\frac{\mathrm{d}^2\tilde{z}}{\mathrm{d}\tilde{r}^2} = \frac{\mathrm{d}}{\mathrm{d}\tilde{r}}\left(\frac{\mathrm{d}\tilde{z}}{\mathrm{d}\tilde{r}}\right) = \frac{\mathrm{d}}{\mathrm{d}\tilde{r}}\left(\pm\tan\tilde{\phi}\right) = \pm\frac{1}{\cos^2\tilde{\phi}}\frac{\mathrm{d}\tilde{\phi}}{\mathrm{d}\tilde{r}} = \pm\left(1+\tan^2\tilde{\phi}\right)\frac{\mathrm{d}\tilde{\phi}}{\mathrm{d}\tilde{r}},
\end{aligned} \tag{8.17}$$

the following dimensionless form of the Young–Laplace equation is obtained:

$$\frac{\mathrm{d}\tilde{\phi}}{\mathrm{d}\tilde{r}} = \pm\left[La - Bo\cdot\tilde{z} + \frac{1}{2}\left(We\cdot\tilde{r}^2 - Bo_{\mathrm{em}}\right)\right]\cdot\frac{1}{\cos\tilde{\phi}} - \frac{1}{\tilde{r}}\tan\tilde{\phi}. \tag{8.18}$$

Therefore, Equation (8.16) is transformed into the system:

$$\begin{cases}
\dfrac{\mathrm{d}\tilde{z}}{\mathrm{d}\tilde{r}} = \pm\tan\tilde{\phi}\\
\dfrac{\mathrm{d}\tilde{\phi}}{\mathrm{d}\tilde{r}} = \pm\left[La - Bo\cdot\tilde{z} + \dfrac{1}{2}\left(We\cdot\tilde{r}^2 - Bo_{\mathrm{em}}\right)\right]\cdot\dfrac{1}{\cos\tilde{\phi}} - \dfrac{1}{\tilde{r}}\tan\tilde{\phi}.
\end{cases} \tag{8.19}$$

The mathematical models given by the systems (8.13), (8.14) or (8.19) are very useful for obtaining information concerning the meniscus behaviour (shape, monotony, attainment of the growth angle, etc.). They were successfully applied only after the development of computers powerful enough to permit the computation of menisci.

8.1.2 Initial and Boundary Conditions of the Meniscus Problem

The initial and/or boundary conditions required for solving the axisymmetric Young–Laplace equation are determined by the structural features of each specific configuration and will be analysed in the following sections for EFG, Cz, and dewetted Bridgman crystal growth techniques. In this section, common features corresponding to typical boundary conditions of the capillary problem are discussed: the *catching* and *wetting boundary conditions*.

The *catching boundary condition* is specific for materials that are wetted by the melt. It is used when one meniscus end is partially fixed, e.g. for the EFG technique the counter line of the meniscus surface is fixed by the internal or external edge counter (see Chapter 2, Figure 2.4b, d, j, k or Figure 2.4e, f). This condition can be expressed as:

$$z|_{r=r_0} = \text{const.},$$

where r_0 represents the radial coordinate of the point situated at the meniscus end, and the value of the constant depends on the position of the horizontal axis of the (rOz) frame, i.e. this constant is set to zero if the meniscus end is on the Or axis, or is equal to the distance between the horizontal axis Or and its parallel which passes through the meniscus end (see Chapter 2, section 2.6.1.1).

The *wetting boundary condition* is also known as the *angle of fixation boundary condition* because it expresses the angle made between the tangent to the meniscus at its endpoint situated at the base, and the tangent to the shaper or crucible wall (see also Chapter 2, section 2.6.1.2). For the axisymmetric Young–Laplace equation written for the configurations presented in Figure 2.4a, c, g, h, i (see Chapter 2) or Figure 8.18 (see dewetted Bridgman technique), the wetting boundary condition can be expressed as follows:

$$\left.\frac{\mathrm{d}z}{\mathrm{d}r}\right|_{r=r_0} = \tan\left(\theta - \frac{\pi}{2}\right)$$

where θ represents the wetting angle (see Chapter 1, and Figures 8.4 and 8.18).

From the physical point of view, the catching and wetting conditions cannot be applied simultaneously at the same point $r = r_0$. However, for certain configurations, it is useful from the mathematical point of view to perform calculations with a given angle applied at the catching condition point. Then the angle is varied in order to find a physically acceptable solution to the problem. In such cases, the systems (8.13), (8.14) or (8.19) have two initial conditions. Thus, an initial value problem is obtained and its unique solution represents the meniscus surface $z = z(r)$. The existence and uniqueness of the meniscus is assured on the basis of the Cauchy theorem, because functions from the right-hand terms of the system (8.13), (8.14) or (8.19) are real analytically. The meniscus can be computed numerically using Runge–Kutta method (see Appendix to this chapter in which the procedure for the fourth–order Runge–Kutta method is presented).

After the meniscus shape is obtained, the *growth angle criterion* should be imposed. It asserts that the crystal is obtained when the *growth angle* α is attained at the place where the meniscus contacts the crystal (see Chapter 1, section 1.3). This condition is expressed as

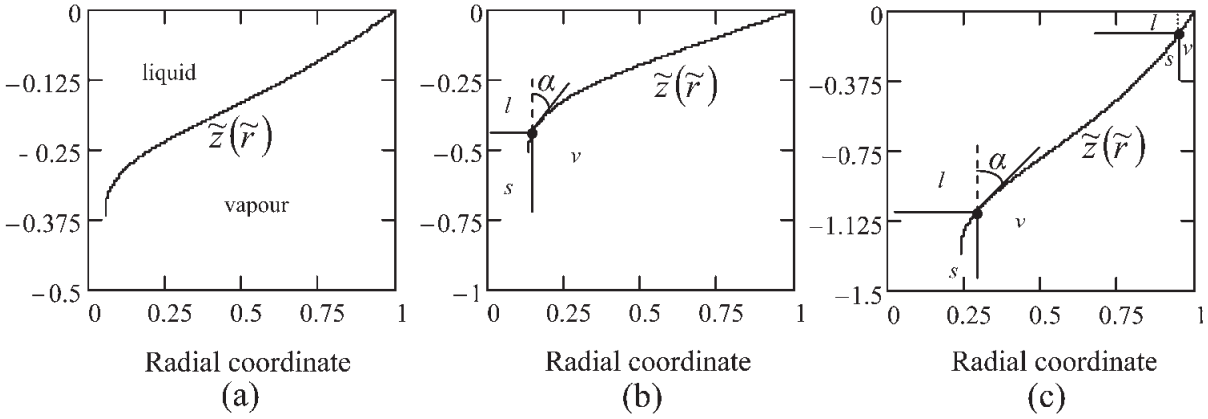

Figure 8.2 *Numerical meniscus shape and attainment of the growth angle for InSb (*Bo = *3.84,* α = *25°): (a)* La = *0.105: the growth angle cannot be achieved; (b)* La = *0.262: the growth angle is achieved once; (c)* La = *0.393: the growth angle is achieved twice.*

$$\phi|_{r=r_c} = \frac{\pi}{2} - \alpha,$$

where r_c represents the crystal radius.

Even if the IVP of the Young–Laplace equation has a unique solution, it is nevertheless possible that this solution does not satisfy the condition for attainment of the growth angle. If this condition is satisfied then a crystal having a radius r_c can be obtained (Figure 8.2); otherwise, a crystal cannot be obtained.

The attainment of the growth angle is exemplified in Figure 8.2. More precisely, in the configuration shown in Figure 8.2a, there is no place along the meniscus where the angle is equal to α, so it is impossible to grow a crystal under conditions giving this meniscus. In Figure 8.2b, it is possible to grow a crystal from this meniscus. In Figure 8.2c, the growth angle can be achieved twice on the meniscus. This means that, under the same capillary conditions, it is possible to grow crystals with two different diameters. The choice is realized by heating or cooling the system in order to fix the height of the solid–liquid interface.

As already explained in Chapter 2, in some configurations, the wetting boundary condition does not exist (or it does so at infinity and hence cannot be used in numerical solutions; see section 8.2). In these cases, to solve the Young–Laplace equation, the growth angle should represent one boundary condition, and the second condition should be expressed using the meniscus height, which is unknown. These kinds of problems are very difficult from a mathematical and numerical point of view, so they should be treated separately, e.g. see section 8.2.

8.1.3 Approximate Solutions of the Axisymmetric Meniscus Problem

Some authors have proposed *simple approximations* of the axisymmetric Young–Laplace equation used especially for unbounded extent (i.e. Ω is an unbounded axisymmetric domain), when numerical solution of the BVP is very difficult [Huh 1969]. For example, in 1960 Nutt neglected the second curvature:

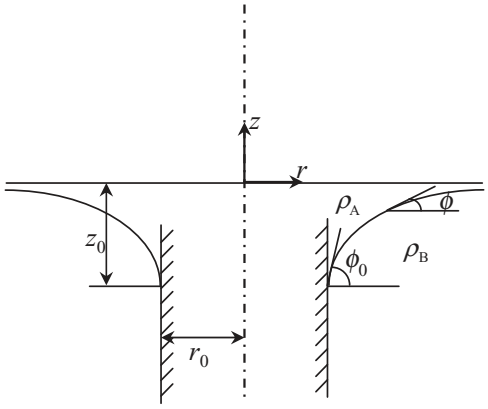

Figure 8.3 *The meniscus for a vertical circular cylinder positioned in a fluid (Reprinted with permission from [Huh 1969], copyright (1969) Elsevier Ltd).*

$$\frac{1}{R_2} = \frac{\frac{1}{r}\cdot\frac{\mathrm{d}z}{\mathrm{d}r}}{\left[1+\left(\frac{\mathrm{d}z}{\mathrm{d}r}\right)^2\right]^{1/2}}$$

from Equation (8.11) [Nutt 1960], leading an analytical expression for the meniscus. More precisely, for the configuration presented in Figure 8.3, the Equation (8.11) is reduced to

$$\frac{\frac{\mathrm{d}^2 z}{\mathrm{d}r^2}}{\left[1+\left(\frac{\mathrm{d}z}{\mathrm{d}r}\right)^2\right]^{3/2}} = \frac{(\rho_B-\rho_A)gz}{\gamma_{lv}}$$

which is equivalent to:

$$\frac{\mathrm{d}\phi}{\mathrm{d}r} = \frac{(\rho_B-\rho_A)gz}{\gamma_{lv}}\cdot\frac{1}{\cos\phi}$$

where $\mathrm{d}z/\mathrm{d}r = +\tan\phi$ (the positive sign is due to the configuration). This equation can be integrated between r_0 and r (here $r>r_0$, see Figure 8.3), and the meniscus z can be expressed as a function of ϕ:

$$z(\phi) = -2\sqrt{\frac{\gamma_{lv}}{(\rho_B-\rho_A)g}}\cdot\sin\left(\frac{\phi}{2}\right).$$

Another approximation was reported by Tsivinski [Tsivinski 1962]. He considered both curvatures but expanded the curvature $1/R_2$ in a Taylor series, considering only the first two terms from the Taylor series:

$$\frac{1}{R_2} = \frac{1}{R_2}(h) + (z-h)\cdot\frac{\mathrm{d}}{\mathrm{d}z}\left(\frac{1}{R_2}\right)\Bigg|_{z=h},$$

where h represents the meniscus height. Using this approximation, Tsivinski obtained an analytical formula for the meniscus height as function of the crystal radius r_c and the growth angle α (for more details, see section 8.2):

$$h_T(r_c) = -\left(\frac{\cos\alpha}{2r_c}\right)\cdot\frac{\gamma_{lv}}{\rho_l g} + \sqrt{\left(\frac{\cos\alpha}{2r_c}\right)^2\cdot\frac{\gamma^2}{\rho_l^2 g^2} - \frac{2\gamma}{\rho_l g}\cdot(\sin\alpha - 1)}.$$

This formula has been intensively cited and used for finding the analytical formulas of the meniscus. For example, Hurle obtained:

$$r(z) = r_c + \sqrt{\frac{2}{A} - h^2} - \sqrt{\frac{2}{A} - z^2} - \frac{1}{\sqrt{2A}}\cdot\ln\left|\frac{z}{h}\cdot\frac{\sqrt{2} + \sqrt{2 - A\cdot h^2}}{\sqrt{2} + \sqrt{2 - A\cdot z^2}}\right|,$$

where

$$A = \frac{1}{2}\left(\frac{\sin\left(\frac{\pi}{2} - \alpha\right)}{r_c\cdot h} + \frac{\rho_l g}{\gamma_{lv}}\right).$$

(see details in section 8.1) [Hurle 1983].

Other approximations of the axisymmetric Young–Laplace equation are based on Bessel functions [Boucher 1980, Ferguson 1912]. Boucher obtained a most useful mathematical approximation involving zero- and first-order modified Bessel functions:

$$z = \sqrt{1 + \cos\phi}\cdot\frac{K_0\left(r\sqrt{2}\right)}{K_1\left(r\sqrt{2}\right)}, \tag{8.20}$$

where

$$\frac{K_0\left(r\sqrt{2}\right)}{K_1\left(r\sqrt{2}\right)} \approx \frac{1}{\sqrt{1 + 1/\left(r\sqrt{2}\right)}}$$

Equation (8.20) can be used to give $z = z(r)$ at constant ϕ, or $z = z(\phi)$ at constant r.

Comparisons between these analytical formulas [Hurle 1983] and the computed menisci reported by Huh and Scriven [Huh 1969] showed that the explicit approximations of the meniscus are adequate for the range of values of crystal radius and contact angle encountered in crystal growth.

The most recent approximation was given by Hernandez-Baltazar [Hernandez-Baltazar 2005] who solved the Young–Laplace equation with an elliptic representation, i.e. the principal curvatures

$$\frac{1}{R_1} = \frac{\frac{d^2z}{dr^2}}{\left[1 + \left(\frac{dz}{dr}\right)^2\right]^{3/2}}, \quad \frac{1}{R_2} = \frac{\frac{1}{r}\cdot\frac{dz}{dr}}{\left[1 + \left(\frac{dz}{dr}\right)^2\right]^{\frac{1}{2}}}$$

were approximated by

$$\frac{1}{R_1} = \frac{a^4 b^4}{\left[a^4 z^2 + b^4 r^2\right]^{3/2}} \quad \text{and} \quad \frac{1}{R_2} = \frac{b^2}{\left[a^4 z^2 + b^4 r^2\right]^{3/2}},$$

assuming that the meniscus profile is very close to an elliptic profile with *a, b* representing the length of the semimajor (one half of the longest axis of the ellipse) and semiminor (one half of the shortest axis) axes of the ellipse centred at the origin. The elliptical analytical solution proposed by these authors is dependent on the parameter *a* in square form and its predictive capacity depends on a cubic expression. The parameters *a* and *b* are obtained from solving the Young–Laplace equation with the elliptical equation:

$$\frac{a}{b} + \frac{a^3}{b^3} = 2 + \beta^* \cdot a^2, \quad \text{where} \quad \beta^* = \frac{(\rho_B - \rho_A) \cdot g}{\gamma_{lv}}.$$

When the results of the analytical solution and the literature data for different profiles are compared, a correlation with acceptable error in the fifth digit is obtained. This means that that the error in the parameter β^*, after applying the differential expression, would be less than 0.1%.

8.2 Analytical and Numerical Solutions for the Meniscus Equation in the Cz Method

For the Cz growth method (see Figure 8.4), the axisymmetric meniscus is given by the Young–Laplace equation (8.12). In the Cz process, the meniscus height *h* is controlled by heat transfer and the problem is to find the relation between the crystal radius and the meniscus height.

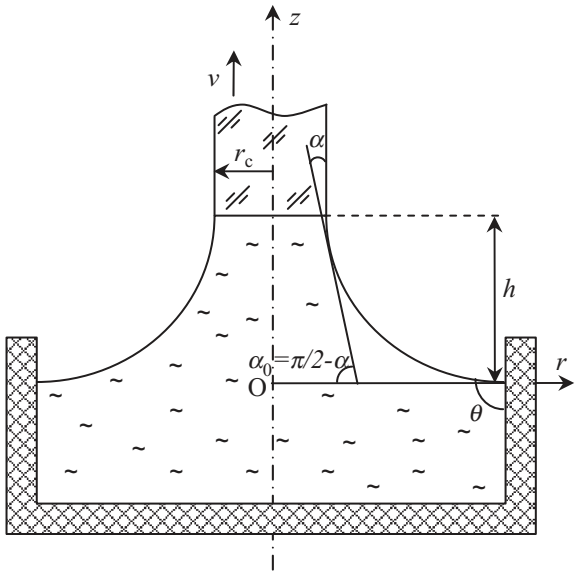

Figure 8.4 *Axisymmetric model for a cylindrical crystal grown by the Cz method.*

The pressure due to rotation in Cz is only a few pascals and is commonly neglected. If the growth process takes place without a magnetic field, Equation (8.12) becomes:

$$\frac{\mathrm{d}^2 z}{\mathrm{d}r^2} = -\frac{(p_\mathrm{O} - p_\mathrm{v}) - \rho_\mathrm{l} g z}{\gamma_\mathrm{lv}} \cdot \left[1 + \left(\frac{\mathrm{d}z}{\mathrm{d}r}\right)^2\right]^{3/2} - \frac{1}{r} \cdot \frac{\mathrm{d}z}{\mathrm{d}r} \cdot \left[1 + \left(\frac{\mathrm{d}z}{\mathrm{d}r}\right)^2\right]. \tag{8.21}$$

The solution $z = z(r)$ of Equation (8.21) has to satisfy the following boundary conditions:

$$z(r_\mathrm{c}) = h, \quad \frac{\mathrm{d}z}{\mathrm{d}r}(r_\mathrm{c}) = -tg\alpha_0; \quad \alpha_0 \in (0, \pi/2), \tag{8.22}$$

where $r_\mathrm{c} > 0$ is the crystal radius, $\alpha_0 = \pi/2 - \alpha$ where α is the growth angle, h is the meniscus height (an unknown in the problem if a crystal with given r_c is to be pulled). Moreover, if the meniscus extends untouched far enough outwards its equilibrium shape becomes effectively flat at some distance from the crystal. The meniscus may then, for all intents and purposes, be regarded as unbounded, i.e. as extending to infinity [Huh 1969]:

$$z|_{r\to\infty} = 0. \tag{8.23}$$

From this peculiarity (no curvature of the meniscus at $r \to \infty$) it follows that the pressure in the melt at $z = 0$ is equal to the vapour pressure $p_\mathrm{O} = p_\mathrm{v}$.

Because of (8.23), it is very difficult to find a numerical method for solving the meniscus surface equation, (8.21). To avoid this inconvenience, many authors have tried to find sufficiently accurate analytical approximations to the real meniscus profile. The most often cited results are those reported by Tsivinski [Tsivinski 1962] which derived an analytical expression for the meniscus height (i.e. the unknown h from the boundary condition (8.22)), in a Czochralski configuration using a particular form of the meniscus equation (8.11):

$$-\frac{\dfrac{\mathrm{d}^2 z}{\mathrm{d}r^2}}{\left[1 + \left(\dfrac{\mathrm{d}z}{\mathrm{d}r}\right)^2\right]^{3/2}} - \frac{\dfrac{1}{r} \cdot \dfrac{\mathrm{d}z}{\mathrm{d}r}}{\left[1 + \left(\dfrac{\mathrm{d}z}{\mathrm{d}r}\right)^2\right]^{1/2}} = \frac{\rho_\mathrm{l} g z}{\gamma_\mathrm{lv}}, \tag{8.24}$$

where

$$\frac{\dfrac{\mathrm{d}^2 z}{\mathrm{d}r^2}}{\left[1 + \left(\dfrac{\mathrm{d}z}{\mathrm{d}r}\right)^2\right]^{3/2}} = \frac{1}{R_1} \quad \text{and} \quad \frac{\dfrac{1}{r} \cdot \dfrac{\mathrm{d}z}{\mathrm{d}r}}{\left[1 + \left(\dfrac{\mathrm{d}z}{\mathrm{d}r}\right)^2\right]^{1/2}} = \frac{1}{R_2}$$

represent principal curvatures. Tsivinski considered both curvatures but he expanded the curvature $1/R_2$ in a Taylor series at the point h, as follows:

$$\frac{1}{R_2} = \frac{1}{R_2}(h) + (z - h) \cdot \frac{\mathrm{d}}{\mathrm{d}z}\left(\frac{1}{R_2}\right)\bigg|_{z=h}. \tag{8.25}$$

Using $1/R_2 = (\sin\phi)/r$, where ϕ is the angle between the tangent to the meniscus (at an arbitrary point) and the horizontal axis, the terms $(1/R_2)\,(h)$ and $(\mathrm{d}/\mathrm{d}z)\,(1/R_2)\big|_{z\,=\,h}$ from the above representation are obtained as function of the growth angle α and the crystal radius r_c:

$$\frac{1}{R_2}(h) = \frac{\sin\phi(h)}{r_c} = \frac{\sin\left(\frac{1}{2}\pi - \alpha\right)}{r_c} = \frac{\sin\alpha_0}{r_c},$$

$$\frac{\mathrm{d}}{\mathrm{d}z}\left(\frac{1}{R_2}\right)\Big|_{z=h} \cong \frac{(1/R_2)(h) - (1/R_2)(0)}{h} = \frac{(\sin\phi(h))/r_c - 0}{h} = \frac{\sin\left(\frac{1}{2}\pi - \alpha\right)}{r_c \cdot h}.$$

After computations, the following formula for the curvature $1/R_2$ is obtained:

$$\frac{1}{R_2} = \frac{\sin\left(\frac{1}{2}\pi - \alpha\right)}{r_c} \cdot \frac{z}{h}. \tag{8.26}$$

Thus, the meniscus equation (8.24) becomes

$$-\frac{z''}{\left[1 + z'^2\right]^{3/2}} - \frac{\sin\left(\frac{1}{2}\pi - \alpha\right)}{r_c} \cdot \frac{z}{h} = \frac{\rho_l g z}{\gamma_{lv}}, \tag{8.27}$$

where $z' = \mathrm{d}z/\mathrm{d}r$ and $z'' = \mathrm{d}^2z/\mathrm{d}r^2$. Multiplying this equation by z', and integrating between 0 and z gives:

$$-\frac{1}{\sqrt{1+z'^2}} - \frac{\sin\left(\frac{1}{2}\pi - \alpha\right)}{r_c \cdot h} \cdot \frac{z^2}{2} - \frac{\rho_l g}{\gamma_{lv}} \cdot \frac{z^2}{2} + \left(\frac{1}{\sqrt{1+z'^2}}\right)\Big|_{z=0} = 0. \tag{8.28}$$

Because $1\Big/\sqrt{1+z'^2} = \cos\phi(r)$, it follows that:

$$-\cos\phi(r) - \frac{\sin\left(\frac{1}{2}\pi - \alpha\right)}{r_c \cdot h} \cdot \frac{z^2}{2} - \frac{\rho_l g}{\gamma_{lv}} \cdot \frac{z^2}{2} + 1 = 0. \tag{8.29}$$

For $z = h$, $\phi(h) = \frac{1}{2}\pi - \alpha = \alpha_0$, and hence Equation (8.29) will represent an equation of the second degree for the meniscus height h:

$$\frac{\rho_l g}{\gamma_{lv}} \cdot \frac{h^2}{2} + \frac{\sin\alpha_0}{2r_c} \cdot h - (1 - \cos\alpha_0) = 0. \tag{8.30}$$

Solving this equation, the following analytical approximations on the meniscus height [Tsivinski 1962] is obtained:

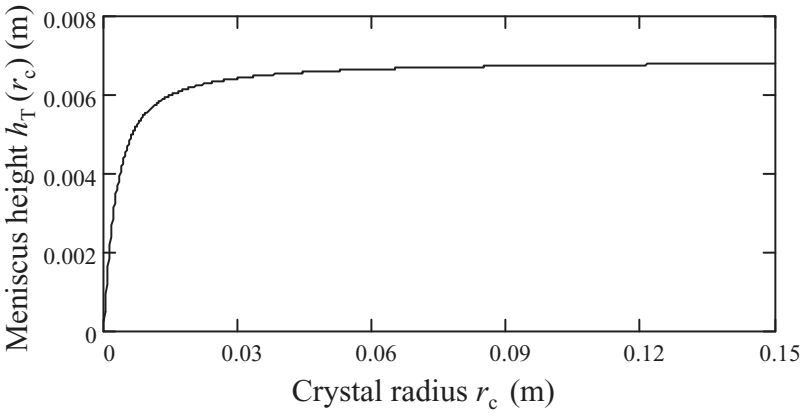

Figure 8.5 *Meniscus height profile* h_T *as a function of the cylindrical silicon crystal radius* r_c.

$$h_{1,2} = -\left(\frac{\sin\alpha_0}{2r_c}\right)\cdot\frac{\gamma_{lv}}{\rho_l g} \pm \sqrt{\left(\frac{\sin\alpha_0}{2r_c}\right)^2\cdot\frac{\gamma_{lv}^2}{\rho_l^2 g^2} + \frac{2\gamma_{lv}}{\rho_l g}\cdot(1-\cos\alpha_0)}. \tag{8.31}$$

It is easy to see that $h_{1,2}$ can be positive or negative, but for physical reasons only the positive meniscus will be considered:

$$h = -\left(\frac{\sin\alpha_0}{2r_c}\right)\cdot\frac{\gamma_{lv}}{\rho_l g} + \sqrt{\left(\frac{\sin\alpha_0}{2r_c}\right)^2\cdot\frac{\gamma_{lv}^2}{\rho_l^2 g^2} + \frac{2\gamma_{lv}}{\rho_l g}\cdot(1-\cos\alpha_0)}. \tag{8.32}$$

where α is the growth angle. This is equivalent to:

$$h_T(r_c) = -\left(\frac{\cos\alpha}{2r_c}\right)\cdot\frac{\gamma_{lv}}{\rho_l g} + \sqrt{\left(\frac{\cos\alpha}{2r_c}\right)^2\cdot\frac{\gamma_{lv}^2}{\rho_l^2 g^2} + \frac{2\gamma_{lv}}{\rho_l g}\cdot(1-\sin\alpha)} \tag{8.33}$$

which is used to estimate the meniscus height in diameter control techniques ([Bardsley 1974–2, Bardsley 1977, Dijk 1974, Johansen 1992]) (Figure 8.5), or for comparison with other analytic approximations [Bardsley 1974–1, Hurle 1981, Hurle 1983, Johansen 1987, Johansen 1992, Mika 1975, Tatartchenko 1993].

An analytical approximation of the meniscus profile can be obtained only for some particular cases. For example, Hurle considered a reduced form of Equation (8.28):

$$\frac{1}{\sqrt{1+z'^2}} + \left(\frac{\sin\left(\frac{1}{2}\pi-\alpha\right)}{r_c\cdot h} + \frac{\rho_l g}{\gamma_{lv}}\right)\cdot\frac{z^2}{2} - 1 = 0. \tag{8.34}$$

Writing the equation in the form:

$$\frac{1}{\sqrt{1+z'^2}} = 1 - A\cdot z^2,$$

where

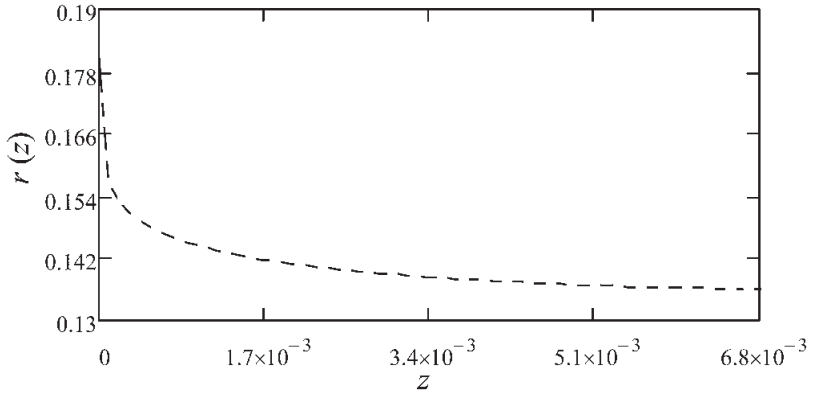

Figure 8.6 *Meniscus profile* $r_T(z)$ *vs* z.

$$A = \frac{1}{2}\left(\frac{\sin\left(\frac{1}{2}\pi - \alpha\right)}{r_c \cdot h} + \frac{\rho_l g}{\gamma_{lv}} \right), \tag{8.35}$$

the following ordinary differential equation is obtained:

$$\frac{1 - A \cdot z^2}{\sqrt{1 - \left(1 - A \cdot z^2\right)^2}} \mathrm{d}z = \mathrm{d}r.$$

After integrating between h and z, using $r(h) = r_c$, the following explicit analytical formula $r_T(z)$ for the meniscus is obtained:

$$r_T(z) = r_c + \sqrt{\frac{2}{A} - h^2} - \sqrt{\frac{2}{A} - z^2} - \frac{1}{\sqrt{2A}} \cdot \ln\left| \frac{z}{h} \cdot \frac{\sqrt{2} + \sqrt{2 - A \cdot h^2}}{\sqrt{2} + \sqrt{2 - A \cdot z^2}} \right|. \tag{8.36}$$

Replacing A and h by (8.35) and (8.33) respectively, the meniscus profile for a cylindrical silicon crystal of radius $r_c = 0.136\,\mathrm{m}$ is shown in Figure 8.6.

The second analytical expression for the meniscus height reported in the literature is based on Bessel functions (see section 8.1.3) [Hurle 1983, Johansen 1992, Johansen 1994]:

$$h_{B\cdot}(r_c) = \sqrt{\frac{2\gamma_{lv}}{\rho_l g}} \cdot \sqrt{\frac{1 - \cos\left(\frac{1}{2}\pi - \alpha\right)}{1 + (1/r_c) \cdot \sqrt{\gamma_{lv}/(\rho_l g)}}}, \tag{8.37}$$

equivalent to

$$h_B(r_c) = \sqrt{\frac{2\gamma_{lv}}{\rho_l g}} \cdot \sqrt{\frac{1 - \sin\alpha}{1 + (1/r_c) \cdot \sqrt{\gamma_{lv}/(\rho_l g)}}}. \tag{8.37'}$$

Details of Bessel functions and how they are used to obtain Equation (8.34) will be given later, when a new analytical-numerical solution for computing the meniscus surface will be proposed.

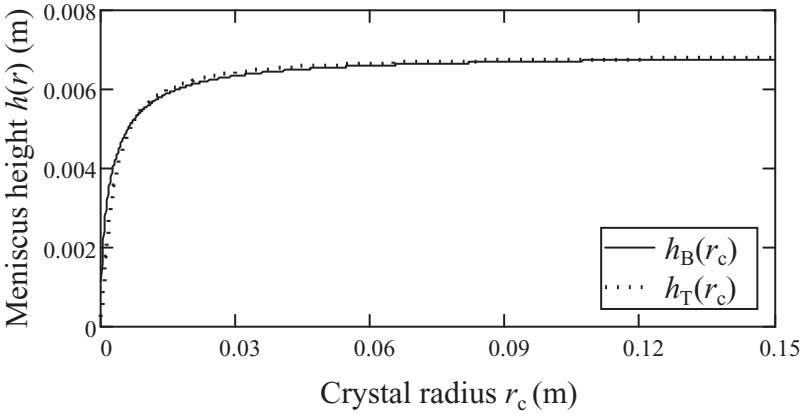

Figure 8.7 *Meniscus heights* h_T *(8.33) and* h_B *(8.37) as function of the crystal radius* r_c.

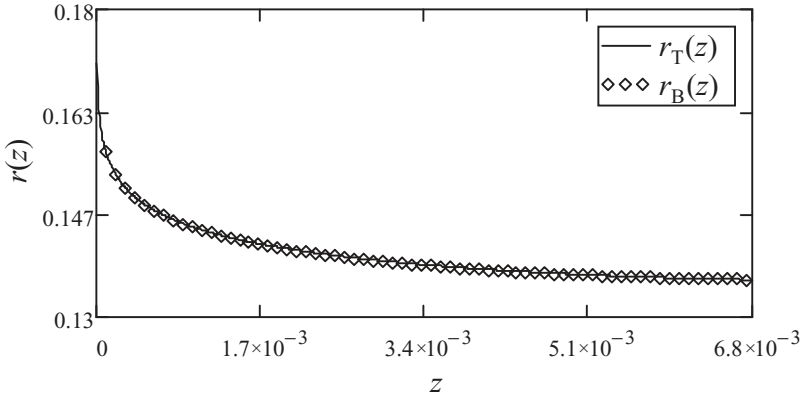

Figure 8.8 *Meniscus profiles* r_T *(8.36) and* r_B *(8.38) vs* z.

A comparison between Equations (8.33) and (8.37) can be seen in Figure 8.7. The figure shows accurate analytical approximations of the meniscus height as a function of the crystal radius. For small crystal radius the error is of the order 10^{-4}, but for large crystal radius, as in Cz crystal growth, the approximation is very good, which is why both formulas have been used by crystal growers. Moreover, for the second of the meniscus height formula $h_B(r_c)$ a similar analytical formula for the meniscus $r_B(z)$ can be found [Hurle 1983]:

$$r_B(z) = \frac{1}{2}\sqrt{\frac{\gamma_{lv}}{\rho_l g}} \cdot \left(P(z) + \sqrt{P^2(z) + \frac{\frac{3}{4}(\rho_l g/\gamma_{lv})^2 \cdot z^2 - 2}{\sqrt{1+(1/r_c)\cdot(\rho_l g/\gamma_{lv})}}} \right) \tag{8.38}$$

where $P(z)$ is given by

$$P(z) = r_c\sqrt{\frac{\rho_l g}{\gamma_{lv}}} + \frac{1}{\sqrt{1+(1/r_c)\cdot(\gamma_{lv}/(\rho_l g))}} \cdot \left(\frac{1}{2r_c}\cdot\sqrt{\frac{\gamma_{lv}}{\rho_l g}} - \ln\left(\frac{z}{h_B(z)}\right) - \frac{3}{16}\left(1+\frac{1}{r_c}\cdot\frac{\gamma_{lv}}{\rho_l g}\right)\cdot\left(\frac{\rho_l g}{\gamma_{lv}}\right)\cdot h_B^2(z) + \frac{3}{16}\cdot\frac{\rho_l g}{\gamma_{lv}}\cdot z^2 \right)$$

The comparison between Equations (8.36) and (8.38) can be seen in Figure 8.8.

Computations show that for the considered cylindrical silicon crystal of radius $r_c = 0.136\,\text{m}$, the errors between these two analytical formulas are of the order 10^{-5}.

The reason why researchers used the above approximations is that it is difficult to obtain a numerical solution because of the condition (8.23). In order to avoid this difficulty, Mika and Uelhoff [Mika 1975] proposed an analytical-numerical solution. More precisely, part of the solution for $r \to \infty$ (called asymptotic part of the solution) can be derived analytically, i.e. for $r \in [r^*; \infty)$, and the remaining part can be solved numerically using Runge–Kutta method on the finite range $r \in (0; r^*]$. The problem is to find the accurate range on which this analytical solution is available, and after that to find initial conditions for computing the numerical solution.

In the following, the asymptotic part of the solution, $r \in [r^*; \infty)$, obtained using modified Bessel functions [Mika 1975] is presented. For the second part of the solution, $r \in (0; r^*]$, mathematical tools for finding initial conditions in order to solve the IVP numerically are used.

The asymptotic solution can be obtained starting from Equation (8.21), in which $(\mathrm{d}z/\mathrm{d}r)^2$ is neglected because $\mathrm{d}z/\mathrm{d}r << 1$ at a large enough distance from the crystal, and $p_O = p_v$:

$$\frac{\mathrm{d}^2 z}{\mathrm{d}r^2} = \frac{\rho_l g z}{\gamma_{lv}} - \frac{1}{r} \cdot \frac{\mathrm{d}z}{\mathrm{d}r}, \tag{8.39}$$

which can be rewritten in the form

$$r^2 \cdot \frac{\mathrm{d}^2 z}{\mathrm{d}r^2} + r \cdot \frac{\mathrm{d}z}{\mathrm{d}r} - r^2 \cdot \frac{\rho_l g}{\gamma_{lv}} \cdot z = 0. \tag{8.40}$$

In order to write this as a standard Bessel equation, $z(r)$ is transformed to $y(x)$ with: $r = x \cdot \sqrt{\gamma_{lv}/(\rho_l g)}$ and $z = y \cdot \sqrt{\gamma_{lv}/(\rho_l g)}$. Thus, Equation (8.40) becomes:

$$x^2 \cdot \frac{\mathrm{d}^2 y}{\mathrm{d}x^2} + x \cdot \frac{\mathrm{d}y}{\mathrm{d}x} - x^2 \cdot y = 0 \tag{8.41}$$

Equation (8.41) is called a homogeneous modified Bessel differential equation, being of the type:

$$x^2 \cdot y'' + x \cdot y' - \left(x^2 + n^2\right) \cdot y = 0, \tag{8.42}$$

with $n = 0$. From the theory of Bessel functions, it is known that the general solution is a linear combination between modified Bessel functions of the first and second order, respectively: $y(x) = C_1 \cdot I_n(x) + C_2 \cdot K_n(x)$, where C_1 and C_2 are constants which should be determined. The general solution of Equation (8.41) is:

$$y(x) = C_1 \cdot I_0(x) + C_2 \cdot K_0(x), \tag{8.43}$$

because $n = 0$. Moreover, it is known that for $x >> n$ (this is available in Cz growth because for the asymptotic solution $r \in [r^*; \infty)$, and hence $r >> 0$), the modified Bessel

functions become: $I_n(x) \approx e^x / \sqrt{2\pi x}$ and $K_n(x) \approx e^{-x} / \sqrt{2\pi x}$. Thus, the general solution (8.43) is

$$y(x) = C_1 \cdot \frac{e^x}{\sqrt{2\pi x}} + C_2 \cdot \frac{e^{-x}}{\sqrt{2\pi x}}. \tag{8.44}$$

Returning to the problem in $z(r)$, the following general solution for the asymptotic part of meniscus shape is obtained:

$$z(r) = \sqrt{\frac{\gamma_{lv}}{\rho_l g}} \cdot \left(C_1 \cdot \frac{\exp\left\{ r \cdot \sqrt{\frac{\rho_l g}{\gamma_{lv}}} \right\}}{\sqrt{2\pi r \sqrt{\frac{\rho_l g}{\gamma_{lv}}}}} + C_2 \cdot \frac{\exp\left\{ -r \sqrt{\frac{\rho_l g}{\gamma_{lv}}} \right\}}{\sqrt{2\pi r \sqrt{\frac{\rho_l g}{\gamma_{lv}}}}} \right). \tag{8.45}$$

The first modified Bessel function $I_0(r) = J_0(ir)$ is complex, but only the real part of the solution (8.45) is considered:

$$z(r) = \sqrt{\frac{\gamma_{lv}}{\rho_l g}} \cdot \left(C_2 \cdot \frac{\exp\left\{ -r \sqrt{\frac{\rho_l g}{\gamma_{lv}}} \right\}}{\sqrt{2\pi r \sqrt{\frac{\rho_l g}{\gamma_{lv}}}}} \right), \tag{8.46}$$

which is equivalent to $y(x) = C_2 \cdot K_0(x)$, according to [Mika 1975].

The solution (8.46) satisfies the boundary condition (8.23):

$$z|_{r \to \infty} = 0.$$

In order to find the unique solution, the constant C_2 must be computed. For that, the continuity condition of the first derivative at the connection point r^* is imposed, i.e. the continuity of the first derivatives for asymptotic analytical and numerical solutions at r^*, $dz/dr|_{r = r^*} = -\tan\phi\,(r^*)$. Thus, deriving the asymptotic analytical solution $z(r)$ given by (8.46) and equating that with the corresponding derivative available for the numerical solution ($-\tan\phi\,(r^*)$), gives:

$$z(r) = \sqrt{\frac{\gamma_{lv}}{\rho_l g}} \cdot \frac{K_0\left(r \sqrt{\frac{\rho_l g}{\gamma_{lv}}} \right)}{K_1\left(r^* \sqrt{\frac{\rho_l g}{\gamma_{lv}}} \right)} \cdot \tan\phi(r^*). \tag{8.47}$$

Here the derivative property of the modified Bessel function: $(d/dx)\,(K_0(x)) = -K_1(x)$ is used. Moreover, in this computation the previously used approximation:

$$\frac{K_0(r)}{K_1(r)} \approx \frac{1}{\sqrt{1 + (1/r)}}, \tag{8.48}$$

was considered. If $r = r^* = r_c$ in (8.47), and using the approximation (8.48), then the formula of the meniscus height given by (8.37) is obtained. Nowadays, it is not necessary to use approximation (8.48) because modern computers can compute modified Bessel functions; this makes it possible to compute the initial conditions:

$$z(r^*) = h^*, \quad \frac{\mathrm{d}z}{\mathrm{d}r}(r^*) = -\tan\phi(r^*), \tag{8.49}$$

necessary for solving numerically the nonlinear system of differential equations corresponding to Equation (8.21):

$$\begin{cases} \dfrac{\mathrm{d}z}{\mathrm{d}r} = -\tan\phi \\ \dfrac{\mathrm{d}\phi}{\mathrm{d}r} = -\dfrac{\rho_l \cdot g}{\gamma_{lv}} \cdot \dfrac{z}{\cos\phi} - \dfrac{1}{r} \cdot \tan\phi. \end{cases} \tag{8.50}$$

In what follows, the meniscus will be computed, using the analytical-numerical solution described above, for a cylindrical silicon crystal grown by the Cz technique.

First, it is necessary to find the region for which the asymptotic analytical solution is accurate. Using the material parameters of silicon and computing the modified Bessel functions

$$K_0\left(r\sqrt{\frac{\rho_l g}{\gamma_{lv}}}\right), \quad K_1\left(r\sqrt{\frac{\rho_l g}{\gamma_{lv}}}\right) \quad \text{for} \quad r \in (0;\infty),$$

it follows that their ratio increases to 1 for $r \leq 3.7$ m, and after that the modified Bessel functions exponentially decay to zero, i.e. for $x >> n$,

$$K_n(x) \approx \frac{\mathrm{e}^{-x}}{\sqrt{(2/\pi)\cdot x}};$$

in our case $n = 0$ or 1, and x represents $r\sqrt{\rho_l g/\gamma_{lv}}$. This shows that a crucible radius 0.25 ≤ 3.7 m and a value for r^* which is not far from the crucible radius, e.g. $r^* = 0.19$ m, should be considered, in order to have an almost flat meniscus. Hence, we set $r^* = 0.19$ m and then find h^*, i.e. the corresponding meniscus height, and $-\tan\phi\,(r^*)$, necessary for conditions (8.49).

Replacing $r = r^* = 0.19$ m in Equations (8.47) and (8.33) the following system is obtained:

$$\begin{cases} h^* = \sqrt{\dfrac{\gamma_{lv}}{\rho_l g}} \cdot \dfrac{K_0\left(r^*\sqrt{\dfrac{\rho_l g}{\gamma_{lv}}}\right)}{K_1\left(r^*\sqrt{\dfrac{\rho_l g}{\gamma_{lv}}}\right)} \cdot \tan\phi(r^*) \\ h^* = -\left(\dfrac{\sin\phi(r^*)}{2r^*}\right) \cdot \dfrac{\gamma_{lv}}{\rho_l g} + \sqrt{\left(\dfrac{\sin\phi(r^*)}{2r^*}\right)^2 \cdot \dfrac{\gamma_{lv}^2}{\rho_l^2 g^2} - \dfrac{2\gamma_{lv}}{\rho_l g} \cdot (\cos\phi(r^*) - 1)}. \end{cases} \tag{8.51}$$

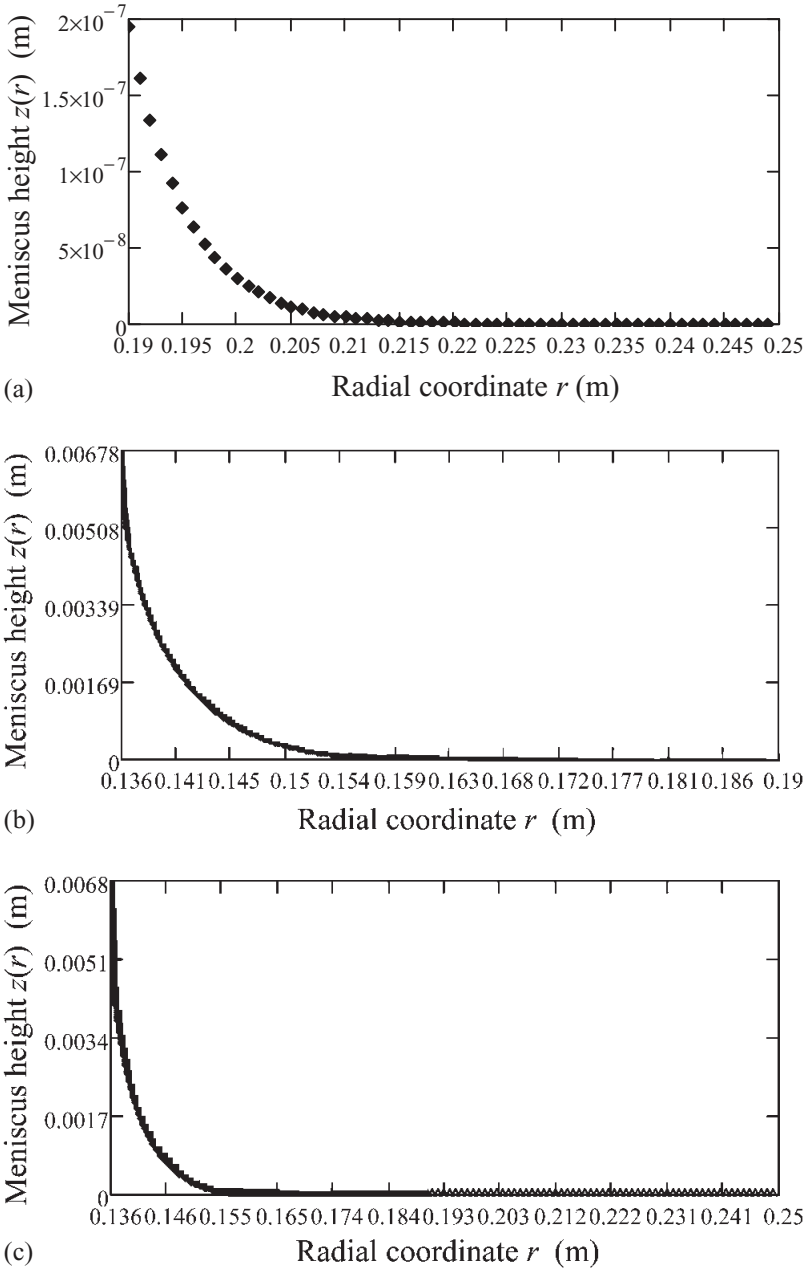

Figure 8.9 *(a) Meniscus given by the asymptotic analytical solution on the interval [0.19; 0.25]. (b) Computed meniscus obtained by numerical solution of the initial value problem on the interval [0; 0.19]. (c) The analytical-numerical meniscus for a cylindrical silicon crystal grown in a crucible of radius 0.25 m.*

In solving this system we considered those values of $\phi\,(r^*)$ that belong to the interval $(0, \frac{1}{2}\pi)$. For the above values, only one value is in the required interval: $\phi\,(r^*) = 7.2\,\text{s}$. Replacing this in first or second equation gives $h^* = 0.2\,\mu\text{m}$. In this way the initial condition is computed, which permits to find the numerical solution. The asymptotic analytical approximation of the meniscus is obtained by plotting function given by (8.47), as can be seen in Figure 8.9a. The numerical solution of the meniscus is obtained solving the system (8.50) with the boundary conditions (8.49). The computed meniscus is shown in Figure 8.9b. The union between the analytical and numerical menisci forms the final required meniscus (Figure 8.9c).

The error between the meniscus height $h = 0.0067\,\text{m}$ computed using the analytical-numerical solution, and those computed using only the analytical formulas h_T (8.32) and h_B (8.37), are of the order 10^{-5}, for a crystal radius $r_c = 0.0136\,\text{m}$.

In the above analytical-numerical model, the idea reported in the literature concerning approximation of the meniscus using Bessel functions was used, but the first part of the meniscus (situated in the neighbourhood of the crucible) was obtained by computing modified Bessel functions, not using the approximation (8.48). From these calculations, initial conditions necessary to solve the IVP (8.49)–(8.50) were found, and the second part of the meniscus (situated near the crystal) was computed numerically. In comparison with previous approximations [Huh 1969, Hurle 1983, Mika 1975], this represents an improved result over the analytical-numerical method which gave errors of the order 10^{-4}.

As can be seen in the developments presented above, no exact solution of the meniscus shape, neither analytical nor numerical, can exist. Always an approximated part of the solution should be used and the difficulty is to keep this approximation as low as possible.

8.3 Analytical and Numerical Solutions for the Meniscus Equation in the EFG Method

The meniscus surface equation (8.3) and its corresponding boundary conditions for the EFG method are considered for sheets and cylindrical crystals. *Qualitative analyses* are performed, and when possible (i.e. in very particular cases) *analytical solutions* are given. The properties of the menisci obtained from the qualitative studies, are exemplified through *numerical examples*.

In the EFG technique, the main question is: what is the relation between the meniscus height h (which can be controlled through heat transfer) and the crystal sheet half-thickness or crystal rod radius?

8.3.1 Sheets

The central component of the EFG growth method is the die. The shape of the die defines the shape and the size of the meniscus, i.e. the liquid bridge retained between the die and the crystal (see Chapters 2 and 5). In order to obtain a sheet, the upper surface of the die has to be rectangular. The main characteristic of the sheet is its thickness (or half-thickness x_c). Then solutions $z = z(x)$ of Equation (8.3), depending only on the coordinate x, are sought. This means that the border effects (which occur on both edges of the sheet) are not considered. This approximation is equivalent to those given by Nutt [Nutt 1960] who neglected the curvature $1/R_2$ from Equation (8.1) written in the (xOz) frame (Figure 8.10). It is possible to consider the borders of the sheet as half-cylinders, and the meniscus computed for an EFG crystal rod can be used as a first approximation. However, the junction between the axisymmetric border meniscus and the two-dimensional sheet meniscus remains a problem.

Thus, the meniscus equation (8.1) without magnetic field and without rotation of the liquid becomes:

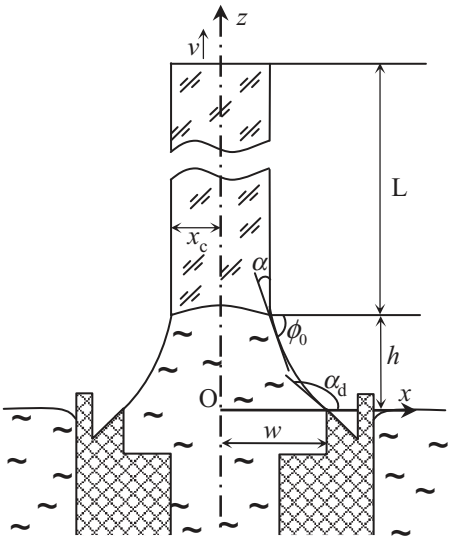

Figure 8.10 *Two-dimensional model for a sheet grown by the EFG method.*

$$\frac{\dfrac{\mathrm{d}^2 z}{\mathrm{d}x^2}}{\left[1+\left(\dfrac{\mathrm{d}z}{\mathrm{d}x}\right)^2\right]^{3/2}} = \frac{\rho_\mathrm{l} g z - (p_\mathrm{O} - p_\mathrm{v})}{\gamma_\mathrm{lv}}, \tag{8.52}$$

which is equivalent to

$$\frac{\mathrm{d}^2 z}{\mathrm{d}x^2} = \frac{\rho_\mathrm{l} g z - (p_\mathrm{O} - p_\mathrm{v})}{\gamma_\mathrm{lv}} \cdot \left[1+\left(\frac{\mathrm{d}z}{\mathrm{d}x}\right)^2\right]^{3/2}. \tag{8.53}$$

In the EFG method, the pressure p_O is the pressure at the origin and it depends on the position of the liquid surface outside the die. For example, referring to Figure 8.10, because a liquid surface plane coinciding with the shaper edge plane has been chosen, $p_\mathrm{O} = p_\mathrm{v}$, and hence Equation (8.53) becomes:

$$\frac{\mathrm{d}^2 z}{\mathrm{d}x^2} = \frac{\rho_\mathrm{l} g z}{\gamma_\mathrm{lv}} \cdot \left[1+\left(\frac{\mathrm{d}z}{\mathrm{d}x}\right)^2\right]^{3/2}. \tag{8.54}$$

The solution $z(x)$ of Equation (8.54) has to satisfy the following catching boundary condition:

$$z(w) = 0, \tag{8.55}$$

where $w > 0$ is the inner half-thickness of the die. It is assumed that the bottom line of the meniscus on the die is fixed on the edge of the die; i.e. $z(w) = 0$ and $z(x) > 0$ for $x < w$ (x close to w) [Braescu 2003].

At the other end of the meniscus, the growth angle criterion should be imposed, i.e.:

$$z(x_\mathrm{c}) = h \quad \text{and} \quad \frac{\mathrm{d}z}{\mathrm{d}x}(x_\mathrm{c}) = -\tan\alpha \tag{8.56}$$

where the meniscus height h and the sheet half-thickness x_c are unknown. In order to find the relation between h and x_c for a given inner die half-thickness w, an intermediate parameter α_d (see Figure 8.10) satisfying:

$$\frac{dz}{dx}(w) = \tan\alpha_d \tag{8.57}$$

is used, or ϕ_c if we denote by $\phi_c = \pi - \alpha_d$:

$$\frac{dz}{dx}(w) = -\tan\phi_c, \phi_c \in \left(0; \frac{1}{2}\pi\right). \tag{8.58}$$

In the following, Equation (8.54) will be solved satisfying conditions (8.55) and (8.58) for a given die half-thickness w, and a given angle ϕ_c. After that, for the obtained meniscus $z(x)$, the growth angle criteria (8.56) will be imposed and the dependence of the sheet half-thickness x_c as a function of the meniscus height h will be found.

In the particular case of zero gravity the solution $z(x)$ can be expressed in an analytical form: Equation (8.54) becomes $d^2z/dx^2 = 0$ for which the solution is $z(x) = c_1 \cdot x + c_2$, where c_1 and c_2 can be determined from the conditions (8.55) and (8.58). In this way, the obtained *analytical solution*

$$z(x) = -(\tan\phi_c)\cdot x + w\cdot\tan\phi_c \tag{8.59}$$

shows that in zero gravity the meniscus is a straight line.

Imposing the growth angle criterion, the parameter ϕ_c is eliminated and the following dependence of the sheet half-thickness x_c as a function of the meniscus height h is obtained:

$$x_c(h) = w - \frac{h}{\tan\alpha}. \tag{8.60}$$

Using material parameters for silicon (growth angle $\alpha = 11° = 0.1919$ radians), and a die half-thickness $w = 0.002$ m, the representation shown in Figure 8.11 is obtained.

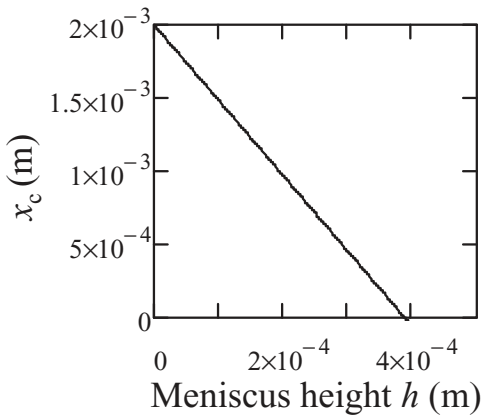

Figure 8.11 *Dependence of the sheet half-thickness* x_c *as a function of the meniscus height* h *in zero gravity.*

If gravity is considered, then *an analytical form of the meniscus cannot be obtained*, but *qualitatively* it is possible to get information about the shape of the meniscus, and *the meniscus shape can be computed* using Runge–Kutta method.

Thus, using the technique set out in the first section, the nonlinear Equation (8.54) is transformed into a nonlinear system of two differential equations:

$$\begin{cases} \dfrac{\mathrm{d}z}{\mathrm{d}x} = -\tan\phi \\ \dfrac{\mathrm{d}\phi}{\mathrm{d}x} = -\dfrac{\rho_\mathrm{l}\cdot g\cdot z}{\gamma_\mathrm{lv}}\cdot\dfrac{1}{\cos\phi} \end{cases} \tag{8.61}$$

for which the boundary conditions (8.55), (8.58) become:

$$z(w)=0, \quad \phi(w)=\phi_\mathrm{c}; \quad \phi_\mathrm{c}\in(0,\pi/2). \tag{8.62}$$

The functions from the right-hand side of Equation (8.61) are defined for $z \in (-\infty; \infty)$, $\phi \in (-\pi/2; \pi/2)$ and are independent of x (the system is autonomous). These functions depend also on the material parameters $\rho_\mathrm{l} \in (0; \infty)$, $\gamma_\mathrm{lv} \in (0; \infty)$. The functions are real analytical, i.e. they can be expanded in a Taylor series in the neighbourhood of any point $(z, \phi, \rho_\mathrm{l}, \gamma_\mathrm{lv})$ from $D = (-\infty; +\infty) \times (-\pi/2; \pi/2) \times (0; +\infty) \times (0; +\infty)$. Therefore, for the Cauchy problem (8.61)–(8.62), all the conditions of the Cauchy–Lipschitz theorem concerning the existence and uniqueness of the solution of the problem (8.61)–(8.62) are satisfied. It follows that the problem (8.61)–(8.62) has a unique saturated solution defined on an interval $(a; b)$. The solution of (8.61)–(8.62) will be denoted by:

$$z = z(x; w, \phi_\mathrm{c}, \gamma_\mathrm{lv}, \rho_\mathrm{l}), \quad \phi = \phi(x; w, \phi_\mathrm{c}, \gamma_\mathrm{lv}, \rho_\mathrm{l}) \tag{8.63}$$

and depends on x and on the parameters w, ϕ_c, γ_lv, ρ_l; a and b also depend on w, ϕ_c, γ_lv, ρ_l and satisfy $a < w < b$.

In general, the solution (8.63) cannot be expressed in an explicit form (because the system is nonlinear). For this reason, the behaviour of the solution will be analysed in the neighbourhood of w [Balint 2005].

From (8.61) and (8.62) we have:

$$\left.\frac{\mathrm{d}z}{\mathrm{d}x}\right|_{x=w} = -\tan\phi_\mathrm{c} < 0, \tag{8.64}$$

which shows that there exists $\varepsilon' > 0$ such that for any $x \in (w - \varepsilon'; w]$ we have $\mathrm{d}z/\mathrm{d}x < 0$. It follows that the function $z = z\,(x;\ w,\ \phi_\mathrm{c},\ \gamma_\mathrm{lv},\ \rho_\mathrm{l})$ is strictly decreasing on the interval $(w - \varepsilon'; w]$ and is strictly positive on $(w - \varepsilon'; w)$:

$$z = z(x; w, \phi_\mathrm{c}, \gamma_\mathrm{lv}, \rho_\mathrm{l}) > 0, \quad \forall\ x \in (w-\varepsilon'; w).$$

Taking into account the equality:

$$\frac{\mathrm{d}^2 z}{\mathrm{d}x^2} = -\frac{1}{\cos^2\phi}\cdot\frac{\mathrm{d}\phi}{\mathrm{d}x}$$

it follows that, in the neighbourhood of w, the meniscus is convex at any point, which is obvious from the Young–Laplace equation:

$$\frac{\mathrm{d}^2 z}{\mathrm{d}x^2} = -\frac{1}{\cos^2\phi}\cdot\frac{\mathrm{d}\phi}{\mathrm{d}x} = \frac{1}{\cos^3\phi}\cdot\frac{\rho_\mathrm{l}\cdot g\cdot z}{\gamma_\mathrm{lv}} > 0.$$

The equality:

$$\frac{\mathrm{d}\phi}{\mathrm{d}x} = -\frac{\rho_\mathrm{l}\cdot g\cdot z}{\gamma_\mathrm{lv}}\cdot\frac{1}{\cos\phi}$$

shows that there exists $\varepsilon'' > 0$ such that on $(w - \varepsilon''; w)$ the function $\phi(x; w, \phi_\mathrm{c}, \gamma_\mathrm{lv}, \rho_\mathrm{l})$ is strictly decreasing and

$$\phi = \phi(x; w, \phi_\mathrm{c}, \gamma_\mathrm{lv}, \rho_\mathrm{l}) > \phi_\mathrm{c}, \quad \forall\, x \in (w - \varepsilon''; w).$$

The growth angle is achieved if the following equality holds:

$$\phi(x; w, \phi_\mathrm{c}, \gamma_\mathrm{lv}, \rho_\mathrm{l}) = \frac{\pi}{2} - \alpha = \phi_0. \tag{8.65}$$

In order to obtain more information about the solution (8.63), an approximation of the solution (8.63) by Taylor polynomials, obtained by expansion in w, is considered:

$$\begin{aligned} z(x; w, \phi_\mathrm{c}, \gamma_\mathrm{lv}, \rho_\mathrm{l}) \approx\ & z(w; w, \phi_\mathrm{c}, \gamma_\mathrm{lv}, \rho_\mathrm{l}) \\ & + \frac{\mathrm{d}z}{\mathrm{d}x}(w; w, \phi_\mathrm{c}, \gamma_\mathrm{lv}, \rho_\mathrm{l})\cdot(x - w) \\ & + \frac{1}{2}\cdot\frac{\mathrm{d}^2 z}{\mathrm{d}x^2}(w; w, \phi_\mathrm{c}, \gamma_\mathrm{lv}, \rho_\mathrm{l})\cdot(x - w)^2 \\ & + \frac{1}{6}\cdot\frac{\mathrm{d}^3 z}{\mathrm{d}x^3}(w; w, \phi_\mathrm{c}, \gamma_\mathrm{lv}, \rho_\mathrm{l})\cdot(x - w)^3, \end{aligned} \tag{8.66}$$

$$\begin{aligned} \phi(x; w, \phi_\mathrm{c}, \gamma_\mathrm{lv}, \rho_\mathrm{l}) \approx\ & \phi(w; w, \phi_\mathrm{c}, \gamma_\mathrm{lv}, \rho_\mathrm{l}) \\ & + \frac{\mathrm{d}\phi}{\mathrm{d}x}(w; w, \phi_\mathrm{c}, \gamma_\mathrm{lv}, \rho_\mathrm{l})\cdot(x - w) \\ & + \frac{1}{2}\cdot\frac{\mathrm{d}^2\phi}{\mathrm{d}x^2}(w; w, \phi_\mathrm{c}, \gamma_\mathrm{lv}, \rho_\mathrm{l})\cdot(x - w)^2. \end{aligned} \tag{8.67}$$

The coefficients of these polynomials are obtained from Equations (8.61) and conditions (8.62), and are given by:

$$z(w) = z(w; w, \phi_\mathrm{c}, \gamma_\mathrm{lv}, \rho_\mathrm{l}) = 0; \tag{8.68}$$

$$z'(w) = \frac{\mathrm{d}z}{\mathrm{d}x}(w; w, \phi_\mathrm{c}, \gamma_\mathrm{lv}, \rho_\mathrm{l}) = -\tan\phi_\mathrm{c}; \tag{8.69}$$

$$z''(w) = \frac{\mathrm{d}^2 z}{\mathrm{d}x^2}(w; w, \phi_c, \gamma_{lv}, \rho_l) = 0; \tag{8.70}$$

$$z'''(w) = \frac{\mathrm{d}^3 z}{\mathrm{d}x^3}(w; w, \phi_c, \gamma_{lv}, \rho_l) = -\frac{1}{\cos^3 \phi_c} \cdot \frac{\rho_l \cdot g}{\gamma_{lv}} \cdot \tan \phi_c; \tag{8.71}$$

$$\phi(w) = \phi(w; w, \phi_c, \gamma_{lv}, \rho_l) = \phi_c; \tag{8.72}$$

$$\phi'(w) = \frac{\mathrm{d}\phi}{\mathrm{d}x}(w; w, \phi_c, \gamma_{lv}, \rho_l) = 0; \tag{8.73}$$

$$\phi''(w) = \frac{\mathrm{d}^2 \phi}{\mathrm{d}x^2}(w; w, \phi_c, \gamma_{lv}, \rho_l) = \frac{1}{\cos^2 \phi_c} \cdot \frac{\rho_l \cdot g}{\gamma_{lv}} \cdot \sin \phi_c. \tag{8.74}$$

Replacing these coefficients into (8.66)–(8.67) gives the following approximations to the solution (8.63):

$$z(x; w, \phi_c, \gamma_{lv}, \rho_l) \approx -(\tan \phi_c) \cdot (x - w) - \frac{1}{6} \cdot \frac{1}{\cos^3 \phi_c} \cdot \frac{\rho_l \cdot g}{\gamma_{lv}} \cdot \tan \phi_c \cdot (x - w)^3, \tag{8.75}$$

$$\phi(x; w, \phi_c, \gamma_{lv}, \rho_l) \approx \phi_c + \frac{1}{2} \cdot \frac{1}{\cos^2 \phi_c} \cdot \frac{\rho_l \cdot g}{\gamma_{lv}} \cdot \sin \phi_c \cdot (x - w)^2. \tag{8.76}$$

These approximations are valid only for x close to w [Balint 2005]. This will be shown numerically for silicon sheets.

The attainment of the growth angle at a point (0; w] means that the equation:

$$\phi_c + \frac{1}{2} \cdot \frac{1}{\cos^2 \phi_c} \cdot \frac{\rho_l \cdot g}{\gamma_{lv}} \cdot \sin \phi_c \cdot (x - w)^2 = \frac{\pi}{2} - \alpha \tag{8.77}$$

has at least one solution on (0; w]. Because

$$(x - w)^2 = \frac{\frac{1}{2}\pi - \alpha - \phi_c}{\frac{1}{2} \cdot \frac{\sin \phi_c}{\cos^2 \phi_c} \cdot \frac{\rho_l \cdot g}{\gamma_{lv}}},$$

it is easy to see that Equation (8.77) can have only one solution on (0; w] if the following inequalities hold:

(i) $0 < \phi_c < \frac{1}{2}\pi - \alpha$

(ii) $w - \sqrt{\frac{\frac{1}{2}\pi - \alpha - \phi_c}{\frac{1}{2} \cdot \frac{\sin \phi_c}{\cos^2 \phi_c} \cdot \frac{\rho_l \cdot g}{\gamma_{lv}}}} > 0$

These inequalities express the range of the parameter ϕ_c for which the growth angle can be achieved. For example, using parameters for silicon and a die half-thickness

$w = 0.002\,\text{m}$, the inequalities (i)–(ii) show that condition of the growth angle is satisfied for $1.11 \le \phi_c < 1.3787$.

Indeed, considering 30 values of the parameter ϕ_c and integrating by Runge–Kutta the problem (8.61)–(8.62), it is found that the growth angle is achieved for $1.04 \le \phi_c < 1.3787$. This proves that the above Taylor approximation is useful for finding the range of the parameter ϕ_c.

Concerning the meniscus shape: from Equations (8.75)–(8.76), it is easy to see that the functions $z\,(x;\, w,\, \phi_c,\, \gamma_{lv},\, \rho_l)$, $\phi(x;\, w,\, \phi_c,\, \gamma_{lv},\, \rho_l)$ are convex in the neighbourhood of w. The growth angle condition imposes the same monotony on the whole interval $(x_c,\, w)$ for the function $\phi(x;\, w,\, \phi_c,\, \gamma_{lv},\, \rho_l)$, i.e. $d\phi/dx < 0$. This implies:

$$\frac{d^2 z}{dx^2} = -\frac{1}{\cos^2\phi}\cdot\frac{d\phi}{dx} > 0,$$

i.e. the meniscus convexity on the interval $(x_c,\, w)$, as can be seen in Figure 8.12.

The couples $(x_c,\, h)$ in which the growth angle is attained were computed for every parameter ϕ_c considered. Plotting these couples gives the dependence shown in Figure 8.13.

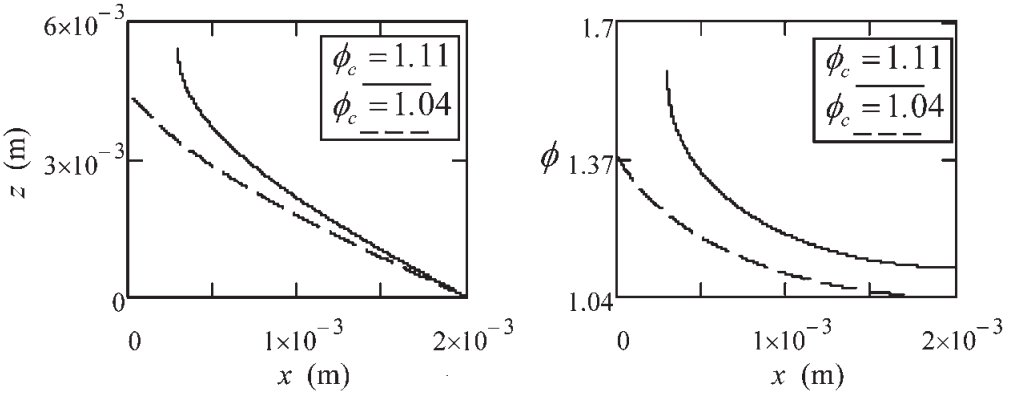

Figure 8.12 *Numerical representation of the functions* $z = z(x;\, w,\, \phi_c,\, \gamma_{lv},\, \rho_l)$ *and* $\phi = \phi(x;\, w,\, \phi_c,\, \gamma_{lv},\, \rho_l)$ *for silicon sheets grown using a die with half-thickness* $w = 0.002\,\text{m}$, *and* $\phi_c = 1.04$ *or* 1.11 *radians.*

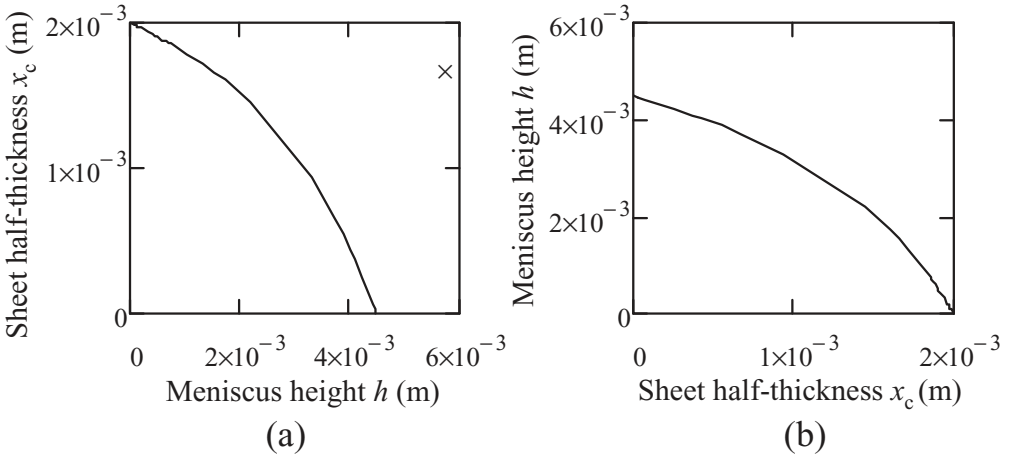

Figure 8.13 *The computed dependencies* $x_c(h)$ *(a) and* $h(x_c)$ *(b).*

Because an analytical expression fitting the above data is useful for practical crystal growers, the dependence of the sheet half-thickness x_c as function of the meniscus height h:

$$x_c(h) = \frac{0.002 - 0.42 \cdot h + 87 \cdot h^2 - 20500 \cdot h^3}{1 - 116.2 \cdot h + 35500 \cdot h^2 - 3825000 \cdot h^3}, \quad h \in [0; 0.0045], \tag{8.78}$$

and the dependence of the meniscus height h as function of the sheet half-thickness x_c:

$$h(x_c) = \frac{0.004 - 5.64 \cdot x_c + 2400 \cdot x_c^2 - 334000 \cdot x_c^3}{1 - 1044 \cdot x_c + 357000 \cdot x_c^2 - 3.86 \cdot 10^7 \cdot x_c^3 + 3 \cdot 10^8 \cdot x_c^4}, \quad x_c \in [0.0000012; 0.002], \tag{8.78*}$$

are obtained, for a silicon sheet grown using a die half-thickness $w = 0.002\,\text{m}$.

The above *qualitative analyses* show that the dependences $x_c(h)$ and $h(x_c)$ are decreasing functions. For the configuration shown in Figure 8.10, i.e. $p_O = p_v$, and zero gravity these dependences are linear functions, and the growth angle is always attained. In normal gravity conditions the above dependences are concave functions (the second derivative is negative), and the growth angle is attained if the parameter ϕ_c satisfies inequalities (i)–(ii).

8.3.2 Cylindrical Crystals

In order to obtain a cylindrical crystal a circular die is used (see Figure 8.14). In this case, the equation of the meniscus surface is the axisymmetric Young–Laplace equation (8.12), which becomes:

$$\frac{d^2z}{dr^2} = \frac{\rho_l g z - (p_O - p_v)}{\gamma_{lv}} \cdot \left[1 + \left(\frac{dz}{dr}\right)^2\right]^{3/2} - \frac{1}{r} \cdot \frac{dz}{dr} \cdot \left[1 + \left(\frac{dz}{dr}\right)^2\right], \tag{8.79}$$

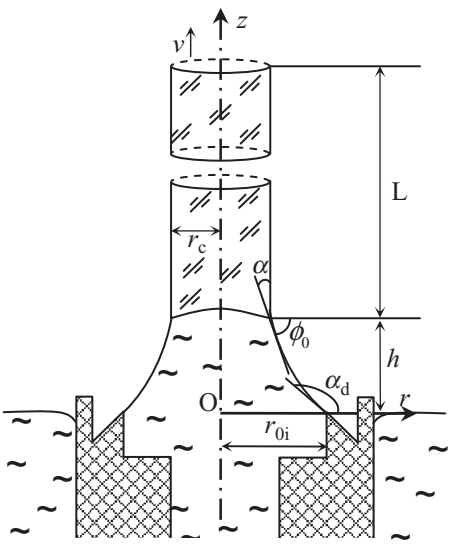

Figure 8.14 *Axisymmetric model of a cylindrical crystal grown by the EFG method.*

if the growth process takes place without a magnetic field and without rotation of the crucible [Borodin 1979, Braescu 2004–1, Braescu 2004–2, Brener 1979–1, Brener 1979–2]. In the configuration in Figure 8.14, the liquid surface plane coincides with the shaper edge plane and hence $p_O = p_v$. Equation (8.79) becomes:

$$\frac{d^2z}{dr^2} = \frac{\rho_l g z}{\gamma_{lv}} \cdot \left[1 + \left(\frac{dz}{dr}\right)^2\right]^{3/2} - \frac{1}{r} \cdot \frac{dz}{dr} \cdot \left[1 + \left(\frac{dz}{dr}\right)^2\right]. \tag{8.80}$$

The solution $z(r)$ of Equation (8.80) has to verify the following catching boundary condition:

$$z(r_{0i}) = 0, \tag{8.81}$$

where $r_{0i} > 0$ is the inner radius of the die. It is assumed that the bottom line of the meniscus on the die is fixed on the edge of the die; i.e. $z(r_{0i}) = 0$ and $z(r) > 0$ for $r < r_{0i}$ (r close to r_{0i}).

At the other end of the meniscus, the growth angle criteria should be imposed, i.e.:

$$z(r_c) = h \quad \text{and} \quad \frac{dz}{dr}(r_c) = -\tan\alpha \tag{8.82}$$

where the meniscus height h and the crystal radius r_c are unknown. For finding h and r_c for a given inner die radius r_{0i}, an intermediate parameter α_d will be used (see Figure 8.14) satisfying:

$$\frac{dz}{dr}(r_{0i}) = \tan\alpha_d, \tag{8.83}$$

or ϕ_c if we denote by $\phi_c = \pi - \alpha_d$:

$$\frac{dz}{dr}(r_{0i}) = -\tan\phi_c, \quad \phi_c \in \left(0; \frac{\pi}{2}\right). \tag{8.84}$$

In the following, Equation (8.80) satisfying conditions (8.81) and (8.84) will be solved for a given die radius r_{0i} and a given angle ϕ_c. After that, for the obtained meniscus $z(r)$, the growth angle criteria (8.82) will be imposed and the dependence of the crystal radius r_c as function of the meniscus height h will be found.

In the particular case of zero gravity the solution $z(r)$ can be expressed in an analytical form. Equation (8.80) becomes:

$$\frac{d^2z}{dr^2} + \frac{1}{r} \cdot \frac{dz}{dr} \cdot \left[1 + \left(\frac{dz}{dr}\right)^2\right] = 0, \tag{8.85}$$

which is equivalent to

$$\frac{d}{dr}\left(\frac{r \cdot \frac{dz}{dr}}{\sqrt{1 + \left(\frac{dz}{dr}\right)^2}}\right) = 0, \quad \text{i.e.} \quad \frac{r \cdot \frac{dz}{dr}}{\sqrt{1 + \left(\frac{dz}{dr}\right)^2}} = c_1,$$

where c_1 is a constant. From this an analytical expression for the derivative of the function $z(r)$ is obtained:

$$\frac{\mathrm{d}z}{\mathrm{d}r}(r) = \pm\frac{c_1}{\sqrt{r^2 - c_1^2}}. \tag{8.86}$$

Imposing the condition (8.84) gives the value of the constant $c_1 = r_{0i} \cdot \sin\phi_c$ and the function $z(r)$ becomes:

$$z(r) = r_{0i} \cdot \sin\phi_c \cdot \int_r^{r_{0i}} \frac{1}{\sqrt{u^2 - r_{0i}^2 \cdot \sin^2\phi_c}}\mathrm{d}u.$$

Thus, the *analytical expression of the meniscus* as function of the parameters is:

$$z(r) = r_{0i} \cdot \sin\phi_c \cdot \ln\frac{r_{0i} + \sqrt{r_{0i}^2 - r_{0i}^2 \cdot \sin^2\phi_c}}{r + \sqrt{r^2 - r_{0i}^2 \cdot \sin^2\phi_c}}, \tag{8.87}$$

for which the condition $r \in [r_{0i} \cdot \sin\phi_c, r_{0i}]$ is imposed, in order to assure the existence of the functions employed [Braescu 2005].

Imposing the growth angle criterion, the parameter ϕ_c can be eliminated and the dependence of the meniscus height as function of the crystal radius can be found. From the condition

$$\frac{\mathrm{d}z}{\mathrm{d}r}(r_c) = -\tan\alpha$$

we get

$$\sin\phi_c = \frac{r_c}{r_{0i}} \cdot \sin\alpha, \tag{8.88}$$

which substituted into (8.87) gives:

$$z(r_c) = r_c \cdot (\sin\alpha) \cdot \ln\frac{r_{0i} + \sqrt{r_{0i}^2 - r_c^2 \cdot \sin^2\alpha}}{r_c + \sqrt{r_c^2 - r_c^2 \cdot \sin^2\alpha}}.$$

Since $z\,(r_c) = h$, the analytical formula of the meniscus height as a function of the crystal radius is obtained:

$$h(r_c) = r_c \cdot (\sin\alpha) \cdot \ln\frac{r_{0i} + \sqrt{r_{0i}^2 - r_c^2 \cdot \sin^2\alpha}}{r_c(1 + \cos\alpha)}. \tag{8.89}$$

Using material parameters for silicon (growth angle $\alpha = 11^\circ = 0.1919$ radians), and a die radius $r_{0i} = 0.002\,\mathrm{m}$, the representation for the curve (8.89) is found as shown in Figure 8.15.

If gravity is considered, then *an analytical form of the meniscus cannot be obtained*, but performing *qualitative studies* gives us information about the shape of the meniscus

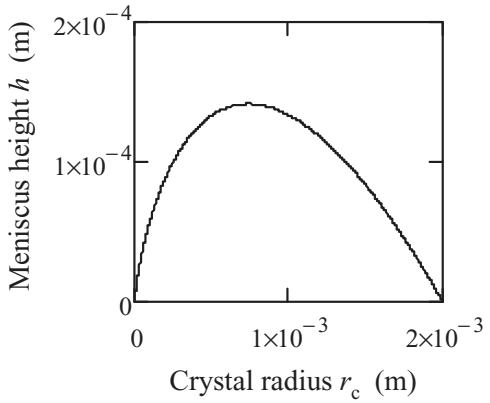

Figure 8.15 *Meniscus height* h *as function of the crystal radius* r_c *in zero gravity.*

which depends on the pressure, and the *meniscus shape* is computed using Runge–Kutta method.

Thus, using the technique presented in previous section, the nonlinear equation (8.60) is transformed into the following nonlinear system of two differential equations:

$$\begin{cases} \dfrac{dz}{dr} = -\tan\phi \\ \dfrac{d\phi}{dr} = -\dfrac{\rho_l \cdot g}{\gamma_{lv}} \cdot \dfrac{z}{\cos\phi} - \dfrac{1}{r} \cdot \tan\phi \end{cases} \tag{8.90}$$

for which the boundary conditions (8.81), (8.84) become [Braescu 2004–2]:

$$z(r_{0i}) = 0, \quad \phi(r_{0i}) = \phi_c; \quad \phi_c \in \left(0, \frac{\pi}{2}\right). \tag{8.91}$$

The functions from the right-hand member of Equations (8.90) are defined for $r \in (0; \infty)$, $z \in (-\infty; \infty)$, $\phi \in (-\pi/2; \pi/2)$. They are real analytic functions, i.e. can be expanded into Taylor series, and hence for the Cauchy problem (8.90)–(8.91) the conditions of existence and uniqueness of a solution are satisfied. It follows that the Cauchy problem (8.90)–(8.91) has a unique saturated solution defined on an interval $(a; b)$:

$$z = z(r; r_{0i}, \phi_c, \gamma_{lv}, \rho_l), \quad \phi = \phi(r; r_{0i}, \phi_c, \gamma_{lv}, \rho_l), \tag{8.92}$$

depending on r and on the parameters r_{0i}, ϕ_c, γ_{lv} , ρ_l. The interval extremities a and b depend on r_{0i}, ϕ_c, γ_{lv}, ρ_l as well and verify $0 < a < r_{0i} < b$ [Braescu 2004-2].

Generally, the solution (8.92) can not be expressed in an explicit form because the system is nonlinear; for this reason it is necessary to analyse the behaviour of the solution in the neighbourhood of r_{0i}.

From the system (8.90) and the conditions (8.91) the following inequalities can be obtained:

$$\left.\frac{dz}{dr}\right|_{r=r_{0i}} = -\tan\phi_c < 0, \tag{8.93}$$

$$\left.\frac{\mathrm{d}\phi}{\mathrm{d}r}\right|_{r=r_{0\mathrm{i}}} = -\frac{1}{r_{0\mathrm{i}}}\cdot\tan\phi_{\mathrm{c}} < 0. \tag{8.94}$$

Inequality (8.93) shows that there exists $\varepsilon' > 0$ such that for $r \in (r_{0\mathrm{i}} - \varepsilon'; r_{0\mathrm{i}}]$, $\mathrm{d}z/\mathrm{d}r < 0$. It follows that the function $z = z(r; r_{0\mathrm{i}}, \phi_{\mathrm{c}}, \gamma_{\mathrm{lv}}, \rho_{\mathrm{l}})$ is strictly decreasing on $(r_{0\mathrm{i}} - \varepsilon'; r_{0\mathrm{i}}]$ and is strictly positive on $(r_{0\mathrm{i}} - \varepsilon'; r_{0\mathrm{i}})$:

$$z = z(r; r_{0\mathrm{i}}, \phi_{\mathrm{c}}, \gamma_{\mathrm{lv}}, \rho_{\mathrm{l}}) > 0, \quad \forall\, r \in (r_{0\mathrm{i}} - \varepsilon'; r_{0\mathrm{i}}).$$

The inequality $\mathrm{d}\phi/\mathrm{d}r|_{r=r_{0\mathrm{i}}} < 0$ shows that the function $\phi = \phi(r; r_{0\mathrm{i}}, \phi_{\mathrm{c}}, \gamma_{\mathrm{lv}}, \rho_{\mathrm{l}})$ is strictly decreasing on $(r_{0\mathrm{i}} - \varepsilon''; r_{0\mathrm{i}}]$ and

$$\phi = \phi(r; r_{0\mathrm{i}}, \phi_{\mathrm{c}}, \gamma_{\mathrm{lv}}, \rho_{\mathrm{l}}) > \phi_{\mathrm{c}}, \quad \forall\, r \in (r_{0\mathrm{i}} - \varepsilon''; r_{0i}).$$

In addition, since

$$\frac{\mathrm{d}^2 z}{\mathrm{d}r^2} = -\frac{1}{\cos^2\phi_{\mathrm{c}}}\cdot\frac{\mathrm{d}\phi}{\mathrm{d}r} > 0$$

in the neighbourhood of $r_{0\mathrm{i}}$, it results that the function $z(r; r_{0\mathrm{i}}, \phi_{\mathrm{c}}, \gamma_{\mathrm{lv}}, \rho_{\mathrm{l}})$ is convex in the neighbourhood of $r_{0\mathrm{i}}$.

In order to get more information about the solution (8.92), it will be approximated by Taylor polynomials obtained by expansion in $r_{0\mathrm{i}}$:

$$\begin{aligned} z(r; r_{0\mathrm{i}}, \phi_{\mathrm{c}}, \gamma_{\mathrm{lv}}, \rho_{\mathrm{l}}) \approx{}& z(r_{0\mathrm{i}}; r_{0\mathrm{i}}, \phi_{\mathrm{c}}, \gamma_{\mathrm{lv}}, \rho_{\mathrm{l}}) + \frac{\mathrm{d}z}{\mathrm{d}r}(r_{0\mathrm{i}}; r_{0\mathrm{i}}, \phi_{\mathrm{c}}, \gamma_{\mathrm{lv}}, \rho_{\mathrm{l}})\cdot(r - r_{0\mathrm{i}}) \\ &+ \frac{1}{2}\cdot\frac{\mathrm{d}^2 z}{\mathrm{d}r^2}(r_{0\mathrm{i}}; r_{0\mathrm{i}}, \phi_{\mathrm{c}}, \gamma_{\mathrm{lv}}, \rho_{\mathrm{l}})\cdot(r - r_{0\mathrm{i}})^2 \\ &+ \frac{1}{6}\cdot\frac{\mathrm{d}^3 z}{\mathrm{d}r^3}(r_{0\mathrm{i}}; r_{0\mathrm{i}}, \phi_{\mathrm{c}}, \gamma_{\mathrm{lv}}, \rho_{\mathrm{l}})\cdot(r - r_{0\mathrm{i}})^3, \end{aligned} \tag{8.95}$$

$$\begin{aligned} \phi(r; r_{0\mathrm{i}}, \phi_{\mathrm{c}}, \gamma_{\mathrm{lv}}, \rho_{\mathrm{l}}) \approx{}& \phi(r_{0\mathrm{i}}; r_{0\mathrm{i}}, \phi_{\mathrm{c}}, \gamma_{\mathrm{lv}}, \rho_{\mathrm{l}}) + \frac{\mathrm{d}\phi}{\mathrm{d}r}(r_{0\mathrm{i}}; r_{0\mathrm{i}}, \phi_{\mathrm{c}}, \gamma_{\mathrm{lv}}, \rho_{\mathrm{l}})\cdot(r - r_{0\mathrm{i}}) \\ &+ \frac{1}{2}\cdot\frac{\mathrm{d}^2\phi}{\mathrm{d}r^2}(r_{0\mathrm{i}}; r_{0\mathrm{i}}, \phi_{\mathrm{c}}, \gamma_{\mathrm{lv}}, \rho_{\mathrm{l}})\cdot(r - r_{0\mathrm{i}})^2. \end{aligned} \tag{8.96}$$

The coefficients of these polynomials are obtained from (8.90) and (8.91), being given by [Braescu 2004-2] as:

$$z(r_{0\mathrm{i}}) = z(r_{0\mathrm{i}}; r_{0\mathrm{i}}, \phi_{\mathrm{c}}, \gamma_{\mathrm{lv}}, \rho_{\mathrm{l}}) = 0; \tag{8.97}$$

$$z'(r_{0\mathrm{i}}) = \frac{\mathrm{d}z}{\mathrm{d}r}(r_{0\mathrm{i}}; r_{0\mathrm{i}}, \phi_{\mathrm{c}}, \gamma_{\mathrm{lv}}, \rho_{\mathrm{l}}) = -\tan\phi_{\mathrm{c}}; \tag{8.98}$$

$$z''(r_{0\mathrm{i}}) = \frac{\mathrm{d}^2 z}{\mathrm{d}r^2}(r_{0\mathrm{i}}; r_{0\mathrm{i}}, \phi_{\mathrm{c}}, \gamma_{\mathrm{lv}}, \rho_{\mathrm{l}}) = \frac{1}{r_{0\mathrm{i}}}\cdot\frac{\sin\phi_{\mathrm{c}}}{\cos^3\phi_{\mathrm{c}}}; \tag{8.99}$$

$$z'''(r_{0i}) = \frac{d^3 z}{dr^3}(r_{0i}; r_{0i}, \phi_c, \gamma_{lv}, \rho_l)$$
$$= -2 \cdot \frac{\sin^3 \phi_c}{\cos^5 \phi_c} \cdot \frac{1}{r_{0i}^2} - \frac{\sin \phi_c}{\cos^5 \phi_c} \cdot \frac{1}{r_{0i}^2} - \frac{1}{\cos^2 \phi_c} \left[\frac{\rho_l \cdot g}{\gamma_{lv}} \cdot \frac{\sin \phi_c}{\cos^2 \phi_c} + \frac{1}{r_{0i}^2} \cdot \tan \phi_c \right]; \quad (8.100)$$

$$\phi(r_{0i}) = \phi(r_{0i}; r_{0i}, \phi_c, \gamma_{lv}, \rho_l) = \phi_c; \quad (8.101)$$

$$\phi'(r_{0i}) = \frac{d\phi}{dr}(r_{0i}; r_{0i}, \phi_c, \gamma_{lv}, \rho_l) = -\frac{\sin \phi_c}{\cos \phi_c} \cdot \frac{1}{r_{0i}}; \quad (8.102)$$

$$\phi''(r_{0i}) = \frac{d^2 \phi}{dr^2}(r_{0i}; r_{0i}, \phi_c, \gamma_{lv}, \rho_l) = \frac{\rho_l \cdot g}{\gamma_{lv}} \cdot \frac{\sin \phi_c}{\cos^2 \phi_c} + \frac{1}{r_{0i}^2} \cdot \tan \phi_c + \frac{\sin \phi_c}{\cos^3 \phi_c} \cdot \frac{1}{r_{0i}^2}. \quad (8.103)$$

Because

$$\phi''(r_{0i}) = \frac{\rho_l \cdot g}{\gamma_{lv}} \cdot \frac{\sin \phi_c}{\cos^2 \phi_c} + \frac{1}{r_{0i}^2} \cdot \tan \phi_c + \frac{\sin \phi_c}{\cos^3 \phi_c} \cdot \frac{1}{r_{0i}^2} > 0$$

and

$$\phi'(r_{0i}) = -\frac{\sin \phi_c}{\cos \phi_c} \cdot \frac{1}{r_{0i}} < 0,$$

the function:

$$\phi(r; \phi_c, \gamma_{lv}, \rho_l) \approx \phi_c - \frac{\sin \phi_c}{\cos \phi_c} \cdot \frac{1}{r_{0i}} \cdot (r - r_{0i})$$
$$+ \frac{1}{2} \cdot \left(\frac{\rho_l \cdot g}{\gamma_{lv}} \cdot \frac{\sin \phi_c}{\cos^2 \phi_c} + \frac{1}{r_{0i}^2} \cdot \tan \phi_c + \frac{\sin \phi_c}{\cos^3 \phi_c} \cdot \frac{1}{r_{0i}^2} \right) \cdot (r - r_{0i})^2 \quad (8.104)$$

has a minimum which is achieved at the point $r_{min} > r_{0i}$:

$$r_{min} = r_{0i} - \frac{\phi'(r_{0i})}{\phi''(r_{0i})},$$

i.e. the polynomial function of second degree $\phi(r; r_{0i}, \phi_c, \gamma_{lv}, \rho_l)$ decreases until r_{min} and increases after that.

The position of r_{min} shows that the function $\phi(r; r_{0i}, \phi_c, \gamma_{lv}, \rho_l)$ decreases and is convex on $(0; r_{0i}]$. This implies convexity of the meniscus, too. Indeed, because $\phi(r; r_{0i}, \phi_c, \gamma_{lv}, \rho_l)$ decreases, $d\phi/dr < 0$, and hence

$$\frac{d^2 z}{dr^2} = -\frac{1}{\cos^2 \phi_c} \cdot \frac{d\phi}{dr} > 0 \text{ on } (0; r_{0i}],$$

which proves convexity of the function $z\,(r; r_{0i}, \phi_c, \gamma_{lv}, \rho_l)$.

Concerning the growth angle condition: from the monotonicity of $\phi(r;\, r_{0i},\, \phi_c,\, \gamma_{lv},\, \rho_l)$, the growth angle can be achieved in $(0;\, r_{0i})$ only if the contact angle ϕ_c is in $(0;\, \pi/2 - \alpha]$. Thus if $\phi_c = \pi/2 - \alpha$, then the growth angle is achieved in r_{0i}. If $\phi_c < \pi/2 - \alpha$, then the growth angle can be attained on $(0;\, r_{0i})$ only once (because $\phi\,(r;\, r_{0i},\, \phi_c,\, \gamma_{lv},\, \rho_l)$ decreases). Imposing the growth angle condition on the function $\phi\,(r;\, r_{0i},\, \phi_c,\, \gamma_{lv},\, \rho_l)$, the following equation is obtained:

$$\frac{1}{2}\left(\frac{\rho_l \cdot g}{\gamma_{lv}} \cdot \frac{\sin\phi_c}{\cos^2\phi_c} + \frac{1}{r_{0i}^2} \cdot \tan\phi_c + \frac{\sin\phi_c}{\cos^3\phi_c} \cdot \frac{1}{r_{0i}^2}\right) \cdot (r - r_{0i})^2 - \frac{\sin\phi_c}{\cos\phi_c} \cdot \frac{1}{r_{0i}} \cdot (r - r_{0i}) + \phi_c = \frac{\pi}{2} - \alpha$$

which should have one root in $(0;\, r_{0i})$. This condition can be satisfied if:

$$\text{(i)} \quad \Delta = \left(\frac{\sin\phi_c}{\cos\phi_c} \cdot \frac{1}{r_{0i}}\right)^2 - 2\left(\frac{\rho_l \cdot g}{\gamma_{lv}} \cdot \frac{\sin\phi_c}{\cos^2\phi_c} + \frac{1}{r_{0i}^2} \cdot \tan\phi_c + \frac{\sin\phi_c}{\cos^3\phi_c} \cdot \frac{1}{r_{0i}^2}\right) \cdot \left(\phi_c - \frac{\pi}{2} + \alpha\right) > 0,$$

$$\text{(ii)} \quad \frac{\dfrac{\sin\phi_c}{\cos\phi_c} \cdot \dfrac{1}{r_{0i}} - \sqrt{\Delta}}{\dfrac{\rho_l \cdot g}{\gamma_{lv}} \cdot \dfrac{\sin\phi_c}{\cos^2\phi_c} + \dfrac{1}{r_{0i}^2} \cdot \tan\phi_c + \dfrac{\sin\phi_c}{\cos^3\phi_c} \cdot \dfrac{1}{r_{0i}^2}} < 0.$$

These inequalities express the range of the parameter ϕ_c for which the growth angle can be achieved. For example, using parameters for silicon and a die radius $r_{0i} = 0.002\,\text{m}$, the inequalities (i)–(ii) show that the growth angle condition can be satisfied for $0 < \phi_c < 1.378$. Indeed, considering 30 values of the parameter ϕ_c and integrating by Runge–Kutta for the problem (8.90)–(8.91), the growth angle is achieved for $0.01 \le \phi_c < 1.378$. The previous described convexity and the monotonicity of the functions $z = z(r;\, r_{0i},\, \phi_c,\, \gamma_{lv},\, \rho_l)$, $\phi = \phi(r;\, r_{0i},\, \phi_c,\, \gamma_{lv},\, \rho_l)$ can be seen in Figure 8.16. For every considered parameter ϕ_c, the couples $(r_c,\, h)$ in which the growth angle is achieved were computed. Plotting these couples gives the dependence showing Figure 8.17.

Because an analytical expression fitting the above data is useful for practical crystal growers, the dependence of the meniscus height h as function of the crystal radius r_c:

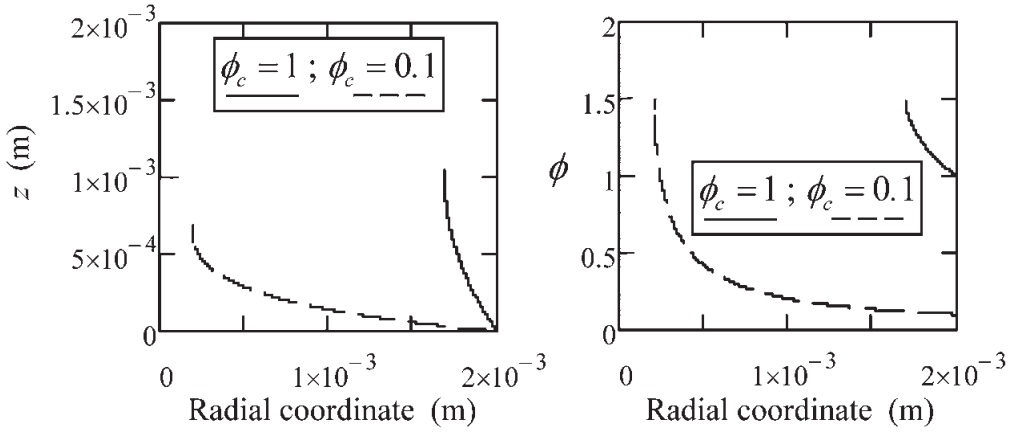

Figure 8.16 *Numerical representation of the functions* $z = z(r;\, r_{oi},\, \phi_c,\, \gamma_{lv},\, \rho_l)$ *and* $\phi = \phi(r;\, r_{oi},\, \phi_c,\, \gamma_{lv},\, \rho_l)$ *for cylindrical silicon rods grown using a die radius* $r_{0i} = 0.002\,\text{m}$, *and* $\phi_c = 1;\, 0.1$ *radians.*

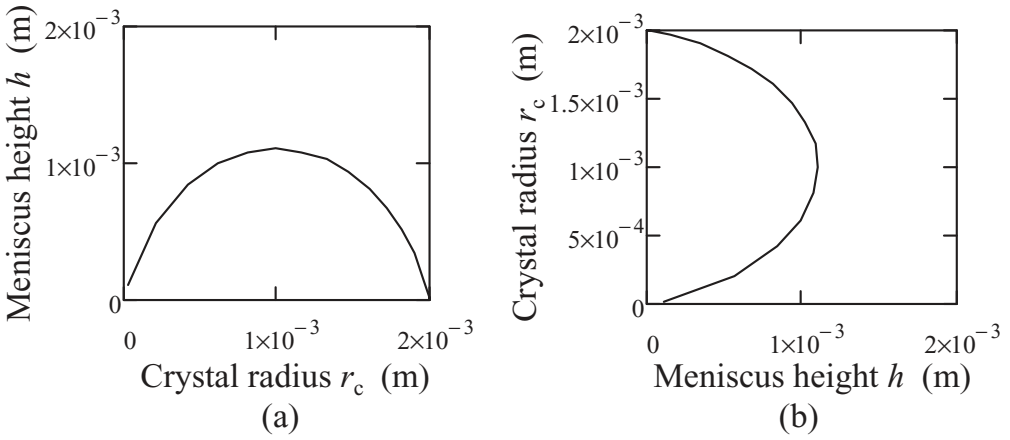

Figure 8.17 *The dependencies* $h(r_c)$ *(a) and* $r_c(h)$ *(b).*

$$h(r_c) = \frac{0.002 + 0.0009 \ln r_c + 0.00017 \ln^2 r_c + 1.2 \times 10^{-5} \ln^3 r_c + 3.26 \times 10^{-7} \ln^4 r_c}{1 + 0.60 \ln r_c + 0.14 \ln^2 r_c + 0.015 \ln^3 r_c + 0.0006 \ln^4 r_c},$$
$$h \in [0; 0.0011],$$

and the dependence of the crystal radius r_c as function of the meniscus height h are obtained for a cylindrical silicon crystal grown using a die radius $r_{0i} = 0.002\,\text{m}$.

The above *qualitative analyses* show that the dependencies $r_c(h)$ and $h(r_c)$ are parabolic functions. For the configuration presented in Figure 8.14, i.e. $p_O = p_v$, and zero gravity, the growth angle is always attained for $r \in [r_{0i} \sin\phi_c, r_{0i}]$. On Earth, the growth angle is achieved if the parameter ϕ_c satisfies inequalities (i)–(ii).

8.4 Analytical and Numerical Solutions for the Meniscus Equation in the Dewetted Bridgman Method

Dewetted Bridgman is a crystal growth technique in which the crystal is detached from the crucible wall by a liquid free surface at the level of the solid–liquid interface, called *liquid meniscu*s, which creates a gap between the crystal and the ampoule (Figure 8.18).

The dewetting is explained in Chapter 6 and involves the wetting angle θ, the growth angle α, possible modification of these parameters due to pollution of the melt by the gas phase and possible pressure difference between the hot and cold sides of the crucible.

There are two problems of interest in dewetting (see Chapter 6):

- What is the gap thickness e, therefore the crystal radius $r_c = r_a - e$?
- What is the shape of the meniscus? This shape is related to the stability of the process.

In order to understand the process which leads to a crystal with a constant radius under normal gravity, analytical and numerical studies of axisymmetric meniscus shapes must be made and the dependence of the meniscus shape on the pressure difference must be established, starting from the Young–Laplace equation of a capillary surface (8.11) written in agreement with the above configuration [Duffar 2000]:

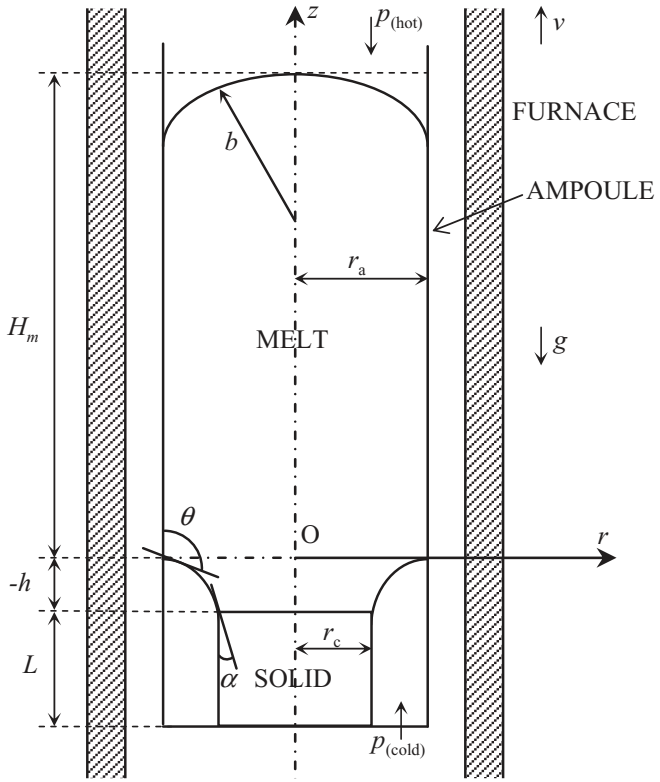

Figure 8.18 *Schematic dewetted Bridgman crystal growth system.*

$$\frac{\dfrac{\mathrm{d}^2 z}{\mathrm{d}r^2}}{\left[1+\left(\dfrac{\mathrm{d}z}{\mathrm{d}r}\right)^2\right]^{3/2}}+\frac{\dfrac{1}{r}\cdot\dfrac{\mathrm{d}z}{\mathrm{d}r}}{\left[1+\left(\dfrac{\mathrm{d}z}{\mathrm{d}r}\right)^2\right]^{1/2}}=\frac{p_{\mathrm{O}}-p_{\mathrm{v}}-\rho_{\mathrm{l}}gz}{\gamma_{\mathrm{lv}}}.$$

Here, the external pressure on the melt $p_{\mathrm{v}} = p_{\mathrm{cold}}$ and the internal pressure applied on the liquid, p_{O} is defined as:

$$p_{\mathrm{O}} = p_{\mathrm{hot}} + \rho_{\mathrm{l}} g H_{\mathrm{m}} + \frac{2\gamma_{\mathrm{lv}}}{b},$$

where p_{hot} and p_{cold} are the vapour pressure at the hot and cold sides of the sample and b is the radius of curvature at the apex of the liquid. Thus the Young–Laplace equation can be written as follows:

$$\frac{\dfrac{\mathrm{d}^2 z}{\mathrm{d}r^2}}{\left[1+\left(\dfrac{\mathrm{d}z}{\mathrm{d}r}\right)^2\right]^{3/2}}+\frac{\dfrac{1}{r}\cdot\dfrac{\mathrm{d}z}{\mathrm{d}r}}{\left[1+\left(\dfrac{\mathrm{d}z}{\mathrm{d}r}\right)^2\right]^{1/2}}=\frac{\rho_{\mathrm{l}} g\,(H_{\mathrm{m}}-z)-\Delta p}{\gamma_{\mathrm{lv}}}+\frac{2}{b}, \tag{8.105}$$

where $\Delta p = p_{\mathrm{cold}} - p_{\mathrm{hot}}$ represents the pressure difference between the cold and hot sides of the sample and the term $2/b$ is due to the curvature at the top which depends on the

wetting angle θ and on the crucible radius r_a [Duffar 1997]. Under microgravity this can be written as follows:

$$\frac{1}{b} = -\frac{\cos\theta}{r_a}.$$

What is specific for dewetted Bridgman is that the contribution due to the curvature $2/b$ at the top of the free liquid must be considered in Equation (8.105). It is important to emphasize that for crucibles with a reasonable practical radius (larger than the melt capillary constant), the curvature of the upper free liquid surface is very small in normal gravity conditions, and hence it can be neglected. This is not true in microgravity conditions, which is why these cases are treated separately in what follows.

From the physical point of view, the dewetting phenomenon is governed by the Young–Laplace equation through the Bond (*Bo*), and Laplace (*La*) dimensionless numbers. Thus, using the dimensionless numbers (8.15) obtained by using the ampoule radius r_a as length scale, Equation (8.110) becomes [Epure 2010]:

$$\frac{\dfrac{d^2\tilde{z}}{d\tilde{r}^2}}{\left[1+\left(\dfrac{d\tilde{z}}{d\tilde{r}}\right)^2\right]^{3/2}} + \frac{\dfrac{1}{\tilde{r}}\cdot\dfrac{d\tilde{z}}{d\tilde{r}}}{\left[1+\left(\dfrac{d\tilde{z}}{d\tilde{r}}\right)^2\right]^{1/2}} = \left[Bo\left(\tilde{H}_m - \tilde{z}\right) - La - 2\cos\theta\right], \tag{8.106}$$

where $\tilde{H}_m = H_m/r_a$, $Bo = \rho_l.g\cdot r_a^2/\gamma_{lv}$, and $La = \Delta p\cdot r_a/\gamma_{lv}$.

8.4.1 Zero Gravity

In zero gravity conditions, the dimensionless Young–Laplace equation becomes:

$$\frac{\dfrac{d^2\tilde{z}}{d\tilde{r}^2}}{\left[1+\left(\dfrac{d\tilde{z}}{d\tilde{r}}\right)^2\right]^{3/2}} + \frac{\dfrac{1}{\tilde{r}}\cdot\dfrac{d\tilde{z}}{d\tilde{r}}}{\left[1+\left(\dfrac{d\tilde{z}}{d\tilde{r}}\right)^2\right]^{1/2}} = [-La - 2\cos\theta], \tag{8.107}$$

for which the following wetting boundary condition must be satisfied:

$$\frac{d\tilde{z}}{d\tilde{r}}(1) = \tan\left(\theta - \frac{\pi}{2}\right), \quad \theta \in \left(\frac{\pi}{2}, \pi\right) \tag{8.108}$$

and the choice of axis gives $\tilde{z}(1) = 0$.

Equation (8.107) can be written as

$$\frac{\tilde{r}\cdot\dfrac{d^2\tilde{z}}{d\tilde{r}^2} + \dfrac{d\tilde{z}}{d\tilde{r}}\cdot\left[1+\left(\dfrac{d\tilde{z}}{d\tilde{r}}\right)^2\right]}{\left[1+\left(\dfrac{d\tilde{z}}{d\tilde{r}}\right)^2\right]^{3/2}} = -(La + 2\cos\theta)\cdot\tilde{r}$$

which is equivalent to

$$\frac{\mathrm{d}}{\mathrm{d}\tilde{r}}\left(\frac{\tilde{r}\cdot\frac{\mathrm{d}\tilde{z}}{\mathrm{d}\tilde{r}}}{\sqrt{1+\left(\frac{\mathrm{d}\tilde{z}}{\mathrm{d}\tilde{r}}\right)^2}}\right)=-(La+2\cos\theta)\cdot\tilde{r}.$$

Integrating, we obtain the analytical expression for the derivative of the function $\tilde{z}(\tilde{r})$:

$$\frac{\mathrm{d}\tilde{z}}{\mathrm{d}\tilde{r}}(\tilde{r})=\frac{-\tilde{r}^2\cdot\cos\theta-\tilde{r}^2\cdot(La/2)+c_1}{\sqrt{\tilde{r}^2-\left(-\tilde{r}^2\cdot\cos\theta-\tilde{r}^2\cdot(La/2)+c_1\right)^2}}. \tag{8.109}$$

The constant c_1 is determined from the boundary condition $(\mathrm{d}\tilde{z}/\mathrm{d}\tilde{r})\ (1) = \tan(\theta - \pi/2)$. It follows that

$$\frac{\mathrm{d}\tilde{z}}{\mathrm{d}\tilde{r}}(\tilde{r})=\frac{-\tilde{r}^2\cdot\cos\theta-\tilde{r}^2\cdot(La/2)+(La/2)}{\sqrt{\tilde{r}^2-\left(-\tilde{r}^2\cdot\cos\theta-\tilde{r}^2\cdot(La/2)+(La/2)\right)^2}}. \tag{8.110}$$

Further, the analytical expression of the meniscus can be obtained by integration. The integral can be expressed using elementary functions only in some particular cases.

8.4.1.1 Case I: La = 0, g = 0

Integrating Equation (8.110) gives:

$$\tilde{z}(\tilde{r})=\frac{1}{\cos\theta}\cdot\sqrt{1-\tilde{r}^2\cos^2\theta}+c_2. \tag{8.111}$$

Using the boundary condition $\tilde{z}(1) = 0$, the *analytical expression* of the meniscus surface in *zero gravity* when $La = 0$ is obtained:

$$\tilde{z}(\tilde{r})=\frac{1}{\cos\theta}\cdot\left(\sqrt{1-\tilde{r}^2\cos^2\theta}-\sin\theta\right), \tag{8.112}$$

where $\tilde{r} \in [0, 1]$. Dewetting occurs when the growth angle α is achieved at least at one point on the meniscus surface, i.e. when the equation:

$$\tilde{\phi}(\tilde{r})=(\pi/2)-\alpha \tag{8.113}$$

has at least one solution in the range (0, 1); where $\tilde{\phi}$ is the angle between the plane $\tilde{z}=0$ and the tangent plane to the meniscus. For this angle the equality $\tan\tilde{\phi}=\mathrm{d}\tilde{z}/\mathrm{d}\tilde{r}$ holds, and hence information concerning attainment of the growth angle is given by the equation:

$$\tan\tilde{\phi}=\frac{-\tilde{r}^2\cdot\cos\theta}{\sqrt{\tilde{r}^2-\left(-\tilde{r}^2\cdot\cos\theta\right)^2}}$$

from whence:

$$\sin\tilde{\phi}=-\tilde{r}\cdot\cos\theta \tag{8.114}$$

which is equivalent to

$$\tilde{\phi} = \arcsin(-\tilde{r} \cdot \cos\theta), \tag{8.115}$$

for any $\tilde{r} \in [0, 1]$. What is remarkable is that Equation (8.115) gives a condition for dewetting that depends on the growth angle α and contact angle θ. From the positivity of the derivative

$$\frac{\mathrm{d}\tilde{\phi}}{\mathrm{d}\tilde{r}} = -\frac{\cos\theta}{\sqrt{1-\tilde{r}^2\cos^2\theta}} > 0, \quad \theta \in \left(\frac{\pi}{2}, \pi\right)$$

it follows that the function $\tilde{\phi}(\tilde{r})$ is strictly increasing for $\tilde{r} \in [0, 1]$. Considering this monotonicity and the boundary condition $(\mathrm{d}\tilde{z}/\mathrm{d}\tilde{r})\ (1) = \tan(\theta - \pi/2)$ which is equivalent to $\tilde{\phi}(1) = (\pi/2) - \alpha$, the growth angle $(\pi/2) - \alpha$ can be achieved if $\tilde{\phi}(\tilde{r})$ decreases from $\theta - (\pi/2)$ to $(\pi/2) - \alpha$. This means that $(\pi/2) - \alpha < \theta - (\pi/2)$ and hence $\alpha + \theta > \pi$. In the opposite case, when $\alpha + \theta < \pi$, the growth angle cannot be achieved because of the monotonicity of $\tilde{\phi}(\tilde{r})$.

Assuming that the growth angle can be achieved, i.e. $\alpha + \theta > \pi$, Equations (8.113) and (8.114) give:

$$\sin((\pi/2) - \alpha) = -(1 - \tilde{e}) \cdot \cos\theta$$

where $\tilde{e}$ represents the nondimensional gap thickness and $\tilde{r}_c = 1 - \tilde{e}$ the nondimensional crystal radius. The following *nondimensional gap thickness formula* [Duffar 1997] results:

$$\tilde{e} = \frac{\cos\theta + \cos\alpha}{\cos\theta} \tag{8.116}$$

valid under *zero gravity* conditions, $La = 0$, and $\alpha + \theta > \pi$.

We now have a remarkable new result concerning the meniscus shape. Because $\tan\tilde{\phi} = \mathrm{d}\tilde{z}/\mathrm{d}\tilde{r}$ and $\mathrm{d}\tilde{\phi}/\mathrm{d}\tilde{r} > 0$, the second derivative is:

$$\frac{\mathrm{d}^2\tilde{z}}{\mathrm{d}\tilde{r}^2} = \frac{\mathrm{d}}{\mathrm{d}\tilde{r}}\left(\frac{\mathrm{d}\tilde{z}}{\mathrm{d}\tilde{r}}\right) = \frac{\mathrm{d}}{\mathrm{d}\tilde{r}}\left(\tan\tilde{\phi}\right) = \frac{1}{\cos^2\tilde{\phi}} \cdot \frac{\mathrm{d}\tilde{\phi}}{\mathrm{d}\tilde{r}}.$$

This equation proves that $\mathrm{d}^2\tilde{z}/\mathrm{d}\tilde{r}^2 > 0$, and hence under *zero gravity* and $La = 0$, the *meniscus is globally convex* for any $\tilde{r} \in [0, 1]$.

8.4.1.2 Case II: La ≠ 0, g = 0

To obtain the meniscus equation, Equation (8.110) should be integrated, but if $La \neq 0$ this integral can not be expressed using elementary functions. In order to obtain information about the meniscus shape, attainment of the growth angle, and gap thickness, a qualitative study is necessary.

Introducing $\tan\tilde{\phi} = \mathrm{d}\tilde{z}/\mathrm{d}\tilde{r}$ in Equation (8.110) gives:

$$\sin\tilde{\phi} = -(\cos\theta) \cdot \tilde{r} - \frac{La}{2} \cdot \tilde{r} + \frac{La}{2} \cdot \frac{1}{\tilde{r}}, \tag{8.117}$$

which is equivalent to

$$\tilde{\phi} = \arcsin\left(-(\cos\theta)\cdot\tilde{r} - \frac{La}{2}\cdot\tilde{r} + \frac{La}{2}\cdot\frac{1}{\tilde{r}}\right), \tag{8.118}$$

for any $\tilde{r} \in [0, 1]$. In a similar way to previous calculations, the sign of the derivative $\mathrm{d}\tilde{\phi}/\mathrm{d}\tilde{r}$ will give information about the shape of the meniscus, and about the condition that must be imposed on the sum of the wetting and growth angles to ensure that attainment of the growth angle is feasible. Deriving the relation (8.118) gives:

$$\frac{\mathrm{d}\tilde{\phi}}{\mathrm{d}\tilde{r}} = \left[1\Big/\sqrt{1-\left(-(\cos\theta)\cdot\tilde{r} - \frac{La}{2}\cdot\tilde{r} + \frac{La}{2}\cdot\frac{1}{\tilde{r}}\right)^2}\right]\cdot\left[\left(-\cos\theta - \frac{La}{2}\right)\tilde{r}^2 - \frac{La}{2}\right]\cdot\frac{1}{\tilde{r}^2}. \tag{8.119}$$

The sign of this derivative depends on the sign of the expression depending on $\tilde{r}$ and La:

$$E(\tilde{r}, La) = \left(-\cos\theta - \frac{La}{2}\right)\tilde{r}^2 - \frac{La}{2}. \tag{8.120}$$

The following three cases should be considered:

- If $La \in (-\infty; 0]$, then $E(\tilde{r}, La) > 0$ and hence $\mathrm{d}\tilde{\phi}/\mathrm{d}\tilde{r} > 0$. Moreover,

$$\frac{\mathrm{d}^2\tilde{z}}{\mathrm{d}\tilde{r}^2} = \frac{1}{\cos^2\tilde{\phi}}\cdot\frac{\mathrm{d}\tilde{\phi}}{\mathrm{d}\tilde{r}} > 0,$$

  i.e. the meniscus is globally convex, and the growth angle can be achieved only if $\alpha + \theta > \pi$.
- If $La \in (0; -2\cos\theta)$, then the meniscus changes its curvature (concave to convex) at the point $\tilde{r}_1 = \sqrt{La/(-2\cdot\cos\theta - La)}$, i.e. $E(\tilde{r}_1, La) = 0$, which is equivalent to

$$\frac{\mathrm{d}\tilde{\phi}}{\mathrm{d}\tilde{r}}(\tilde{r}_1) = \frac{\mathrm{d}^2\tilde{z}}{\mathrm{d}\tilde{r}^2}(\tilde{r}_1) = 0,$$

  and the growth angle can be achieved either once or twice, depending on its value.
- If $La \in [-2\cos\theta; +\infty)$, then $E(\tilde{r}, La) < 0$ and hence $\mathrm{d}\tilde{\phi}/\mathrm{d}\tilde{r} < 0$. In this case the meniscus is globally concave, i.e. $\mathrm{d}^2\tilde{z}/\mathrm{d}\tilde{r}^2 < 0$, and the growth angle can be achieved only if $\alpha + \theta < \pi$.

The above ranges for the pressure difference give information about the meniscus shape and the corresponding cases $\alpha + \theta < \pi$ or $\alpha + \theta > \pi$, in which the growth angle can be achieved or, in other words, when dewetting is feasible.

Assuming that La, θ, and α are chosen such that the growth angle can be achieved, the growth angle condition (8.113) is satisfied somewhere along the meniscus. From (8.117):

$$\sin\left(\frac{\pi}{2} - \alpha\right) = -(\cos\theta)\cdot(1-\tilde{e}) - \frac{La}{2}\cdot(1-\tilde{e}) + \frac{La}{2}\cdot\frac{1}{(1-\tilde{e})}, \tag{8.121}$$

from which the following *gap thickness formulas* available in *zero gravity* [Duffar 1997] are obtained:

$$\tilde{e}_1 = \frac{\cos\alpha + 2\cdot\cos\theta + La + \sqrt{\cos^2\alpha + La^2 + 2\cdot La\cdot\cos\theta}}{La + 2\cdot\cos\theta}, \tag{8.122}$$

$$\tilde{e}_2 = \frac{\cos\alpha + 2\cdot\cos\theta + La - \sqrt{\cos^2\alpha + La^2 + 2\cdot La\cdot\cos\theta}}{La + 2\cdot\cos\theta}, \tag{8.123}$$

The gap formula (8.122) is valid when the growth angle is reached on the convex part of the meniscus, and formula (8.123) is valid when attainment of the growth angle takes place on the concave part of the meniscus. More precisely, the numerical results obtained by solving the problem (8.90)–(8.91) by the Runge–Kutta method for InSb crystals grown in zero gravity by the dewetted Bridgman technique (the parameters for InSb are those presented in [Balint 2008, Braescu 2008-2]), confirm the results obtained from the qualitative study:

- If $La \in (-\infty; 0]$, then the meniscus is globally convex and the growth angle can be achieved once. When the growth angle is reached the gap thickness is given by $\tilde{e}_1$, as in (8.122). The numerical results reveal this behaviour for $La = -0.655 \in (-\infty; 0]$ and $\theta + \alpha = 160° + 25° > \pi$, as can be seen in Figure 8.19. The figure shows that the meniscus is globally convex and that the growth angle is achieved. The computed gap thickness $\tilde{e} = 1 - \tilde{r}_{c1} = 1 - 0.97915 = 0.02085$ is equal to the value given by formula (8.122), i.e. $\tilde{e}_1 = 0.02085$.
- If $La \in (0; -2\cos\theta)$, then the meniscus is concave–convex (i.e it has a point of inflexion). If the growth angle is attained on the concave part the gap thickness is given by $\tilde{e}_2$ in (8.123); if on the convex part, the gap thickness is given by $\tilde{e}_1$ in (8.122). The numerical results confirm this behaviour. The menisci are concave–convex and the growth angle can be achieved either once or twice: (a) for $\theta + \alpha = 112° + 25° < \pi$ and $La = 0.105 \in (0; -2\cos\theta) = (0; 0.749)$ the growth angle is not achieved (see Figure

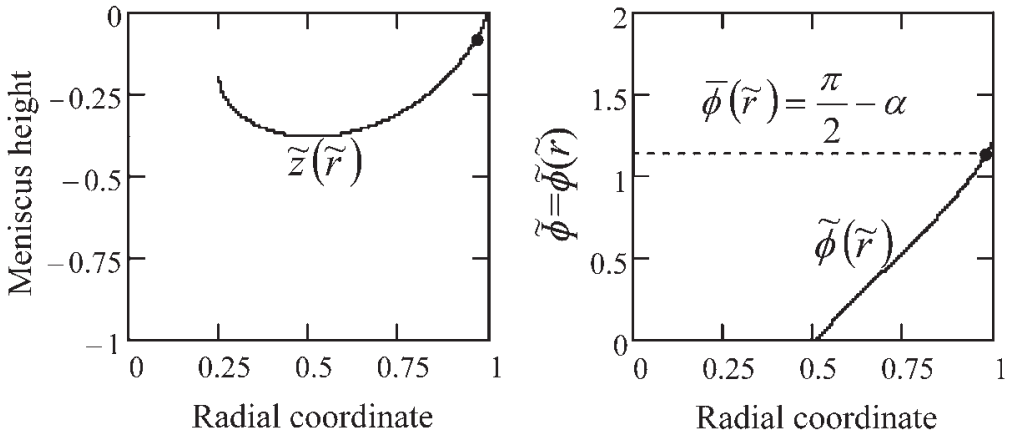

Figure 8.19 *Meniscus shape* z̃(r̃) *and meniscus angle* φ̃(r̃) *corresponding to* La = *–0.655 and* θ + α = *160° + 25° for InSb,* g = *0. The place where the growth angle ((π/2) – α = 1.13446 radians) is reached is shown by the black dot.*

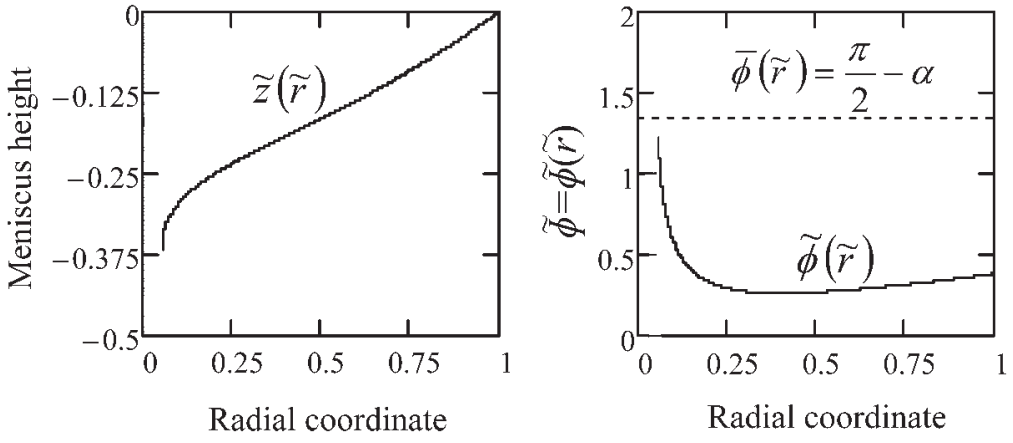

Figure 8.20 *Meniscus shape* $\tilde{z}(\tilde{r})$ *and meniscus angle* $\tilde{\phi}(\tilde{r})$ *corresponding to* La = *0.105 and* $\theta + \alpha = 112° + 25°$ *for InSb,* g = *0. The growth angle cannot be achieved.*

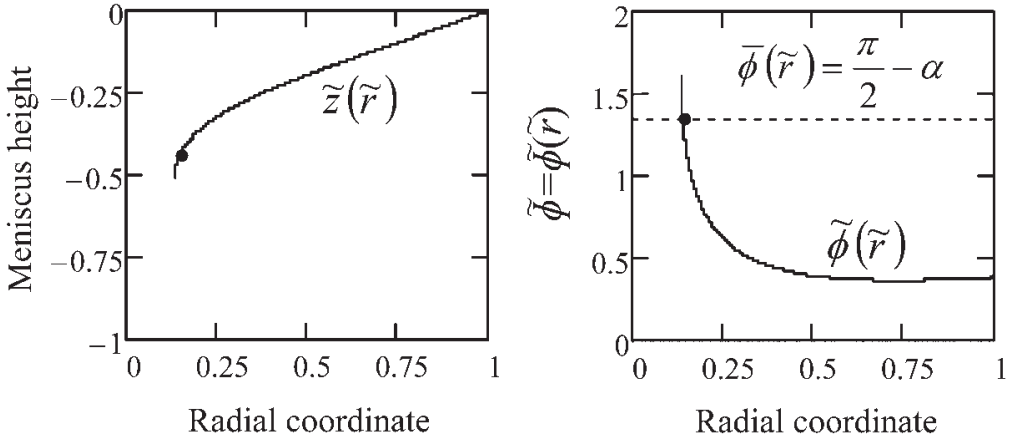

Figure 8.21 *Meniscus shape* $\tilde{z}(\tilde{r})$ *and meniscus angle* $\tilde{\phi}(\tilde{r})$ *corresponding to* La = *0.262 and* $\theta + \alpha = 112° + 25°$ *for InSb,* g = *0. The place where the growth angle* $((\pi/2) - \alpha = 1.13446$ *radians) is achieved is shown by the black dot.*

8.20), but for $La = 0.262 \in (0; 0.749)$ the growth angle is achieved once, as can be seen in Figure 8.21; (b) for $\theta + \alpha = 160° + 25° > \pi$ and $La = 0.393 \in (0; -2\cos\theta) = (0; 1.879)$ the growth angle is achieved twice (Figure 8.22). If the growth angle is achieved on the concave part of the meniscus, then the computed gap thickness in Figure 8.21 $\tilde{e} = 1 - \tilde{r}_{c1} = 1 - 0.1505 = 0.8494$ is equal to $\tilde{e}_2 = 0.8494$ given by (8.123) and in Figure 8.22, $\tilde{e} = 1 - \tilde{r}_{c1} = 1 - 0.2819 = 0.7181$ is equal to $\tilde{e}_2$. If the growth angle is reached on the convex part of the meniscus, then the computed gap thickness $\tilde{e} = 1 - \tilde{r}_{c2} = 1 - 0.9374 = 0.0626$ is equal to $\tilde{e}_1 = 0.0626$ given by (8.122), as can be seen in Figure 8.21.

- If $La \in [-2\cos\theta; +\infty)$, then the meniscus is concave and the growth angle can be achieved once. When the growth angle is attained the gap thickness is given by $\tilde{e}_2$ in (8.123). The numerical results show that the meniscus is concave, and that the growth angle is achieved for $\theta + \alpha = 112° + 25° < \pi$, $La = 0.85 \in [-2\cos\theta; +\infty) = [0.749; +\infty)$ (Figure 8.23). The computed gap thickness $\tilde{e} = 1 - \tilde{r}_{c2} = 1 - 0.4573 = 0.5427$ is equal to $\tilde{e}_2$ as given by (8.123).

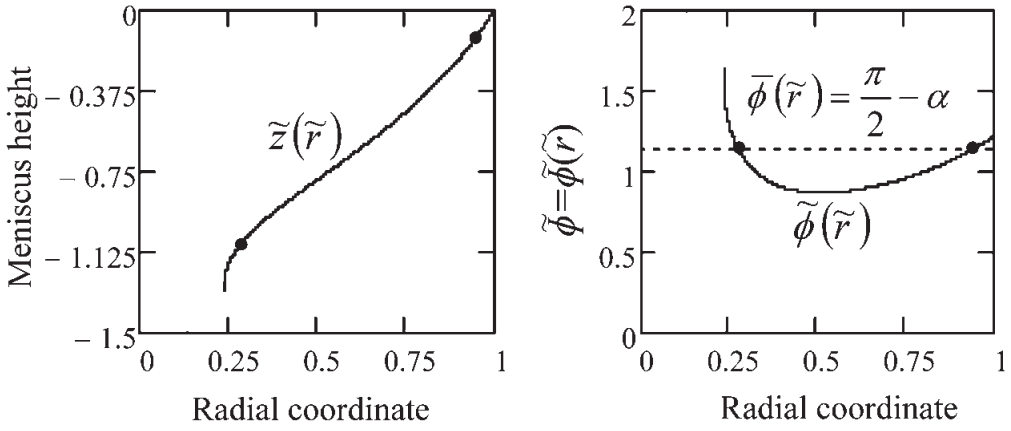

Figure 8.22 *Meniscus shape* $\tilde{z}(\tilde{r})$ *and meniscus angle* $\tilde{\phi}(\tilde{r})$ *corresponding to* La = *0.393 and* $\theta + \alpha = 160° + 25°$ *for InSb,* g = *0. The places where the growth angle* $((\pi/2) - \alpha = 1.13446$ *radians) is achieved are shown by the black dots.*

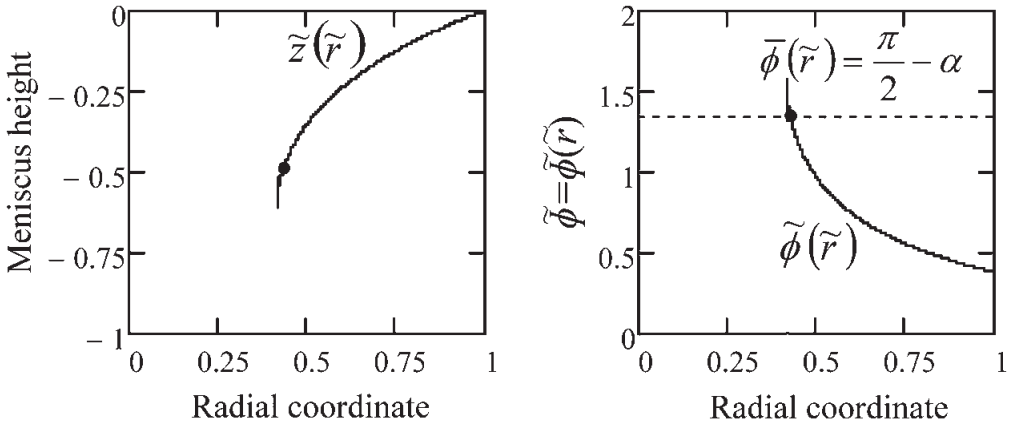

Figure 8.23 *Meniscus* $\tilde{z}(\tilde{r})$ *and meniscus angle* $\tilde{\phi}(\tilde{r})$ *corresponding to* La = *0.85 and* $\theta + \alpha = 112° + 25°$ *for InSb,* g = *0. The place where the growth angle* $((\pi/2) - \alpha = 1.13446$ *radians) is achieved is shown by the black dot.*

8.4.2 Normal Gravity

Under normal gravity conditions, for a crucible radius larger than the capillary constant of the material, the curvature of the upper free liquid surface can be neglected (it is very small), and hence the Young–Laplace equation (8.105) becomes:

$$\frac{\mathrm{d}^2\tilde{z}}{\mathrm{d}\tilde{r}^2} = \left[Bo\cdot\left(\tilde{H}_{\mathrm{m}} - \tilde{z}\right) - La\right]\cdot\left[1+\left(\frac{\mathrm{d}\tilde{z}}{\mathrm{d}\tilde{r}}\right)^2\right]^{3/2} - \frac{1}{\tilde{r}}\left[1+\left(\frac{\mathrm{d}\tilde{z}}{\mathrm{d}\tilde{r}}\right)^2\right]\cdot\frac{\mathrm{d}\tilde{z}}{\mathrm{d}\tilde{r}}, \tag{8.124}$$

where the axisymmetric solution $\tilde{z} = \tilde{z}(\tilde{r})$ has to satisfy the following boundary condition:

$$\frac{\mathrm{d}\tilde{z}}{\mathrm{d}\tilde{r}}(1) = \tan\left(\theta - \frac{\pi}{2}\right), \quad \theta \in \left(\frac{\pi}{2}, \pi\right). \tag{8.125}$$

and, by the choice of origin, $\tilde{z}(1) = 0$.

Using the technique presented in section 8.1, the nonlinear equation (8.124) is transformed into the following nonlinear system of two differential equations:

$$\begin{cases} \dfrac{\mathrm{d}\tilde{z}}{\mathrm{d}\tilde{r}} = \tan\tilde{\phi} \\ \dfrac{\mathrm{d}\tilde{\phi}}{\mathrm{d}\tilde{r}} = \left[Bo\cdot\left(\tilde{H}_{\mathrm{m}} - \tilde{z}\right) - La\right]\cdot\dfrac{1}{\cos\tilde{\phi}} - \dfrac{1}{\tilde{r}}\cdot\tan\tilde{\phi} \end{cases} \tag{8.126}$$

for which the boundary condition (8.125) becomes [Balint 2008, Braescu 2008-2]:

$$\tilde{z}(1) = 0, \quad \tilde{\phi}(1) = \theta - \frac{\pi}{2}; \quad \theta \in \left(\frac{\pi}{2}, \pi\right). \tag{8.127}$$

The functions on the right-hand side of Equations (8.126) are real analytic, i.e. they can be expanded in Taylor series, and the conditions of existence and uniqueness of a solution are satisfied for the problem (8.126)–(8.127). The meniscus shape is described by the solution

$$\tilde{z} = \tilde{z}\left(\tilde{r}; \theta, La, Bo, \tilde{H}_{\mathrm{m}}\right), \quad \tilde{\phi} = \tilde{\phi}\left(\tilde{r}; \theta, La, Bo, \tilde{H}_{\mathrm{m}}\right)$$

which depends on $\tilde{r}$ and on the parameters θ, *La, Bo,* $\tilde{H}_{\mathrm{m}}$. In what follows, this solution is denoted by $\tilde{z} = \tilde{z}(\tilde{r})$, $\tilde{\phi} = \tilde{\phi}(\tilde{r})$.

Because of the high nonlinearity of the problem, *an analytical formula for the meniscus cannot be obtained,* hence analytical and numerical studies of meniscus shapes are necessary. With this aim, the dependence of meniscus shape on the pressure difference will be established, and inequalities of the pressure intervals which assure the feasibility of dewetting will be determined.

Because of the different behaviours of the meniscus shape in the cases $\alpha + \theta < \pi$, and $\alpha + \theta > \pi$, as already shown in zero gravity, qualitative studies will be performed on each case separately. Recent experimental developments [Sylla 2008–1], confirmed by thermodynamic analysis [Sylla 2008–2], show that contamination of the system during the growth process may greatly increase the wetting angle, leading to an unexpected inequality between the wetting angle θ and growth angle α, i.e. $\alpha + \theta > \pi$.

8.4.2.1 Case I: $\alpha + \theta < \pi$

In order to make a qualitative study of the meniscus shape (convex, concave–convex, convex–concave, concave) as a function of the Laplace number, the function $\tilde{z} = \tilde{z}(\tilde{r})$ is approximated by a Taylor polynomial of third degree $T^3_{\tilde{z}}(\tilde{r})$ in the neighbourhood of $\tilde{r} = 1$. To establish the inequalities of the pressure intervals (i.e. *La* numbers) which assure the feasibility of dewetting, the information obtained from Taylor approximation (approximate meniscus) will be combined with properties deduced from the problem (8.126)–(8.127) which describes the shape of the real meniscus. Thus, approximating the function $\tilde{z} = \tilde{z}(\tilde{r})$ by a Taylor polynomial of third degree $T^3_{\tilde{z}}(\tilde{r})$ in the neighbourhood of $\tilde{r} = 1$, accurate qualitative results are obtained only in a sufficiently small neighbourhood of r_{a}. The third-order Taylor polynomial $T^3_{\tilde{z}}(\tilde{r})$ which approximates the meniscus surface $\tilde{z} = \tilde{z}(\tilde{r})$ is given by:

$$T_{\tilde{z}}^{3}(\tilde{r}) = \tilde{z}'(1)\cdot(\tilde{r}-1) + \frac{\tilde{z}''(1)}{2}\cdot(\tilde{r}-1)^2 + \frac{\tilde{z}'''(1)}{6}\cdot(\tilde{r}-1)^3 \tag{8.128}$$

where $\tilde{z}'(1)$, $\tilde{z}''(1)$, $\tilde{z}'''(1)$ represent the first-, second- and third-order derivatives of the function $\tilde{z} = \tilde{z}(\tilde{r})$ at $\tilde{r} = 1$, and are obtained from the system (8.126) and boundary conditions (8.127) as follows [Braescu 2008-2]:

$$\tilde{z}'(1) = A_{\tilde{z}}^{1} = -\frac{\cos\theta}{\sin\theta}, \tag{8.129}$$

$$\tilde{z}''(1) = -A_{\tilde{z}}^{2}\cdot La + B_{\tilde{z}}^{2} = -\frac{1}{\sin^3\theta}\cdot La + \frac{\cos\theta}{\sin^3\theta} + \frac{Bo\cdot\tilde{H}_{\mathrm{m}}}{\sin^3\theta}, \tag{8.130}$$

$$\begin{aligned}\tilde{z}'''(1) &= A_{\tilde{z}}^{3}\cdot La^2 - B_{\tilde{z}}^{3}\cdot La + C_{\tilde{z}}^{3}\\ &= -\frac{3\cdot\cos\theta}{\sin^5\theta}La^2 + \left(\frac{6\cdot\cos^2\theta}{\sin^5\theta} + \frac{1}{\sin^3\theta} + \frac{6\cdot Bo\cdot\tilde{H}_{\mathrm{m}}\cdot\cos\theta}{\sin^5\theta}\right)La\\ &\quad + \frac{1}{\sin^3\theta}\cdot\left[-\frac{3\cdot Bo^2\cdot\tilde{H}_{\mathrm{m}}^2\cdot\cos\theta}{\sin^2\theta} - \frac{3\cdot\cos^3\theta}{\sin^2\theta} - 2\cdot\cos\theta + \frac{Bo\cdot\cos\theta}{\sin\theta}\right.\\ &\quad \left. - \frac{6\cdot Bo\cdot\tilde{H}_{\mathrm{m}}\cdot\cos^2\theta}{\sin^2\theta} - Bo\cdot\tilde{H}_{\mathrm{m}}\right].\end{aligned} \tag{8.131}$$

The concavity or convexity of the meniscus $\tilde{z} = \tilde{z}(\tilde{r})$ in a sufficiently small neighbourhood of 1 is given by the sign of the second derivative of the approximated meniscus $\tilde{z}_T(\tilde{r}) = T_{\tilde{z}}^{3}(\tilde{r})$:

$$\begin{aligned}\frac{\mathrm{d}^2T_{\tilde{z}}^{3}}{\mathrm{d}\tilde{r}^2} &= -A_{\tilde{z}}^{2}\cdot La + B_{\tilde{z}}^{2} + \left[A_{\tilde{z}}^{3}\cdot La^2 - B_{\tilde{z}}^{3}\cdot La + C_{\tilde{z}}^{3}\right]\cdot(\tilde{r}-1)\\ &= E_{\tilde{z}}^{2} + E_{\tilde{z}}^{3}\cdot(\tilde{r}-1).\end{aligned} \tag{8.132}$$

The sets of *La* values that define convex, concave–convex, convex–concave and concave shapes of the approximated menisci are determined by the following inequalities:

- if $E_{\tilde{z}}^{2} > 0$ and $E_{\tilde{z}}^{4} < 0$ (or $E_{\tilde{z}}^{2} > 0$ and $E_{\tilde{z}}^{4} > 1$), then the approximated meniscus is convex;
- if $E_{\tilde{z}}^{2} > 0$ and $0 < E_{\tilde{z}}^{4} < 1$, then the approximated meniscus is concave–convex;
- if $E_{\tilde{z}}^{2} < 0$ and $0 < E_{\tilde{z}}^{4} < 1$, then the approximated meniscus is convex–concave;
- if $E_{\tilde{z}}^{2} < 0$ and $E_{\tilde{z}}^{4} < 0$ (or $E_{\tilde{z}}^{2} < 0$ and $E_{\tilde{z}}^{4} > 1$), then the approximated meniscus is concave;

where $E_{\tilde{z}}^{4} = 1 - \left(E_{\tilde{z}}^{2}/E_{\tilde{z}}^{3}\right)$.

Dewetting occurs if the growth angle α is achieved at some point in the interval (0, 1), which is given by the solution of the equation:

$$\tilde{\phi}(\tilde{r}) = \frac{\pi}{2} - \alpha \quad \text{or} \quad \frac{\mathrm{d}T_{\tilde{z}}^{3}}{\mathrm{d}\tilde{r}} = \tan\left(\frac{\pi}{2} - \alpha\right). \tag{8.133}$$

Because $\alpha + \theta < \pi$, the boundary condition for $\tilde{\phi}(\tilde{r})$ shows that the growth angle $(\pi/2) - \alpha$ can be achieved only if $\tilde{\phi}(\tilde{r})$ decreases, i.e. $\mathrm{d}\tilde{\phi}/\mathrm{d}\tilde{r} < 0$. On the other hand,

$$\frac{\mathrm{d}\tilde{\phi}}{\mathrm{d}\tilde{r}}(1) = E_{\tilde{z}}^2 \cdot \sin^2(\theta) \quad \text{and} \quad \frac{\mathrm{d}^2 T_{\tilde{z}}^3}{\mathrm{d}\tilde{r}^2}(1) = E_{\tilde{z}}^2.$$

Hence, if $\tilde{\phi}(\tilde{r})$ decreases then

$$\frac{\mathrm{d}^2 T_{\tilde{z}}^3}{\mathrm{d}\tilde{r}^2}(1) = E_{\tilde{z}}^2 < 0$$

and the real meniscus should be concave in the neighbourhood of 1. For this reason, in what follows special attention is paid to the convex–concave (S-shaped), and concave meniscus shapes. Moreover, the inequality $E_{\tilde{z}}^2 > 0$, which appears in both cases, gives the values of *La* resulting in a concave meniscus at 1:

$$La > \frac{B_{\tilde{z}}^2}{A_{\tilde{z}}^2} = \cos\theta + Bo \cdot \tilde{H}_{\mathrm{m}}. \tag{8.134}$$

The inequality (8.134) states that the gas pressure difference should be larger than the hydrostatic pressure plus a term which depends on the capillary parameters.

For certain values of *La*, the growth angle can be achieved twice for a convex–concave approximated meniscus (Equation (8.133) has two solutions), and once for a concave approximated meniscus (Equation (8.133) has one solution). These values of *La* are given by the following statements (for details see [Braescu 2008-2]):

- *Statement 1:* The set of *La* values for which the growth angle α can be achieved once on the approximated meniscus is defined by the inequality:

$$F_{\tilde{z}}^1 = \left(A_{\tilde{z}}^1 - \frac{\cos\alpha}{\sin\alpha}\right) \cdot \left[\frac{1}{2} \cdot E_{\tilde{z}}^3 - E_{\tilde{z}}^2 + A_{\tilde{z}}^1 - \frac{\cos\alpha}{\sin\alpha}\right] < 0. \tag{8.135}$$

- *Statement 2:* The set of *La* values for which the growth angle α can be achieved twice in the interval (0, 1) on the approximated meniscus is defined by the following inequalities:

$$F_{\tilde{z}}^2 = \left(E_{\tilde{z}}^2\right)^2 - 2 \cdot E_{\tilde{z}}^3 \cdot \left(A_{\tilde{z}}^1 - \frac{\cos\alpha}{\sin\alpha}\right) > 0, \tag{8.136}$$

$$F_{\tilde{z}}^3 = \frac{A_{\tilde{z}}^1 - \dfrac{\cos\alpha}{\sin\alpha}}{E_{\tilde{z}}^3} > 0, \tag{8.137}$$

$$F_{\tilde{z}}^4 = \frac{F_{\tilde{z}}^1}{F_{\tilde{z}}^3} > 0, \tag{8.138}$$

$$F_{\tilde{z}}^5 = \frac{E_{\tilde{z}}^2}{E_{\tilde{z}}^3} \in (0, 1). \tag{8.139}$$

- *Statement 3:* For $\alpha + \theta < \pi$:

(i) If the real meniscus is concave at 1, then $La > Bo \cdot \tilde{H}_m + \cos\theta$;
(ii) If the real meniscus is convex at the triple point r_c in which the growth angle is achieved, then $La < Bo \cdot (\tilde{H}_m - \tilde{h}) - \cos\alpha$.

Inequalities (i) and (ii) define the interval La_I for which dewetted Bridgman growth is feasible with a convex–concave (S-shaped) meniscus. Moreover they show that the value $La_{(concave)}$ for which the meniscus is concave can be deduced from the pressure difference values $La_{(convex–concave)}$ for which the meniscus is S-shaped.

The range La_I can be refined by using the approximation $\tilde{\phi}_T(\tilde{r})$ of the function $\tilde{\phi}(\tilde{r})$, and the condition for attainment of the growth angle on the approximate meniscus $\tilde{z}_T(\tilde{r})$.

- *Statement 4:* A refined range La^{approx} of the interval La_I, for which dewetted Bridgman with convex–concave meniscus is feasible and the growth angle is achieved, is determined by the following inequalities:

(i) $Bo \cdot \tilde{H}_m + \cos\theta < La < Bo \cdot (\tilde{H}_m - \tilde{h}) - \cos\alpha$,

(ii) $F_{\tilde{z}}^1(La) = \left(A_{\tilde{z}}^1 - \frac{\cos\alpha}{\sin\alpha}\right) \cdot \left[\frac{1}{2} \cdot E_{\tilde{z}}^3 - E_{\tilde{z}}^2 + A_{\tilde{z}}^1 - \frac{\cos\alpha}{\sin\alpha}\right] < 0$,

(iii) $Bo \cdot (\tilde{H}_m - \tilde{h}) - \frac{\cos\alpha}{\tilde{r}_1(La)} > La$,

where $\tilde{r}_1$ (La) represents the real root of the equation

$$\frac{1}{2} \cdot E_{\tilde{z}}^3 - E_{\tilde{z}}^2 + A_{\tilde{z}}^1 - \frac{\cos\alpha}{\sin\alpha} = 0$$

and is in (0, 1) [Braescu 2008-2].

Inequalities (i) are related to the shape of the meniscus: concave at 1 and convex later. The inequality (ii) $F_{\tilde{z}}^1(La) < 0$ indicates that the growth angle α is achieved once on the approximated meniscus. Inequality (iii) shows that in $\tilde{r}_1$ (La) the approximated meniscus is convex.

In the following, numerical results are obtained by solving the problem (8.126)–(8.127) for InSb crystals grown in normal gravity by the dewetted Bridgman process [Balint 2008, Braescu 2008-2].

Inequalities (i)–(ii), from Statement 4 give the *La* range [51.353; 52.617]. Through inequality (iii) this is refined to La^{approx} = [51.353; 52.589] which represents the range of the Laplace number for which dewetted Bridgman growth with a convex–concave meniscus is possible and where the growth angle is achieved. Numerically integrating the system (8.126)–(8.127) for different values of the *La* from the refined range La^{approx}, gives La^{real} = [51.726; 52.458] which represents the real range of the pressure difference that gives a convex–concave real meniscus where the growth angle is attained twice (Figure 8.24). If $La^{real} \geq 52.46$ then the real meniscus is concave and the growth angle is achieved only once, as can be seen in Figure 8.25.

Figures 8.24 and 8.25 show that the approximated meniscus given by the third-degree Taylor polynomial $T_{\tilde{z}}^3(\tilde{r})$ is accurate only in the neighbourhood of 1. However, experimental values of the gap thickness are always much smaller than 1 mm (see Chapter 6). The points marked on the figures represent the points at which the growth angle is achieved.

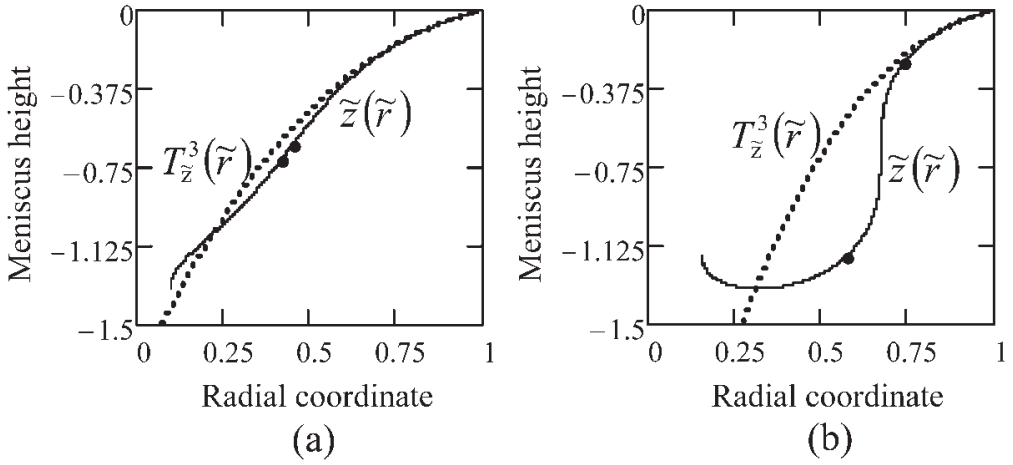

Figure 8.24 *Approximated menisci* $T_{\tilde{z}}^3(\tilde{r})$ *(dotted line) and real (numerical) convex–concave menisci* $\tilde{z}(\tilde{r})$ *corresponding to* La = *51.726 (a) and* La = *52.446 (b) for InSb,* $\tilde{H}_m = 10.9$. *The places where the growth angle* $((\pi/2) - \alpha = 1.13446$ *radians) is achieved are shown by the black dots.*

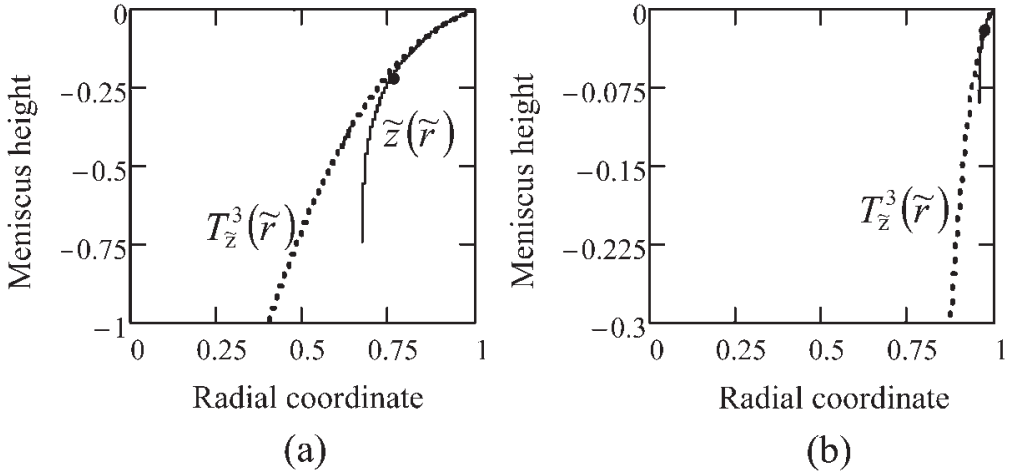

Figure 8.25 *Approximated menisci* $T_{\tilde{z}}^3(\tilde{r})$ *(dotted line) and real (numerical) concave menisci* $\tilde{z}(\tilde{r})$ *corresponding to* La = *52.46 (a) and* La = *64.167 (b) for InSb,* $\tilde{H}_m = 10.9$. *The places where the growth angle* $((\pi/2) - \alpha = 1.13446$ *radians) is achieved are shown by the black dots.*

8.4.2.2 Case II: $\alpha + \theta > \pi$

During the growth process of classical semiconductors grown in uncoated ampoules (i.e. $\alpha + \theta < \pi$), contamination of the system may greatly increase the wetting angle, leading to an unexpected sum of the wetting angle θ and growth angle α, i.e. $\alpha + \theta > \pi$. For this reason, the dependence of the meniscus shape on the pressure difference is studied, in order to get conditions that allow dewetting for classical semiconductors grown in uncoated crucibles with contamination (or in coated crucibles). To study the meniscus shape qualitatively as a function of the Laplace number, only the properties obtained from the problem (8.126)–(8.127) are used. In the case $\alpha + \theta > \pi$, the meniscus height increases

if *La* increases, hence the Taylor polynomial approximations cannot be used because they are valid only in a small neighbourhood of 1 (this is the opposite behaviour to the previous case $\alpha + \theta < \pi$, where increasing *La* leads to a decrease of the meniscus).

Thus, considering the inequality $\alpha + \theta > \pi$ and boundary condition for $\tilde{\phi}(\tilde{r})$, $\tilde{\phi}(1) = \theta - (\pi/2)$, it follows that the growth angle $(\pi/2) - \alpha$ can be achieved if $\tilde{\phi}(\tilde{r})$ decreases from $\theta - (\pi/2)$ to $(\pi/2) - \alpha$, i.e. $\mathrm{d}\tilde{\phi}/\mathrm{d}\tilde{r} > 0$. On the other hand, from Equations (8.126):

$$\frac{\mathrm{d}\tilde{\phi}}{\mathrm{d}\tilde{r}}(1) = \left[Bo \cdot \left(\tilde{H}_{\mathrm{m}} - \tilde{z}(1)\right) - La\right] \cdot \frac{1}{\cos\tilde{\phi}(1)} - \frac{1}{\tilde{r}} \cdot \tan\tilde{\phi}(1),$$

and using the boundary conditions $\tilde{z}(1) = 0$, $\tilde{\phi}(1) = \theta - (\pi/2)$, gives:

$$\frac{\mathrm{d}\tilde{\phi}}{\mathrm{d}\tilde{r}}(1) = \frac{1}{\sin\theta}\left[Bo \cdot \tilde{H}_{\mathrm{m}} - La + \cos\theta\right]. \tag{8.140}$$

As $\mathrm{d}\tilde{\phi}/\mathrm{d}\tilde{r}(1) > 0$, the following inequality for the pressure difference is obtained:

$$La < Bo \cdot \tilde{H}_{\mathrm{m}} + \cos\theta, \tag{8.141}$$

for which the growth angle can be achieved.

Concerning the meniscus shape, because

$$\frac{\mathrm{d}^2\tilde{z}}{\mathrm{d}\tilde{r}^2}(1) = \frac{1}{\cos^2\tilde{\phi}(1)} \cdot \frac{\mathrm{d}\tilde{\phi}}{\mathrm{d}\tilde{r}}(1),$$

$\mathrm{d}^2\tilde{z}/\mathrm{d}\tilde{r}^2 > 0$ in the neighbourhood of 1, which means that the growth angle can be achieved if the meniscus is convex in the neighbourhood of 1.

Then, for a pressure difference which satisfies the inequality (8.141) the meniscus is convex in the neighbourhood of 1 (this includes globally convex or concave–convex menisci), and the growth angle can be achieved.

Numerical results obtained by solving the problem (8.126)–(8.127) for InSb crystals grown on the ground by the dewetted Bridgman process for high apparent wetting angle (i.e. the contamination case $\theta + \alpha = 160^\circ + 25^\circ > \pi$) prove that if the pressure difference satisfies the inequality (8.141), i.e. $La < 49.794$, then the meniscus is globally convex (Figure 8.26) or concave–convex (see Figure 8.27; it is difficult to see this shape on the figure, but it can be seen in the numerical results) and the growth angle is achieved once.

Further, there are cases in which the meniscus is concave at 1 and the growth angle can be achieved. There are two possible situations: (i) convex–concave meniscus, and (ii) globally concave meniscus.

For the *convex–concave meniscus* there is a point of inflexion $\tilde{r}_{\mathrm{I}}$, i.e. $(\mathrm{d}^2\tilde{z}/\mathrm{d}\tilde{r}^2)(\tilde{r}_{\mathrm{I}}) = 0$. This condition implies that $\left(\mathrm{d}\tilde{\phi}/\mathrm{d}\tilde{r}\right)(\tilde{r}_{\mathrm{I}}) = 0$ because

$$\frac{\mathrm{d}^2\tilde{z}}{\mathrm{d}\tilde{r}^2} = \frac{1}{\cos^2\tilde{\phi}} \cdot \frac{\mathrm{d}\tilde{\phi}}{\mathrm{d}\tilde{r}}.$$

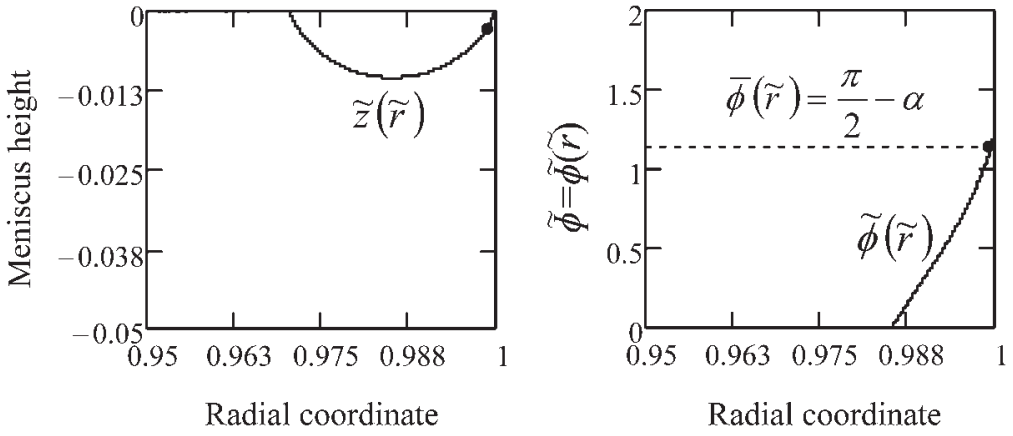

Figure 8.26 *Meniscus shape* $\tilde{z}(\tilde{r})$ *and meniscus angle* $\tilde{\phi}(\tilde{r})$ *corresponding to* La = −13.095 *and* $\theta + \alpha = 160° + 25° > \pi$ *for InSb,* $\tilde{H}_m = 10.9$. *The place where the growth angle* ($(\pi/2) - \alpha = 1.13446$ *radians) is reached is shown by the black dot.*

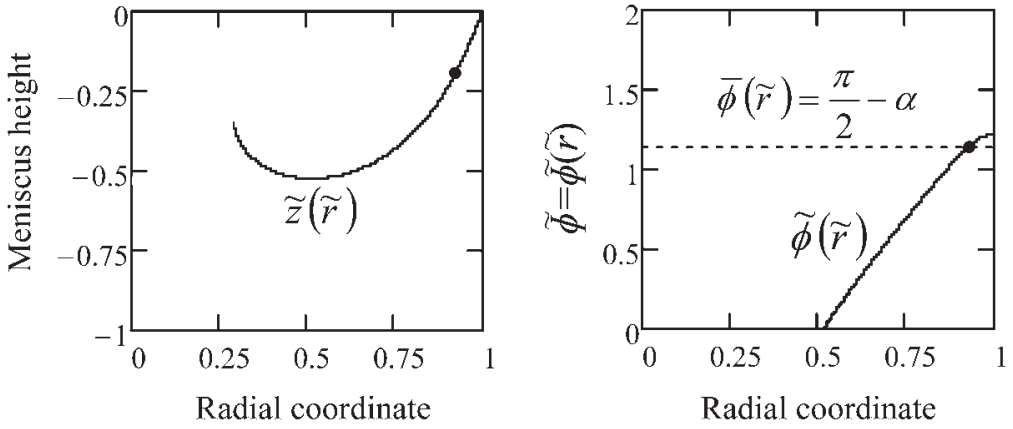

Figure 8.27 *Meniscus* $\tilde{z}(\tilde{r})$ *and meniscus angle* $\tilde{\phi}(\tilde{r})$ *corresponding to* La = 49.788 *and* $\theta + \alpha = 160° + 25° > \pi$ *for InSb,* $\tilde{H}_m = 10.9$. *The place where the growth angle* ($(\pi/2) - \alpha = 1.13446$ *radians) is achieved is shown by the black dot.*

Because the meniscus is concave at 1, i.e. $d\tilde{\phi}/d\tilde{r} < 0$ in the neighbourhood of 1, the meniscus is concave for $\tilde{r} \in [\tilde{r}_I; 1]$ and the function $\tilde{\phi}(\tilde{r})$ decreases. Attainment of the growth angle may be possible on the convex meniscus, i.e. on the left side of $\tilde{r}_I$ the meniscus is convex and $d\tilde{\phi}/d\tilde{r} > 0$. This proves that the growth angle can be achieved if the function $\tilde{\phi}(\tilde{r})$ is concave and its maximum is $(\tilde{r}_I; \tilde{\phi}(\tilde{r}_I))$. This gives a condition on the second derivative $\left(d^2\tilde{\phi}/d\tilde{r}^2\right)(\tilde{r}) < 0$ for $\tilde{r} \in (\tilde{r}_I - \varepsilon; \tilde{r}_I + \varepsilon)$. Thus, deriving the second equation

$$\frac{d\tilde{\phi}}{d\tilde{r}} = \left[Bo \cdot \left(\tilde{H}_m - \tilde{z}\right) - La\right] \cdot \frac{1}{\cos\tilde{\phi}} - \frac{1}{\tilde{r}} \cdot \tan\tilde{\phi}$$

from Equations (8.126), and replacing $\tilde{r}$ by $\tilde{r}_I$, we get:

$$\frac{d^2\tilde{\phi}}{d\tilde{r}^2}(\tilde{r}_I) = \left(\frac{1}{\tilde{r}_I^2} - Bo \cdot \frac{1}{\cos\tilde{\phi}(\tilde{r}_I)}\right) \cdot \tan\tilde{\phi}(\tilde{r}_I) \qquad (8.142)$$

which must be negative. As $\tilde{\phi}(\tilde{r}_1) \in (\theta - (\pi/2); (\pi/2))$ and $\tilde{r}_1 < 1$, from (8.142) we have that $\tilde{r}_1 > \sqrt{(1/Bo) \cdot \sin\theta}$, which gives the following limit for the ampoule radius:

$$1 > \sqrt{(1/Bo) \cdot \sin\theta}. \tag{8.143}$$

Moreover, since $\left(d\tilde{\phi}/d\tilde{r}\right)(\tilde{r}_1) = 0$ the following inequality for the pressure difference is obtained:

$$La < Bo \cdot \tilde{H}_m - Bo \cdot z(r_1). \tag{8.144}$$

Here $\tilde{z}(\tilde{r}_1)$ is unknown but $\tilde{z}(\tilde{r}_1) < 0$, and hence if

$$La < Bo \cdot \tilde{H}_m \tag{8.145}$$

then inequality (8.144) is always satisfied.

In conclusion, for a convex–concave meniscus, the growth angle can be achieved (the crystal can be obtained) if inequalities (8.143) and (8.145) are satisfied. In practice, it is not certain whether the growth angle is always attained; this depends on the material and process parameters.

Numerical results obtained by solving the problem (8.126)–(8.127) for InSb crystals grown under normal gravity by the dewetted Bridgman process for the case $\theta + \alpha = 160° + 25° > \pi$, show that if $La = 50.679 < Bo \cdot \tilde{H}_m = 50.733$ and $1 > \sqrt{(1/Bo) \cdot \sin\theta} = 0.271$, then the meniscus is convex–concave and the growth angle is achieved on the convex part of the meniscus (Figure 8.28).

For the globally concave meniscus $d\tilde{\phi}/d\tilde{r} < 0$, and hence the function $\tilde{\phi}(\tilde{r})$ decreases on the interval (0; 1); because $(\pi/2) - \alpha < \theta - (\pi/2)$ the growth angle cannot be achieved on the globally concave meniscus. Numerical results show that for $La = 51.504 > Bo \cdot \tilde{H}_m = 50.733$ Pa the meniscus is globally concave and the growth angle is not achieved (Figure 8.29).

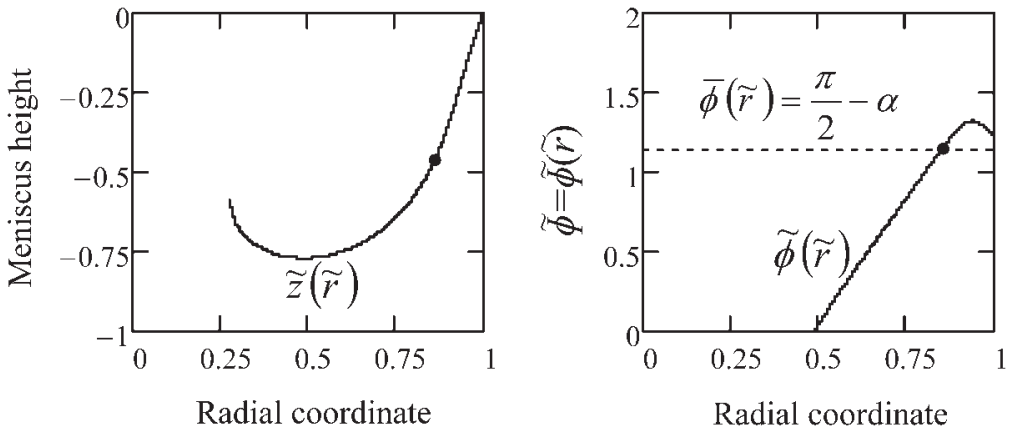

Figure 8.28 *Convex–concave meniscus shape $\tilde{z}(\tilde{r})$ and meniscus angle $\tilde{\phi}(\tilde{r})$ corresponding to* La = *50.679 and* $\theta + \alpha = 160° + 25° > \pi$ *for InSb,* $\tilde{H}_m$ = *10.9. The place where the growth angle ((*$\pi/2$*) −* α = *1.13446 radians) is reached is shown by the black dot.*

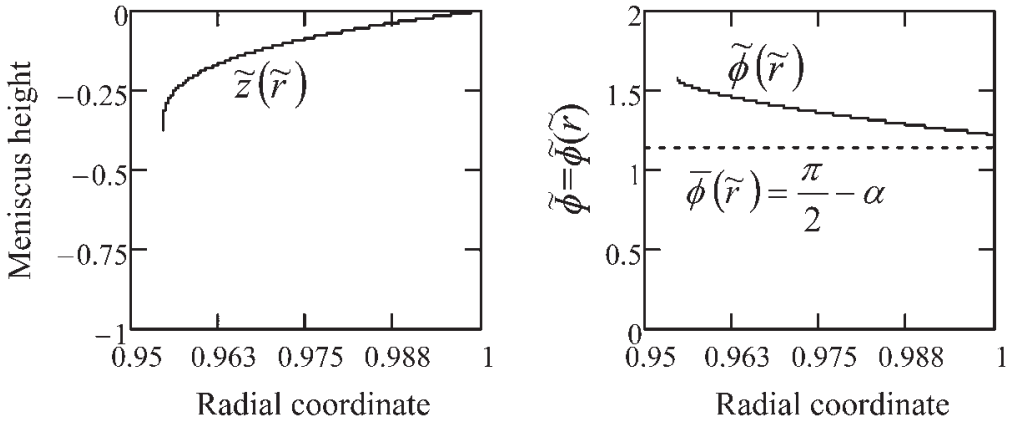

Figure 8.29 *Globally concave meniscus shape* $\tilde{z}(\tilde{r})$ *and meniscus angle* $\tilde{\phi}(\tilde{r})$ *corresponding to* La = *51.504 and* $\theta + \alpha = 160° + 25° > \pi$ *for InSb,* $\tilde{H}_m = 10.9$. *The growth angle* ($(\pi/2) - \alpha = 1.13446$ *radians) cannot be achieved.*

The above analytical and numerical studies of meniscus shapes were performed in order to derive the conditions which allow dewetting and lead to a crystal with a constant radius under normal gravity. The results are useful for *in situ* control of the process and show the importance of a careful calculation of the meniscus shapes for the optimization of stable dewetted Bridgman growth.

8.5 Conclusions

In this chapter, mathematical and numerical analyses of the BVP for the Young–Laplace equation have been presented as an essential part of capillarity problems and processes. First, a mathematical formulation of the capillary problem and the BVP for the Young–Laplace equation in the three-dimenional and axisymmetric cases was presented.

After that, the problems were formulated for the Cz, EFG and dewetted Bridgman growth techniques. For the configurations and specific boundary conditions considered, analytical solutions of the meniscus were found in some special cases. Due to the high nonlinearity of these problems in general cases, the solutions were approached qualitatively and proved by numerical computations using the Runge–Kutta method. From these analytical and numerical studies, information useful for practical crystal growers was reported: meniscus shapes for different growth conditions, the range of some parameters for which the growth angle is achieved (i.e. a crystal is obtained), the dependencies between the meniscus height and the crystal thickness. A relevant computer program (in Mathcad) is presented in the Appendix .

Because of the nonlinearity of the Young–Laplace equation, no simple solution of the problem exists in most cases. It is always necessary to perform a qualitative analysis, which is problem dependent. After that a numerical solution can be sought. However, as shown for the Cz technique, there are configurations for which no exact solution is available.

Appendix: Runge–Kutta Methods

The Runge–Kutta methods are single-step methods which approximate solutions of first-order differential equations (or systems) with given initial conditions. They are based on the Taylor series method in which derivatives are approximated by the forward difference and at the same time, keep the desirable property of higher-order local truncation error [Braescu 2008–1]. These facts imply a better convergence to the solution.

In practice, there are some particular forms of the Runge–Kutta method: the second-order method RK2, the third-order method RK3, the fourth-order (standard) method RK4 and the fifth-order Runge–Kutta–Fehlberg method RKF5. The RK4 method is discussed in more details in the next section, as it is the most commonly used.

A.1 Fourth-Order Runge–Kutta Method (RK4)

Considering the initial value problem:

$$y'(x) = f(x, y)$$
$$y(x_0) = y_0$$

where f:$(a;\ b) \times (c;\ d) \to \mathbb{R}$ is an indefinite derivable function and $x_0 \in (a;\ b)$, $y_0 \in (c;\ d)$. The solution $y(x)$ of IVP can be computed numerically using RK4 method along the interval $[x_0; x_N]$ which is divided in N equidistant subintervals. The RK4 method for this problem is summarized by the following equation with differences:

$$y_i = y_{i-1} + \frac{1}{6}(k_1 + 2k_2 + 2k_3 + k_4),\ i = 1, \ldots, N$$

where $x_i = x_{i-1} + h$, $i = 1, \ldots, N$, h represents the step-size (equidistant nodes are considered), $h = \dfrac{x_N - x_0}{N}$; x_N is the end value of the interval; x_0 is the first value of the interval, N represents the number of the solution values in the interval $[x_0, x_N]$; y_i is the approximation of $y(x_i)$; and …

$$k_1 = h \cdot f(x_{i-1}, y_{i-1}),$$
$$k_2 = h \cdot f\left(x_{i-1} + \frac{h}{2}, y_{i-1} + \frac{k_1}{2}\right),$$
$$k_3 = h \cdot f\left(x_{i-1} + \frac{h}{2}, y_{i-1} + \frac{k_2}{2}\right),$$
$$k_4 = h \cdot f(x_{i-1} + h, y_{i-1} + k_3).$$

Thus the current value y_i is determined by the previous value y_{i-1}, to which is added an estimated slope $\frac{1}{6}(k_1 + 2k_2 + 2k_3 + k_4)$ which represents the weighted average of slopes:

- k_1 is the slope at the beginning of the interval;
- k_2 is the slope at the midpoint of the interval, using the slope k_1 for determining the value of y at the point $x_{i-1} + (h/2)$ by Euler's method (first-order Runge–Kutta method);

- k_3 is the slope at the midpoint of the interval, but now using the slope k_2 for determining the value of y at the point $x_{i-1} + (h/2)$ by Euler's method;
- k_4 is the slope at the end of the interval with its y-value predicted by k_3.

In summary, each value of k_i gives an estimate of the size of the y-jump made by the actual solution across the whole width of the interval. The first one uses Euler's method, the next two use estimates of the solution slope at the midpoint, and the last one uses an estimate of the slope at the endpoint. Each k_i uses the earlier k_i as a basis for its prediction of the y-jump. The local truncation error for RK4 is of the order $O(h^5)$.

A.1.1 RK4 Procedure

Input *a, b, c, N, f // a, b, c* are the problem-dependent values of x_0, x_N and y_0//.

Runge–Kutta4(c, a, b, N, f)

$$
\begin{array}{l}
x_0 \leftarrow a \\
x_N \leftarrow b \\
y_0 \leftarrow c \\
h \leftarrow \dfrac{|x_N - x_0|}{N} \\
for\ i \in 1\,..\,N \\
\quad k_1 \leftarrow h \cdot f(x_{i-1}, y_{i-1}) \\
\quad k_2 \leftarrow h \cdot f\left(x_{i-1} + \dfrac{h}{2}, y_{i-1} + \dfrac{k_1}{2}\right) \\
\quad k_3 \leftarrow h \cdot f\left(x_{i-1} + \dfrac{h}{2}, y_{i-1} + \dfrac{k_2}{2}\right) \\
\quad k_4 \leftarrow h \cdot f(x_{i-1} + h, y_{i-1} + k_3) \\
\quad y_i \leftarrow y_{i-1} + \dfrac{1}{6}(k_1 + 2k_2 + 2k_3 + k_4) \\
\quad y_i \leftarrow y_{i-1} + h \\
augment\ (x, y)
\end{array}
$$

S: = Runge–Kutta4(c, a, b, N, f).

This method is relatively easy to implement and gives good accuracy, but as it is a constant step size method, the calculation time may become very long, especially if a very small step size is needed. Thus, in order to reduce computation time, an *adaptive step size* version of the Runge–Kutta method can be used. The general formula for the adaptive step size Runge–Kutta method is given by:

$$y_{i+1} = y_i + \sum_{n=1}^{6} c_n k_n$$

where:

$$k_1 = h \cdot f(x_i, y_i)$$

$$k_n = h \cdot f\left(x_i + a_n \cdot h,\, y_i + \sum_{m=1}^{n-1} b_{nm} k_m \right),\, n = 2, \ldots, 6$$

with local truncation error of order $O(h^6)$.

Several sets of a_n, b_{nm} and c_n coefficients and computer algorithms for implementation of this method were reported, e.g. those suggested by Cash and Karp [Cash 1990].

Thus, in the *adaptive* Runge–Kutta method, the step size is controlled so that the results are within the desired accuracy. This is why the numerical computations in Chapter 8 are performed using the *adaptive RK4 method*.

Runge–Kutta methods are available in all standard computer mathematical toolboxes such as Matlab, Mathcad, Mathematica, Maple etc. The use of a Runge–Kutta fourth-order method with fixed integration step (a routine called *rkfixed*), and with step-size adaptation (*Rkadapt*) is shown here for Mathcad.

A.2 Rkfixed and Rkadapt Routines for Solving IVP

The case of cylindrical rods grown in zero gravity using the EFG technique (the configuration presented in Figure 8.14) is considered as an example. Equation (8.86) with the initial condition (8.81) is solved numerically and the solutions obtained using the routines *rkfixed* and *Rkadapt* are compared with the analytical solution (8.87).

Thus, the following IVP is solved numerically:

$$\frac{\mathrm{d}z}{\mathrm{d}r}(r) = -\frac{r_{0\mathrm{i}} \cdot \sin\phi_{\mathrm{c}}}{\sqrt{r^2 - (r_{0\mathrm{i}} \cdot \sin\phi_{\mathrm{c}})^2}} \tag{A8.1}$$

$$z(r_{0\mathrm{i}}) = 0 \tag{A8.2}$$

The exact solution represents the analytical expression of the meniscus as function of the parameter ϕ_{c}:

$$z(r) = r_{0\mathrm{i}} \cdot \sin\phi_{\mathrm{c}} \cdot \ln \frac{r_{0\mathrm{i}}(1 + \cos\phi_{\mathrm{c}})}{r + \sqrt{r^2 - r_{0\mathrm{i}}^2 \cdot \sin^2\phi_{\mathrm{c}}}}, \quad r \in (r_{0\mathrm{i}} \cdot \sin\phi_{\mathrm{c}}, r_{0\mathrm{i}}] \tag{A8.3}$$

The obtained solution of *rkfixed* and *Rkadapt* routines is a matrix with two columns (independent variable values, and the corresponding solution function values). The arguments list of these procedures is as follows:

rkfixed(init, x_1, x_2, N, D) and *Rkadapt*(init, x_1, x_2, N, D)

where:

- init is either a vector of n real initial values, where n is the number of unknowns, or a single scalar initial value, for a single ordinary differential equation (ODE);
- x_1 and x_2 are real, scalar initial and end points of the interval over which the solution to the ODE(s) will be evaluated;
- N is the integer number of points beyond the initial point at which the solution is to be approximated;

- D is a derivative vector function of the form $D(x, y)$ specifying the right-hand side of the system.

A.2.1 Example of Implementation in Mathcad

$r_{0i} := 0.002\,[\mathrm{m}]$

$\phi_c := 1.3\,[\mathrm{rad}]$

$a := r_{0i}; c := 0$ // initial value given at the beginning of the interval //

$b := r_{0i} \cdot \sin(\phi_c) + 10^{-9}$ // final value of the interval //

$N := 1000$ // number of the solution value in the interval $[a, b]$ //

$\mathrm{init} := c$

$$D(x, y) := \frac{-r_{0i} \cdot \sin\phi_c}{\sqrt{x^2 - (r_{0i} \cdot \sin\phi_c)^2}}$$

$\mathrm{S\_fixed} := rkfixed(\mathrm{init}, a, b, N, D)$

$\mathrm{R\_fixed} := \mathrm{S\_fixed}^{\langle 0 \rangle}$ $Z\_\mathrm{fixed} := \mathrm{S\_fixed}^{\langle 1 \rangle}$

$\mathrm{S\_adapt} := Rkadapt(\mathrm{init}, a, b, N, D)$

$\mathrm{R\_adapt} := \mathrm{S\_adapt}^{\langle 0 \rangle}$ $Z\_\mathrm{adapt} := \mathrm{S\_adapt}^{\langle 1 \rangle}$

S_fixed =			S_adapt =		
	0	1		0	1
•••	••••••	••••••	•••	••••••	••••••
990	0.001927846	0.000475318	990	0.001927846	0.000475318
991	0.001927773	0.000478036	991	0.001927773	0.000478036
992	0.0019277	0.000480909	992	0.0019277	0.000480909
993	0.001927628	0.000483968	993	0.001927628	0.000483968
994	0.001927555	0.000487253	994	0.001927555	0.000487253
995	0.001927482	0.000490826	995	0.001927482	0.000490826
996	0.001927409	0.000494776	996	0.001927409	0.000494776
997	0.001927336	0.000499258	997	0.001927336	0.000499258
998	0.001927263	0.00050457	998	0.001927263	0.00050457
999	0.00192719	0.000511483	999	0.00192719	0.000511479
1000	0.001927117	0.000532588	1000	0.001927117	0.000526005

A.2.2 Conclusion

Comparing the solution obtained by *rkfixed* (i.e. RK4), *Rkadapt* and the analytical solution, it is easy to see that *Rkadapt* gives better results. In seeking the computed value of the function at the endpoint b of the interval, it can be observed that the difference between the exact solution and the approximate solutions are in the fourth digit for *rkfixed*, and the sixth digit for *Rkadapt*. Note that the error can be decreased by increasing N.

The *exact solution* is given by Equation (A8.3). At the end point of the interval the exact solution is:

$$z(b) = z\left(r_{0i} \cdot \sin(\phi_c) + 10^{-9}\right) = 0.0005263903.$$

The *approximate solution* given by the *rkfixed* routine, computed at the endpoint *b*, is:

z_fixed = 0.000532588 // the last value from the table S_fixed corresponding to *b* //

The *approximate solution* given by the *Rkadapt* routine, computed at the endpoint *b*, is:

z_adapt = 0.000526005 // the last value from the table S_adapt corresponding to *b* //

After plotting the menisci obtained numerically (Figure A8.1a), it is difficult to see a difference of the order of the fourth or sixth digit and for this reason an enlarged image is shown in Figure A8.1b.

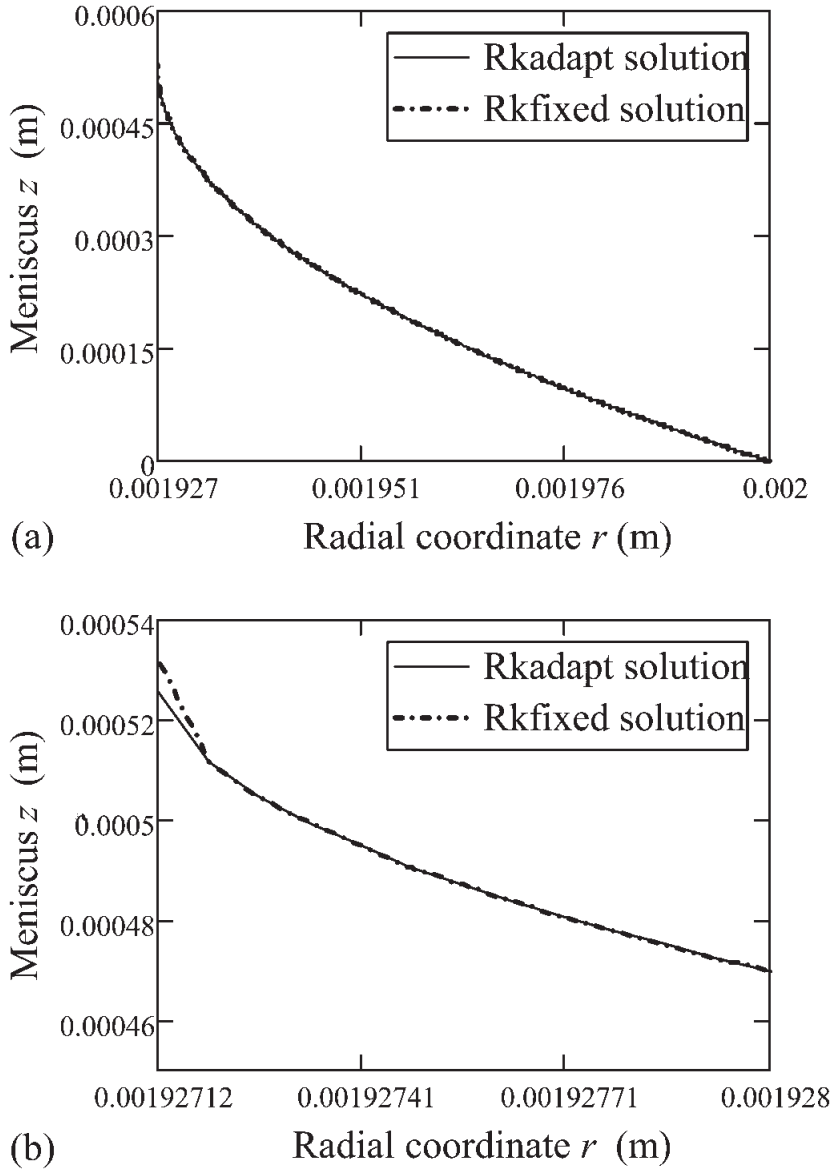

Figure A8.1 *(a) Approximated menisci obtained by RK4 (dotted line) and adaptive RK4 (full line). (b) Approximated menisci obtained by RK4 (dotted line) and adaptive RK4 (enlargement of Figure A8.1a).*

References

[Balint 2005] Balint S., Braescu L., Balint A.M., Szabo R., *J. Cryst. Growth* **283** (2005) 15.

[Balint 2008] Balint S., Braescu L., Sylla L., Epure S., Duffar T., *J. Cryst. Growth* **310** (2008) 1564.

[Bardsley 1974] Bardsley W., Cockayne B., Green G.W., Hurle D.T.J., Joyce G.C., Roslington J.M., Tufton P.J., Webber H.C., Healey M., *J. Cryst. Growth* **24–25** (1974) 369.

[Bardsley 1977-1] Bardsely W., Hurle D.T.J., Joyce G.C., *J. Crystal Growth* **40** (1977) 13.

[Bardsley 1977-2] Bardsley W., Hurle D.T.J., Joyce G.C., Wilson G.C., *J. Cryst. Growth* **40** (1977) 21.

[Borodin 1979] Borodin V.A., Brener E.A., Tatarchenko V.A., *Acta Phys. Sci. Hungar.* **47** (1979) 151.

[Boucher 1980] Boucher E.A., Jones T.G.J., *J. Chem. Soc. Faraday I* **76** (1980) 1419.

[Braescu 2003] Braescu L., Balint A.M., Balint S., *J. Cryst. Growth* **259** (2003) 121.

[Braescu 2004-1] Braescu L., Balint A.M., Balint S., *J. Cryst. Growth* **268** (2004) 284.

[Braescu 2004-2] Braescu L., Balint A.M., Balint S., *J. Cryst. Growth* **269** (2004) 617.

[Braescu 2005] Braescu L., *Nonlinear Stud.* **12**(4) (2005) 361.

[Braescu 2008-1] Braescu L., Balint St., Bonchis N., Kaslik E., *Numerical Methods* (undergraduate course in English), West University Publishing House, Timisoara, Romania (2008).

[Braescu 2008-2] Braescu L., *J. Colloid Interface Sci.* **319** (2008) 309.

[Brener 1979-1] Brener E.A., Tatarchenko V.A., *Acta Phys. Sci. Hungar.* **47** (1979) 133.

[Brener 1979-2] Brener E.A., Tatarchenko V.A., *Acta Phys. Sci. Hungar.* **47** (1979) 139.

[Cash 1990] Cash J.R., Karp A.H., *ACM Trans. Math. Software* **16** (1990) 201–222.

[Clanet 2002] Clanet C., Quere D., *J. Fluid Mech.* **460** (2002) 131.

[Dijk 1974] Dijk H.J.A., Goorissen J., Gross U., Kersten R., Pistorius J., *Acta Electron.* **17** (1974) 45.

[Duffar 1997] Duffar T., Boiton P., Dusserre P., Abadie J., *J. Cryst. Growth* **179** (1997) 397.

[Duffar 2000] Duffar T., Dusserre P., Picca F., Lacroix S., Giacometti N., *J. Cryst. Growth* **211** (2000) 434.

[Epure 2010] Epure S., PhD Thesis, Grenoble Institute of Technology, France and West University of Timisoara, Romania (2010).

[Ferguson 1912] Ferguson A., *Phil. Mag.* **24** (1912) 837.

[Finn 1986] Finn R., *Equilibrium capillary surfaces*, Springer-Verlag, New York (1986), pp. 1–16.

[Gartner 1972] Gartner K.J., Rittinghaus K.F., Seeger A., Uelhoff W., *J. Cryst. Growth* **13–14** (1972) 619.

[Gartner 1973] Gartner K.J., Uelhoff W., *Optik* **37** (1973) 15.

[Hartland 1976] Hartland S., Hartley R.W., *Axisymmetric Fluid-Liquid Interfaces*, Elsevier, Amsterdam (1976).

[Hauksbee 1709] Hauksbee F., *Physico-Mechanical Experiments*, London (1709), pp. 139–169.

[Hernandez-Baltazar 2005] Hernandez-Baltazar E., Gracia-Fadrique J., *J. Colloid Interface Sci.* **287** (2005) 213.

[Huh 1969] Huh C., Scriven L.E., *J. Colloid Interface Sci.* **30** (1969) 323.

[Hurle 1981] Hurle D.T.J., *Advances in Colloid and Interface Science* **15** (1981) 101.

[Hurle 1983] Hurle D.T.J., *J. Crystal Growth* **63** (1983) 13.

[Johansen 1987] Johansen T.H., *J. Crystal Growth* **80** (1987) 343.

[Johansen 1992] Johansen T.H., *J. Cryst. Growth* **118** (1992) 353.

[Johansen 1994] Johansen T.H., *J. Crystal Growth* **141** (1994) 484.

[Landau 1971] Landau L.D., Lifchits E.M., *Mécanique des Fluides* (Mir, Moscow, 1971 (in French).

[Laplace 1806] Laplace P.S., *Traité de Mécanique Céleste; Suppléments au Livre X, Oeuvres Complètes Vol. 4*, Gauthier-Villars, Paris (1806).

[Mika 1975] Mika K., Uelhoff W., *J. Crystal Growth* **30** (1975) 9.

[Nutt 1960] Nutt C.W., *Chem. Eng. Sci.* **12** (1960) 133.

[O'Kane 1972] O'Kane D.F., Kwap T.W., Gulitz L., Bednowitz A.L., *J. Cryst. Growth* **13–14** (1972) 624.
[Princen 1965] Princen H.M., Mason S.G., *J. Colloid Sci.* **20** (1965) 246.
[Sachs 1980] Sachs E.M., Surek T., *J. Cryst. Growth* **50** (1980) 114.
[Sylla 2008-1] Sylla L., Duffar T., *Mater. Sci. Eng. A* **495** (2008) 208–214.
[Sylla 2008-2] Sylla L., *PhD thesis, INP-Grenoble* (2008) (in French).
[Tatartchenko 1993] Tatarchenko Y.A., *Shaped Crystal Growth*, Kluwer, Dordrecht (1993), pp. 19–167.
[Tsivinski 1962] Tsivinski S.V., *Inzheherno Fiz. Zhur.* **5** (1962) 59.
[Young 1805] Young T., *Phil. Trans. R. Soc. London* **95** (1805) 65.